DOCTORAL THESIS

Development of a Pulsed Corona Discharge-Photocatalytic Oxidation System for Environmental Air Treatment

Kristen Altof

TALLINNA TEHNIKAÜLIKOOL
TALLINN UNIVERSITY OF TECHNOLOGY
TALLINN 2026

TALLINN UNIVERSITY OF TECHNOLOGY
DOCTORAL THESIS
/2026

Development of a Pulsed Corona Discharge-Photocatalytic Oxidation System for Environmental Air Treatment

KRISTEN ALTOF

TAL TECH PRESS

TALLINN UNIVERSITY OF TECHNOLOGY
School of Engineering
Department of Materials and Environmental Technology
This dissertation was accepted for the defence of the degree 06/05/2026

Supervisor: Dr. Juri Bolobajev
Department of Materials and Environmental Technology
Tallinn University of Technology
Tallinn, Estonia

Co-supervisor: Assoc. Prof Marina Krichevskaya
Department of Materials and Environmental Technology
Tallinn University of Technology
Tallinn, Estonia

Opponents: Assoc. Prof Taavo Tenno
Institute of Chemistry
University of Tartu
Tartu, Estonia

Prof Bratislav M. Obradović
Faculty of Physics
University of Belgrade
Belgrade, Serbia

Defence of the thesis: 09/06/2026, Tallinn

Declaration:
Hereby I declare that this doctoral thesis, my original investigation and achievement, submitted for the doctoral degree at Tallinn University of Technology has not been submitted for doctoral or equivalent academic degree.

Kristen Altof

---
signature

European Union
European Regional Development Fund

Investing in your future

ISSN 2585-6898 (publication)
ISBN 978-9916-80-504-6 (publication)
ISSN 2585-6901 (PDF)
ISBN 978-9916-80-503-9 (PDF)

TALLINNA TEHNIKAÜLIKOOL
DOKTORITÖÖ
/2026

Impulss-koroonalahenduse ja fotokatalüütilise oksüdatsiooni kombineeritud tehnoloogia arendamine õhu puhastamiseks

KRISTEN ALTOF

TAL TECH
KIRJASTUS

Contents

List of publications

The list of author's publications on which the thesis is based:

I **K. Altof**, M. Krichevskaya, S. Preis, J. Bolobajev. (2024). Oxidation of Airborne *m*-Xylene in Pulsed Corona Discharge: Impact of Water Sprinkling, *ChemEngineering*, 8, 99. https://doi.org/10.3390/chemengineering8050099

II **K. Altof**, M. Krichevskaya, S. Preis, T. Tähemaa, J. Bolobajev. (2024). Ozone-assisted degradation of 2-methoxyethanol in a prototype plug flow photocatalytic reactor, *Chemical Engineering Journal*, 481. https://doi.org/10.1016/j.cej.2023.148488

III **K. Altof**, M. Krichevskaya, S. Preis, J. Bolobajev. (2025). Advanced oxidation of airborne *m*-xylene in combination of pulsed corona discharge and post-plasma photocatalysis, *Journal of Electrostatics*, 138, 104184. https://doi.org/10.1016/j.elstat.2025.104184

Author's contribution to the publications

Contributions to the papers in this thesis are:

I The author prepared and operated the scaled-up PCD reactor equipped with an internal water-sprinkling system, conducted VOC degradation experiments under varying operational conditions, measured pollutant concentrations, performed GC-MS, LC and FT-IR analyses, evaluated energy efficiency, interpreted degradation mechanisms and prepared the manuscript draft in cooperation with co-authors.

II The author contributed to the design and commissioning of the pilot-scale PCO reactor, prepared the photocatalytic reactor configuration, conducted photocatalytic degradation experiments including tests in the presence of ozone, analysed operational parameters and mineralization efficiency, interpreted analytical results, prepared visualizations and wrote the manuscript draft in cooperation with co-authors.

III The author conceptualized the integration of the PCD and PCO reactors into a sequential post-plasma catalytic system, assembled and optimized the combined experimental setup, conducted comparative experiments of standalone and coupled configurations, analysed synergistic effects and system performance, interpreted the results and prepared the original manuscript draft in cooperation with co-authors.

Introduction

The PhD thesis focuses on the development of state-of-the-art technology for the treatment of airborne organic contaminants. Conventional air treatment processes, such as absorption, biofiltration and thermal treatment are respectively either transferring volatile organic compounds (VOCs) to liquid phase or are insufficient in degrading refractory pollutants. These limitations emphasize the need for advanced treatment methods capable of achieving efficient degradation and, ideally, complete mineralization of organic pollutants. Advanced oxidation processes (AOPs) can effectively degrade airborne VOCs reducing these pollutants to less harmful components or completely mineralize organic pollutants to CO_2 and H_2O. The fundamental principles of plasma processes, photocatalysis and AOPs that underpin this research are discussed in Chapter 1.

The main drawback of many AOPs lies in their high consumption of energy and other resources, which consequently leads to elevated treatment costs. From this perspective, the present doctoral study explores the application of an energy-efficient method based on low-temperature plasma generated by gas-phase pulsed corona discharge (PCD) in combination with photocatalytic oxidation (PCO). This approach required fundamental research to evaluate the process performance and to identify the efficiency limitations with respect to airborne contaminants.

The study revealed chemical reaction kinetics, reaction products and operational limitations associated with the treatment of airborne pollutants using gas-phase PCD plasma combined with PCO. The first article focuses on the PCD reactor operating as a standalone cold-plasma oxidation system, analyzing degradation efficiency, energy performance and reaction kinetics. The second article examines the PCO reactor independently, evaluating photocatalytic activity, operational parameters and pollutant transformation. The third article investigates the combination of the PCD reactor followed by the PCO reactor, assessing potential synergistic effects arising from plasma treatment and subsequent photocatalytic oxidation, with particular emphasis on enhanced degradation efficiency.

A tentative list of VOCs emitted by industry in Estonia served as a guide for selecting the target pollutants. 2-Methoxyethanol (2ME) and m-xylene were chosen for their widespread industrial use and their classification as hazardous and toxic compounds. The characterization of the degradation pathways of the target contaminants was performed using gas chromatography–mass spectrometry (GC-MS), liquid chromatography (LC) and Fourier transform infrared spectroscopy (FT-IR).

The thesis is based on data acquired from experiments conducted with a scale-up PCO reactor built for this purpose and a PCD reactor. The research project included the construction and optimization of the experimental setup for the application of plasma-photocatalytic oxidation system, analysis and reporting of experimental results. The methodology, reactor configurations and analytical procedures are described in Chapter 2, while the experimental results, including degradation efficiencies, energy consumption and operational limitations, are presented and discussed in Chapter 3.

The novelty of the study lies in the systematic evaluation of plasma and photocatalytic oxidation processes both individually and in sequence, demonstrating the potential of combining one of the most energy-efficient plasma-based AOPs with heterogeneous photocatalysis for improved treatment of airborne VOCs. The findings contribute to a deeper understanding of reaction mechanisms and provide a foundation for the development of more sustainable air purification technologies.

Abbreviations

2EE	2-ethoxyethanol
2ME	2-methoxyethanol
AOP	Advanced oxidation processes
DBD	Dielectric barrier discharge
E	Energy efficiency
FT-IR	Fourier transform infrared spectroscopy
GC-MS	Gas chromatography mass spectrometry
HPLC	High-performance liquid chromatography
NMVOC	Non-methane volatile organic compounds
PCD	Pulsed corona discharge
PCO	Photocatalytic oxidation
PPC	Post plasma catalysis
pps	Pulses per second
RH	Relative humidity
RONS	Reactive oxygen and nitrogen species
UV-A	Ultraviolet light A radiation (wavelength: 315-400 nanometres)
VOC	Volatile organic compounds

1 Literature overview

1.1 Air emission control technologies

Volatile organic compounds of toxic character present both indoors and outdoors an increasingly relevant health hazard that must be effectively mitigated. It has been found that indoor air pollutants originate from cleaning products, construction materials, kitchen activities, and furniture, whereas outdoor sources include traffic and neighbouring industries (Edwards *et al*., 2001; Schlink *et al*., 2010; Wang *et al*., 2013; Pearson, 2019). Considering that VOCs are generally hazardous, the member states of the European Union have committed to reducing emissions of non-methane volatile organic compounds (NMVOCs) by 40% by 2030, as stated in Directive 2016/2284 of the European Parliament and of the Council on the reduction of national emissions of certain atmospheric pollutants (Directive (EU) 2016). This commitment puts especially the industry in the European Union under pressure to implement innovative technologies to reduce NMVOCs emissions and achieve this ambitious goal.

Air emission control systems used in industry for the removal of volatile organic compounds (VOCs) are presented in Table 1. These technologies can be applied either as stand-alone systems or in combination. The table also illustrates the suggested application ranges for the different techniques (Kiely, 1997).

Table 1. Application ranges of air emission control technologies (Kiely, 1997).

Technology	VOC treatment	Inlet concentration, ppm	Efficiency, %
Adsorption	physico-chemical	> 5000	99
		> 200	90
Absorption	physico-chemical	> 5000	99
		> 200	90
Condensation	physico-chemical	> 5000	95
		> 500	50
Thermal incineration	thermal	> 100	99
		> 20	95
Catalytic incineration	thermal	> 100	95
		> 50	90

Gas separation technologies are based on the principle of physico-chemical separating unwanted pollutants from the airstream, thereby emitting only clean air. This can be achieved through several methods (Henry & Heinke, 1996; Kiely, 1997):

- *Adsorption*. The gas is passed through a porous material with a large surface area trapping the target components (pollutants) through weak adhesion forces while allowing clean air to pass through. This process continues until the porous material becomes saturated with pollutants, after which it must be regenerated or replaced.
- *Absorption*. The gas is brought into contact with a liquid medium, in which the target components (pollutants) are dissolved and thereby removed from the gas stream. The liquid must be continuously circulated, and the absorbed pollutants removed, to prevent saturation.

- *Condensation*. The gas is cooled in a heat exchanger, reducing its temperature and causing pollutants in the gas stream to condense. The condensate can then be collected and potentially reused, leaving the gas stream free from unwanted components.

Polluted air incineration technologies aim to mineralize pollutants to environmentally benign CO_2 and water. This can be achieved by the following methods:

- *Thermal incineration*. The gas is mixed with fuel (e.g. methane or propane) and ignited in a burner, where both the fuel and organic pollutants are oxidized to CO_2 and water.
- *Catalytic incineration*. The gas is passed over a surface of catalytic material, which lowers the activation energy required for the oxidation of pollutants. This leaves the gas stream pure from unwanted substances. Catalytic incineration is operated in continuous mode and typically requires elevated temperatures above 200 °C to further accelerate oxidation (Everaert & Baeyens, 2004).

It should be noted that gas separation technologies offer the advantage of recovering vaporized components. However, this approach is economically viable only when the initial pollutant concentrations exceed approximately 200 ppm, and ideally around 0.5% (5000 ppm). Gas incineration is recommended for pollutant concentrations between 20 to 100 ppm, where recovery is not economically feasible.

The technologies listed above do not include advanced oxidation processes (AOPs), as such methods have not yet reached widespread industrial application. AOP technologies, such as plasma oxidation and photocatalytic oxidation used in air emission control systems constitute the main focus of this thesis.

1.2 Non-thermal plasma

Plasma is the fourth state of matter, following solid, liquid and gas, as seen in Figure 1**.** It is an ionized gas consisting of positive and negative ions, free electrons, excited species, and neutral atoms and molecules. Plasma occurs naturally in phenomena such as auroras, lighting or in stars, and it can be generated artificially using thermal energy, electric fields or radiation (Meichsner *et al*., 2012).

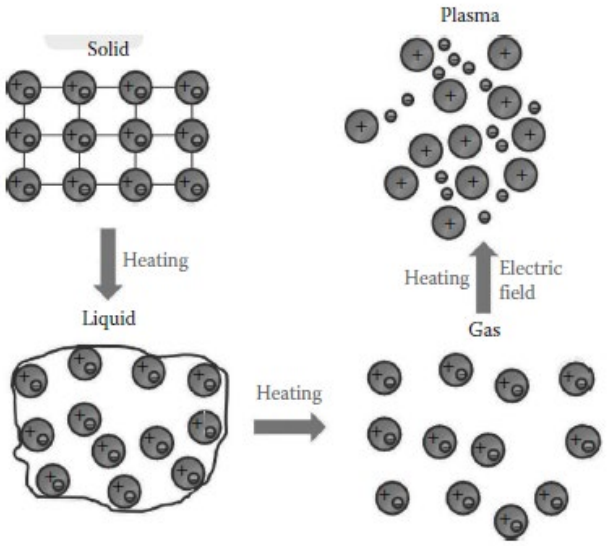

Figure 1. Transition of states of matter (Chu & Lu, 2013).

Plasma can be classified according to three main parameters: ionization, density, and thermal equilibrium. Ionization refers to the ratio between ionized and neutral particles. When this ratio is less than 0.1, the plasma is considered weakly ionized, whereas a ratio close to 1.0 indicates fully ionized plasma.

Plasma density (or pressure) describes the number of particles per unit volume. A particle density above 10^{15} cm^{-3} is considered high-density plasma, characterized by extensive excitation and ionization collisions as well as increased ion bombardment rates. Low-density or low-pressure plasma has a particle density of 10^{14} cm^{-3} or less, where collision rates between particles are negligible.

Thermal equilibrium in plasma refers to the temperature balance between electrons, ions and neutral particles. In thermal equilibrium plasma, all components have approximately the same temperature, and the plasma is regarded as hot. In non-thermal plasma, however, the electron temperature is significantly higher than that of ions and neutral particles. Since electrons have much lower mass, they cannot efficiently transfer energy to heavier particles, meaning that the overall gas temperature remains low. Therefore, non-thermal plasma is often referred to as cold plasma (Chu & Lu, 2013).

Plasma (ionized gas) can be utilized in environmental technologies due to its ability to degrade organic compounds. In emission control systems, cold plasma is of particular interest, as it requires less energy because the gas temperature remains low. Consequently, plasma density also remains lower compared to that of thermal equilibrium plasma. Even when the gas is only partially ionized, its components can form a variety of reactive oxygen and nitrogen species (RONS), as illustrated in Figure 2.

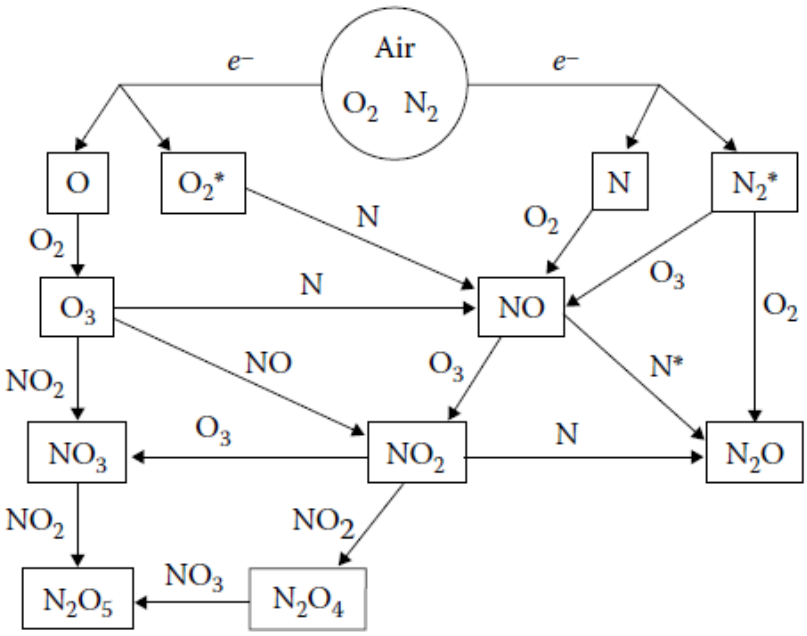

Figure 2. Oxygen and nitrogen species formed in plasma (Meichsner et al., 2012).

In dry air, oxygen and nitrogen form various RONS, such as O, O^+, O•, N• and NO•. In other words, molecular oxygen and nitrogen are dissociated into their atomic and ionic forms (Eq. 1 to 5) when they interact with high-energy free electrons. These reactive species readily undergo further reactions with other compounds in the gas mixture (Ogata *et al*., 2002; Ono & Oda, 2003; Nijdam *et al*., 2012).

$$e^- + O_2 \rightarrow O^+ + O\bullet + 2e^- \quad (1)$$

$$e^- + O_2 \rightarrow 2O\bullet + e^- \quad (2)$$

$$e^- + O_2 \rightarrow O^- + O\bullet \quad (3)$$

$$e^- + N_2 \rightarrow 2N\bullet + e^- \quad (4)$$

$$N\bullet + O_2 \rightarrow NO\bullet + O\bullet \quad (5)$$

In humid air, water molecules participate in the reactions, producing hydrogen-containing species such as H_2O_2, •OH (Eq. 6 and 7). Among these, the hydroxyl radical (•OH) is the most reactive, with a redox potential as high as 2.8 V (Carey, 1992; Schiorlin *et al.,* 2009; Chen *et al*., 2016). It is formed mainly through electron-impact dissociation of water (Eq. 6) (Chu & Lu, 2013):

$$H_2O + e^- \rightarrow \bullet OH + H\bullet + e^- \quad (6)$$

$$\bullet OH + \bullet OH \rightarrow H_2O_2 \quad (7)$$

More stable species that form in plasma include ozone (O_3) (Eq. 8, where M stands for a third body, typically a neutral molecule such as N_2 or O_2) (Ogata et al., 2002) and nitrous

oxide (N_2O). Ozone is generally considered a powerful oxidant in most environmental technologies. However, in gas-phase plug flow plasma reactors, the residence time is often too short for O_3 to play a significant role in pollutant oxidation. Therefore, ozone and nitrous oxide are typically regarded as unwanted by-products that require further attention.

$$O_2 + O\bullet + M \rightarrow O_3 + M \quad (8)$$

All these excited and stable species coexist in air plasma, continuously interacting with one another and with free electrons. More importantly, RONS and hydrogen-containing radicals react with organic pollutants when these are present in the plasma environment. This interaction forms the basis for using cold plasma in environmental applications, where sufficient radical concentrations are generated to degrade pollutants into less harmful substances.

The two primary plasma technologies employed for environmental applications are dielectric barrier discharge (DBD) and pulsed corona discharge (PCD), both capable of producing non-thermal plasma at atmospheric pressure.

Dielectric barrier discharge

DBD is generated between two electrodes separated by a gas gap and dielectric barriers that prevent the formation of arc discharge. The electric field between the electrodes is sufficient to ionize the gas and produce plasma, as illustrated in the schematic (Figure 3) of a cylindrical reactor with a coaxial arrangement of the electrodes and a dielectric barrier in between. According to Meichsner *et al*. (2012), typical operating parameters for DBD in air are voltages between 3-20 kV, repetition frequencies of 50-1000 Hz, an air gap of up to 5 mm, and atmospheric pressure. The dielectric materials commonly used include glass, Al_2O_3 and ferroelectrics (Meichsner *et al*., 2012; Chu & Lu, 2013).

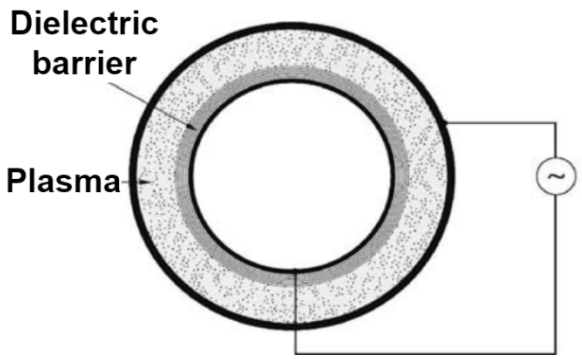

Figure 3. Cylindrical DBD reactor (Meichsner et al., 2012).

Pulsed corona discharge

Corona discharge is a type of partial discharge that occurs in the immediate vicinity of the electrode pin or wire and does not extend fully to the grounded plate. The gas between the high-voltage electrode and the ground is ionized, forming plasma and associated reactive species. PCD operates with nanosecond pulses, allowing voltages to reach tens of kilovolts. Typical configurations of corona discharge plasma generators include pin-to-plate or wire-to-plate systems (Figure 4) (Chu & Lu, 2013).

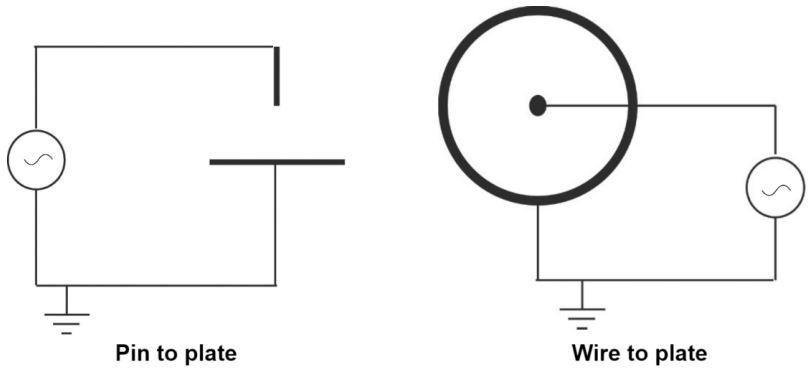

Figure 4. Corona discharge configurations (Chu & Lu, 2013).

1.3 Photocatalytic oxidation

Photocatalytic oxidation (PCO) refers to a process in which a semiconductor material is irradiated with light ($h\upsilon$) of sufficient energy for electrons to overcome the band gap between the valence and conduction bands. When the band gap is breached, electrons migrate to the conduction band (e_{cb}^-), leaving holes (h_{vb}^+) in the valence band, thus creating so-called electron-hole pairs (Sharma & Kumar, 2021).

The semiconductor titanium dioxide (TiO_2) has a band gap between 3.0 and 3.2 eV, depending on its crystalline form: anatase has a band gap of 3.2 eV, while rutile has a band gap of 3.0 eV (Kohtani *et al*., 2012). According to the photon energy equation (Eq. 9) the minimum wavelength of light required to breach the band gap can be calculated:

$$E_p = hc\lambda^{-1} \quad (9)$$

where E_p is the photon energy, h is the Planck's constant (6.626×10^{-34} Js^{-1}), c is the speed of light (3.0×10^8 ms^{-1}) and λ is the wavelength of light. For TiO_2, light with a wavelength of 387.5 nm is sufficient for anatase, and 413.4 nm for rutile. Therefore, UV-A light (315-400 nm) provides adequate energy, while visible light (400 – 700 nm) does not meet the threshold (Sharma & Kumar, 2021).

In the photocatalytic process, which is classified as AOP, the semiconductor is irradiated with light to generate electron-hole pairs. The components on or close to the catalyst surface interact with these charge carriers (Eq. 10). The mechanism functions particularly well with oxygen, which acts as an electron acceptor forming superoxide anion radicals ($O_2\bullet^-$) through reduction (Eq. 11). Simultaneously, water is oxidized to produce hydroxyl radicals (•OH) and protons (H^+) (Eq. 12) (Huang & Li, 2011; Sujatha *et al*., 2020). Both •OH and $O_2\bullet^-$ are powerful oxidants capable of degrading organic pollutants. The mechanism of photocatalysis is illustrated in Figure 5.

$$TiO_2 + h\upsilon \rightarrow TiO_2(h^+) + e^- \quad (10)$$

$$O_2 + e^- \rightarrow O_2\bullet^- \quad (11)$$

$$H_2O + h^+ \rightarrow \bullet OH + H^+ \quad (12)$$

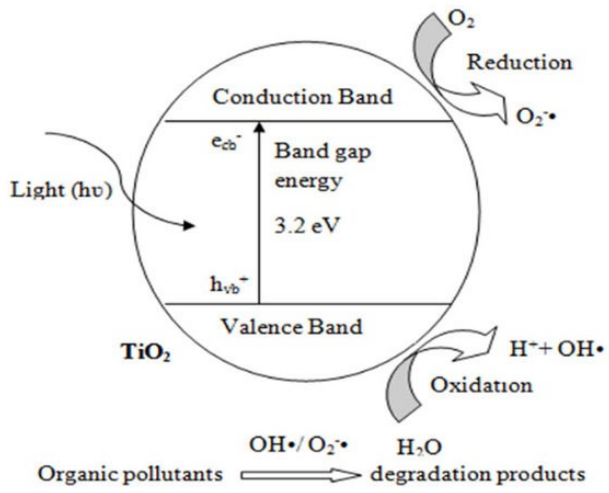

Figure 5. Photocatalytic oxidation mechanism (Sujatha et al., 2020).

The photocatalytic mechanism can be utilized for air purification in photocatalytic oxidation (PCO) reactors. In general, all PCO reactors consist of three essential components: a light source, a substrate or reactor structure, and a semiconductor coating that covers the substrate and is activated by light. The most common reactor designs are summarized in Table 2 (Ren et al., 2017; Zhang et al., 2022; Almaie et al., 2022).

Although, reactor configurations may vary, their objective remains the same: to bring the polluted gas stream into contact with the illuminated photocatalyst while maximizing surface contact area and minimizing the energy required for irradiation.

One of the most important components of a PCO reactor is the photocatalyst material, which determines the energy required for activation. Reducing this energy requirement (band gap) opens the possibility for PCO systems that can be driven by visible light instead of UV. Commonly studied materials include, for example, cerium oxide (CeO_2) and bismuth vanadate ($BiVO_4$) (Ren et al., 2017; Sharma & Kumar, 2021). CeO_2 is known for its stability and resistance to photocorrosion. Notably, Fe-doped (2.0 mol%) CeO_2 has a reduced band gap of 2.35 eV, enabling activation under visible light (Channei et al., 2014). $BiVO_4$ is a low-cost, highly stable semiconductor with a band gap of 2.4 eV, making it a promising candidate for visible-light-driven PCO applications (Fan et al., 2012; Ren et al., 2017). However, when shifting from UV to visible-light photocatalysts with narrower band gaps, the redox potentials of the generated charge carriers decrease. As a result, such catalysts may struggle to degrade more persistent pollutants efficiently, exhibiting undesirable selectivity in air treatment processes and often requiring longer reaction times or failing to achieve complete decomposition of pollutants (Chen et al., 2025).

Table 2. Basic PCO reactor designs.

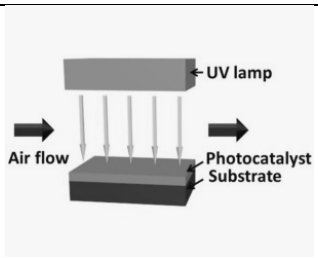	A plate reactor consists of a flat structure coated with a photocatalyst, while the light source is positioned above the semiconductor material to irradiate the surface. The air stream passes through the reactor between the light source and the photocatalyst.
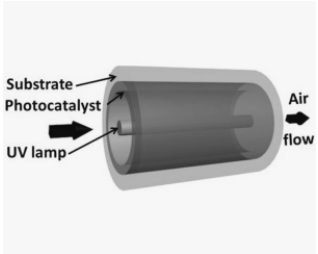	Annular reactors have a tubular shape with the inner surface coated with a photocatalyst. A light source is placed along the central axis of the tube, irradiating the inner walls. Air passes through the annular space between the light source and the photocatalyst-coated walls.
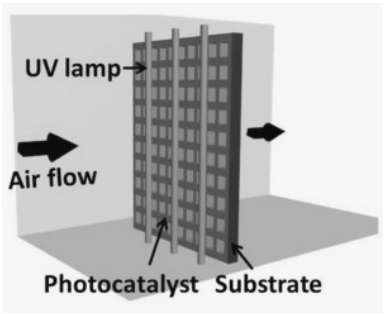	A honeycomb monolith reactor consists of a honeycomb-structured substrate, the inner walls of which are coated with a photocatalyst and irradiated by light sources positioned outside the structure. Air flows through the channels of the honeycomb, allowing contact between the photocatalyst and the gas stream.

Although a number of photocatalytic materials have been studied, TiO_2 remains the most widely used photocatalyst in environmental applications due to its stability, cost efficiency and availability.

The degradation of organic pollutants via PCO has been extensively studied (Almaie *et al*., 2022; Zhang *et al*., 2022), but the technology can also target other pollutants such as O_3 and N_2O, especially when PCO is combined with a PCD reactor. Similarly to oxygen, ozone acts as an electron acceptor, triggering a sequence of reactions (Eq. 13-15) that generate reactive oxygen species (ROS) such as ozonide radical anions, hydrotrioxide radicals, and hydroxyl radicals (Pengyi et al., 2003):

$$O_3 + e_{cb}^- \rightarrow O_3 \bullet^- \quad (13)$$

$$O_3 \bullet^- + H^+ \rightarrow HO_3 \bullet \quad (14)$$

$$HO_3 \bullet \rightarrow O_2 + OH \bullet \quad (15)$$

Ozone is thus degraded in a PCO while simultaneously generating ROS and suppressing electron-hole recombination, thereby extending the availability of h_{vb}^+ for further oxidation of organic pollutants (Krichevskaya *et al*., 2017).

Similarly, PCO has been investigated for N_2O degradation (Obalová *et al*., 2013; Kočí *et al*., 2017; Tan *et al*., 2019). Like oxygen and O_3, N_2O can act as an electron acceptor and react with ROS formed during photocatalysis (Eq. 16-17) (Kočí *et al*., 2017):

$$N_2O + e_{cb}^- \rightarrow N_2 + O\bullet^- \quad (16)$$

$$O\bullet^- + N_2O \rightarrow N_2 + O_2 + e^- \quad (17)$$

The photocatalytic mechanism can be applied in environmental control technologies as a standalone unit. However, its potential for degrading O_3 and N_2O makes it particularly attractive for post-plasma treatment, since these two by-products are among the main drawbacks of plasma reactors such as PCD systems.

1.4 Pollutants under consideration

In 2020, industrial air pollutant emissions reported by industries in Estonia amounted to 1,260 tons of VOCs (Keskkonnaamet, 2022), underscoring industrial exhaust as a significant source of air contamination. Among industrial sectors, wood fabrication and furniture production stand out due to their extensive use of solvent-based materials, including 2-ethoxyethanol (2EE). Twenty-two Estonian enterprises reported emissions of 2EE totalling 13.7 tons. As global demand for manufactured goods continues to rise, VOC emissions from such industries are expected to increase correspondingly, intensifying their environmental and health impacts.

2-Methoxyethanol (2ME) was chosen for experimental studies as it is more hazardous than glycol ether 2EE; both substances are widely used as solvents and carriers in paints (Sax, 1984). The occupational exposure limit for 2ME is 1 ppm (Miller *et al*., 1984; Bagchi and Waxman, 2008; European Chemicals Agency, 2023).

m-Xylene, an aromatic compound frequently used as a solvent in coatings, adhesives, and cleaning agents, represents one of the more hazardous VOCs. In 2020, xylene was reported to have been used by 193 companies in Estonia, with total emissions amounting to 221.2 tons (Keskkonnaamet, 2022). Due to its carcinogenic, mutagenic, and neurotoxic properties, *m*-xylene is regulated under occupational safety standards. The U.S. Occupational Safety and Health Administration sets an 8-hour exposure limit of 100 ppm for xylene isomers, while the European Union limit is 50 ppm (European Chemicals Agency, 2024). Nonetheless, several studies suggest that these limits may still be too high to fully protect human health (Bolden *et al*., 2015). Despite its potential risks, *m*-xylene remains indispensable across numerous industries, resulting in continuous emissions into the environment (Atsdr, 2021; Zoveidavianpoor *et al*., 2012; Niaz *et al*., 2015).

The persistence and widespread industrial use of VOCs such as xylenes and glycol ethers highlight the urgent need to understand their behaviour, transformation, and impacts in the atmosphere. As industrial activity expands, addressing the issue of VOC pollution becomes increasingly critical for ensuring both environmental quality and public health.

1.5 Summary of literature review and aim of the study

The removal of airborne volatile organic compounds remains a major technological and environmental challenge, particularly in industrial applications where high flow rates, fluctuating pollutant concentrations and energy efficiency requirements must be simultaneously addressed. Among advanced oxidation processes, non-thermal plasma

and heterogeneous photocatalysis are of interest due to their ability to generate highly reactive species capable of oxidizing VOCs at moderate operating conditions. Increasingly, research has explored the coupling of plasma and catalytic processes in order to enhance oxidation efficiency and improve mineralization.

Previous studies have demonstrated that combining plasma with catalytic materials can improve VOC degradation and reduce the formation of undesirable by-products (Zhang *et al*., 2022; Belkessa *et al*., 2024; Destrieux *et al*., 2025). Most of this research, however, has focused on laboratory-scale systems and on in-plasma catalysis, where the catalyst is placed directly inside the discharge zone. In contrast, post-plasma catalytic (PPC) configurations, where the catalyst is located downstream of the plasma reactor, remain comparatively rare. The combination of plasma with a dedicated PCO reactor as a post-plasma stage is even less explored. Furthermore, the majority of published studies rely on small-scale experimental setups, and only a few scaled-up prototype reactors have been reported worldwide. To the best of current knowledge, none of these scaled-up systems incorporate an internal water-sprinkling configuration within a plug-flow PCD reactor.

These limitations highlight several open research questions. How does a scaled-up plug-flow PCD reactor equipped with an internal water-sprinkling system perform in VOC oxidation? Can the introduction of a downstream PCO reactor enhance mineralization and overall process efficiency? And does a sequential plasma–photocatalytic configuration offer measurable advantages compared to the individual processes operating separately?

In response to these gaps, the aim of this study is to investigate the performance of a scaled-up plug-flow PCD reactor with internal water sprinkling and its integration with a downstream PCO unit, with particular emphasis on oxidation efficiency and process synergy. To achieve this, the present work develops and systematically evaluates this combined system arranged in a PPC configuration (Figure 6).

Three main objectives were addressed in this thesis:

- *The first objective* was to evaluate the performance of a prototype PCD reactor, equipped with a water-sprinkling system based on patented technology (Preis *et al*., 2016), for the degradation of VOCs. In addition, the study aimed to identify the key operational parameters influencing oxidation efficiency.
- *The second objective* was to design and commission a pilot-scale PCO reactor, quantify its key performance parameters under controlled operating conditions and study PCO performance in the presence of ozone.
- *The third objective* was to integrate the PCD and PCO units into a single PPC system and systematically evaluate the benefits and limitations of their coupled operation.

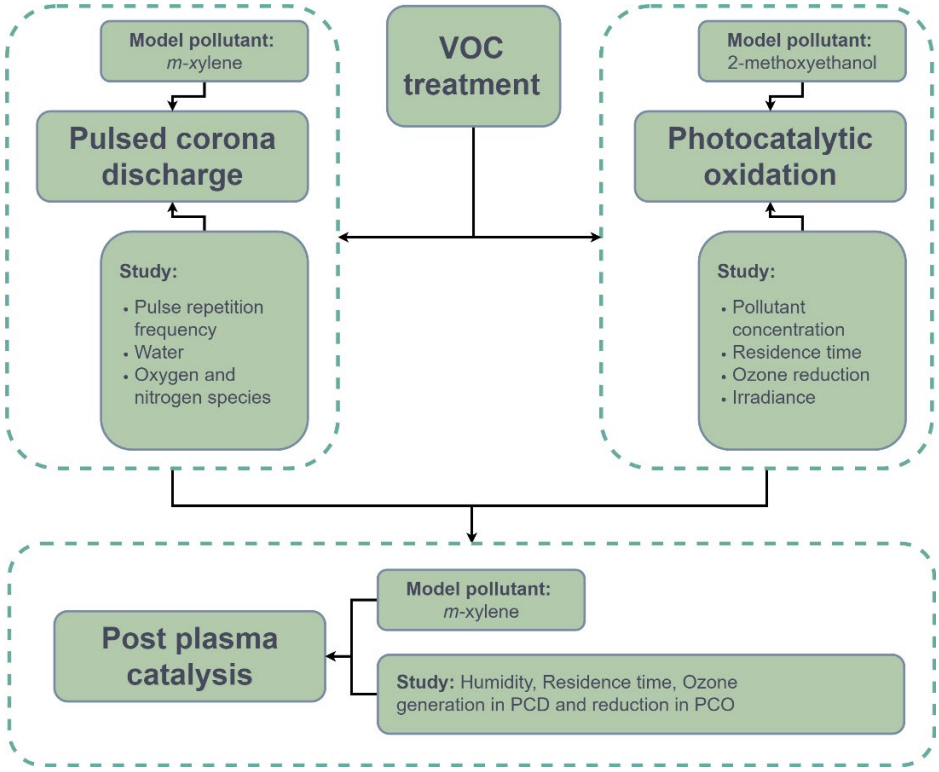

Figure 6. Structure of study.

2 Materials and methods

2.1 Chemicals and materials

Analytical grade *m*-xylene (C_8H_{10}, ≥99%, Thermo Scientific Chemicals, USA) and 2-methoxyethanol (2ME, $C_3H_8O_2$, ≥99%, Fisher Chemicals, USA) were used as model VOC pollutants. For the preparation of glass plates coated with photocatalyst, titanium dioxide P25 (Evonik Industries AG, Germany), and ethanol (C_2H_5OH, ≥99%, Sigma-Aldrich USA) were used. Ozone was generated onsite using a 10G Lab Ozone Generator (A2Z Ozone, USA).

For the high-performance liquid chromatography (HPLC) analyses, methanol (CH_3OH, ≥99.9%, Honeywell International Inc., USA) and Milli-Q ultrapure water (Millipore Simplicity® UV system, EMD Millipore Corporation, USA) were used as eluents. Dichloromethane (CH_2Cl_2, 99+% from Honeywell Riedel-de Haän™, Germany) was used to extract *m*-xylene oxidation by-products from water samples, and the extracts were dried using anhydrous sodium sulfate (Na_2SO_4 ≥ 99.8% from LachNer, Czech Republic). The carrier gas in gas chromatography-mass spectrometry (GC-MS) was helium (He, 99.99%, Elme Messer Gaas AS, Estonia).

Distilled water was used in the PCD experiments employing the water-sprinkling system. pH adjustment was accomplished using sulfuric acid (H_2SO_4, 96%, Lach:Ner, Czech Republic) and sodium hydroxide (NaOH, puriss. p.a., STANCHEM Sp. z o.o., Poland). Silica gel (SiO_2 > 98%) used for drying the inlet air was obtained from International Silica Gel.CO.,LTD (China).

2.2 Polluted air

2ME or *m*-xylene were used as model pollutants depending on the experiment. The setup used for pollutant vaporization is shown in Figure 7. All experiments were conducted in continuous mode with a constant air flow ranging from 1 to 8 $m^3\ h^{-1}$. The flow rate was adjusted by the main valve (1) and monitored with the rotameter (2).

An Eco Air Pump PA200 (Jecod Co. Ltd., People's Republic of China) supplied air at room temperature (22 °C), atmospheric pressure, and a relative humidity (RH) of 35±5%. Pressurized air from a compressor provided air with an RH of 7% and was used for dry-air experiments after passing through an additional drying stage in column (3) packed with silica gel.

Bubble columns (4) and (5) (height = 700 mm, inner diameter = 50 mm) were filled with 400 – 750 mL of liquid 2ME and m-xylene, respectively. Bypass lines controlled by valves (7) and (8) diverted the main airflow through the columns. As the air passed through the column, it became saturated with the target VOC vapor and was then reintroduced into the main airflow. The VOC concentration in the polluted air stream was adjusted by varying the air/bypass flow ratio.

For ozone-assisted PCO experiments, ozone was generated onsite using an ozone generator (A2Z Ozone, USA), and its flow rate was regulated using valve (9) before mixing with the main air stream. Column (6) was filled with silica gel to dry the air prior to entering the ozone generator.

Sampling for ozone, VOC degradation products, and oxidation by-products was performed downstream of the reactors using Fourier-transform infrared spectroscopy (FT-IR), GC-MS, and ozone analyser. The sampling line was controlled by valve (10).

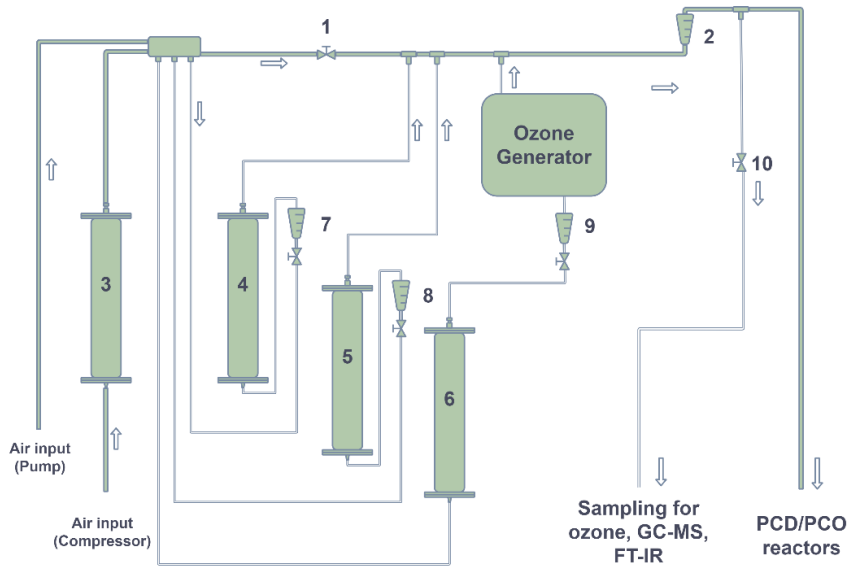

Figure 7. VOC vaporization setup: 1 – main flow control valve, 2 – main flow rotameter, 3 – air dryer filled with silica gel for the experiments with 2.5 % RH, 4 – 2ME column, 5 – m-xylene column, 6 – air dryer filled with silica gel for the generation of ozone, 7 – rotameter and control valve for the 2ME saturation bypass, 8 – rotameter and control valve for the m-xylene saturation bypass, 9 – rotameter and control valve for ozone generator, 10 – valve for input air sampling.

2.3 Gas-phase pulsed corona discharge

The PCD reactor (Flowrox Oy, Finland), illustrated in Figure 8, has a total volume of 75.9 L and comprises a central plasma zone (1275 × 550 × 35 mm, volume 24.5 L) and two side compartments housing high-voltage electrodes mounted on tensioning devices. The active plasma region is formed between two vertical grounded plates and a set of horizontal high-voltage wires suspended between them.

The high-voltage electrode assembly consists of 12 m of wire (0.6 mm diameter) arranged horizontally, with an inter-electrode distance of 17 mm from the grounded plates and 30 mm between adjacent high-voltage wires. The peak voltage is 18 kV, and the peak current can reach 380 A. Corona discharge is generated using nanosecond pulses (100 ns), with pulse repetition frequencies ranging from 50 to 800 pulses per second (pps), corresponding to an input power range of 6.25–100 W depending on the operational settings, as shown in Table 3.

Table 3. Power consumption corresponding to pulse frequency.

Pulse frequency, pps	Power, W
50.00	6.25
100.00	12.50
200.00	25.00
500.00	62.50
800.00	100.00

Water sprinkling was integrated into the system via a 12.7-L stainless steel storage tank, which was filled with 5.0 L of distilled water. A magnet-drive circulation pump (Iwaki Co. Ltd., Tokyo, Japan) delivered the water to the top of the reactor, where it was evenly distributed across a perforated plate (565 × 97 mm) containing 24 holes (3 mm diameter each). The water then cascaded downward through the plasma zone before returning to the storage tank, completing the circulation loop. This configuration ensured effective interaction between the plasma and the liquid phase, facilitating advanced oxidation of pollutants. The reactor generated a low-temperature, non-thermal plasma under atmospheric pressure air conditions, suitable for the oxidative degradation of VOCs.

Energy efficiency of the PCD reactor, expressed in g $kW^{-1}h^{-1}$, was calculated according to Eq. 18.

$$E = \frac{\Delta C \cdot Q}{P} \tag{18}$$

where E – energy efficiency, ΔC – difference in *m*-xylene concentrations between inlet and outlet air streams, g m^{-3}, Q – air volumetric flow rate, m^3 h^{-1}, P – pulsed power input, kW.

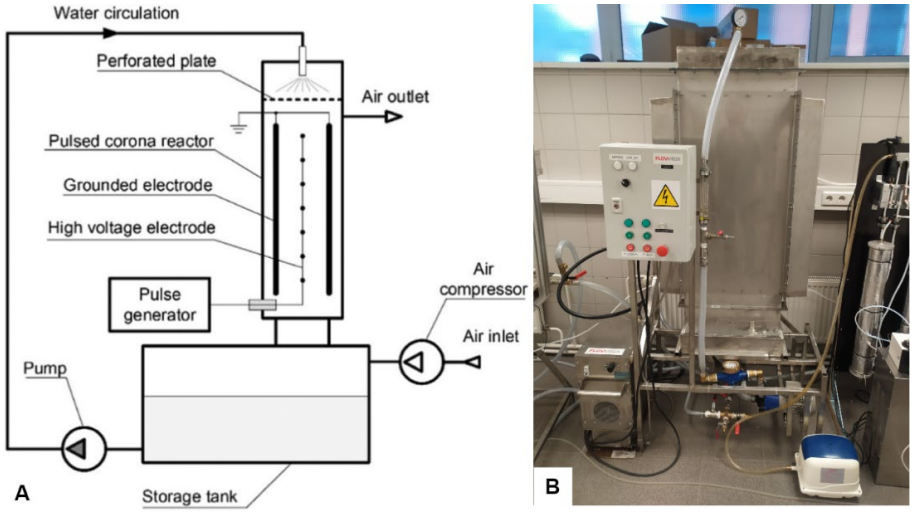

Figure 8. (A) - Pulsed corona discharge reactor schematics (Kask et al., 2021), (B) - Photo of the pulsed corona discharge reactor.

2.4 Gas-phase photocatalytic oxidation

The plug flow PCO reactor used in this study features a flat-bed design enclosed by a transparent 2-mm polyethylene terephthalate cover. This configuration enables external irradiation of the photocatalyst and ensures continuous contact between the polluted gas stream and the photocatalytic surface throughout the reactor chamber. The internal dimensions of the reactor are 996 mm in length, 534 mm in width, and 40 mm in height, corresponding to a total internal volume of 21.3 L.

The reactor is divided into five chambers of equal volume (4.26 L each), separated by stainless-steel partition plates with perforations that direct airflow diagonally between compartments. Additionally, three vertical stainless-steel walls were installed within each section to induce a zigzag flow pattern. This design enhances turbulent mixing and promotes effective contact between the polluted air and the photocatalyst surface.

SolidWorks simulations (Figure 9 A) demonstrate that this configuration provides both turbulence and uniform airflow distribution across the catalyst surface. Experimental comparison of configurations with and without internal partitions showed no significant difference in 2ME degradation efficiency at an average flow rate of 5.0 $m^3 h^{-1}$, confirming that the default flow dynamics provide sufficient mass transfer.

The photocatalyst used was TiO_2, consisting predominantly of anatase with a rutile fraction of 13.4±0.7 wt.%. TiO_2 was applied to 115 × 90 × 2 mm glass plates using a spraying method, as described by Kask et al. (Kask *et al*., 2020). A total of 40 plates, each coated with 1.53±0.11 mg cm^{-2} of TiO_2, were installed in the reactor, providing a total catalyst surface area of 4,140 cm^2.

UV-A radiation was supplied by twenty TL-D 15W lamps (Philips, Germany) positioned 7.0 cm above the catalyst surface (Figure 9 B). Light intensity was controlled by adjusting the number of lamps switched-on in sets of five distributed evenly along the reactor. Spectral analysis of UV-A radiation (315 – 400 nm) were performed using a USB 162 2000+ UV-VIS spectrometer (Ocean Optics, USA). The average irradiance at the photocatalyst surface increased from 29 to 119 W m^{-2} as the nominal power increased, corresponding to activation of 5 to 20 lamps, respectively.

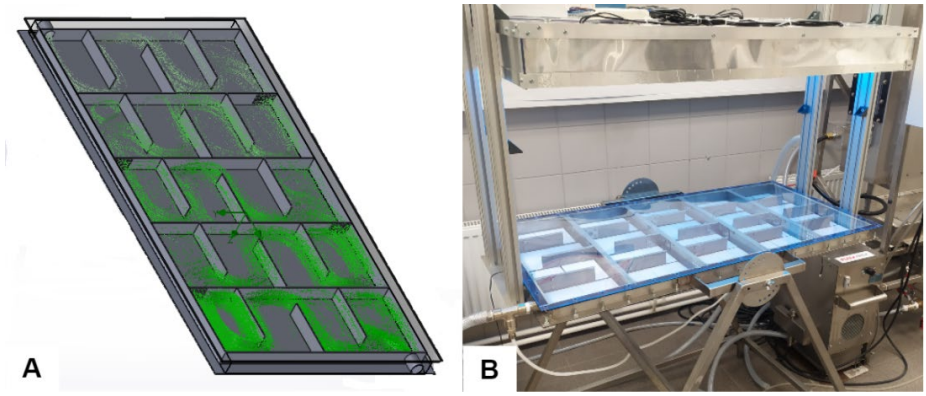

Figure 9. (A) - Air flow trajectories simulated in photocatalytic oxidation reactor at the gas flow of 5.0 m3 h-1, (B) - Photocatalytic oxidation reactor (The picture is for illustration purposes only; for experiments the lamps were lowered to 7 cm above the reactor).

2.5 Post plasma catalysis

For post plasma catalyst studies, the PCD and PCO reactors were connected in series, with plasma treatment serving as the primary stage and photocatalysis as the secondary stage. The combined PPC reactor configuration is shown in Figure 10. Valves (2) and (3) were added to the experimental setup to enable the collection of comparable samples from each reactor individually.

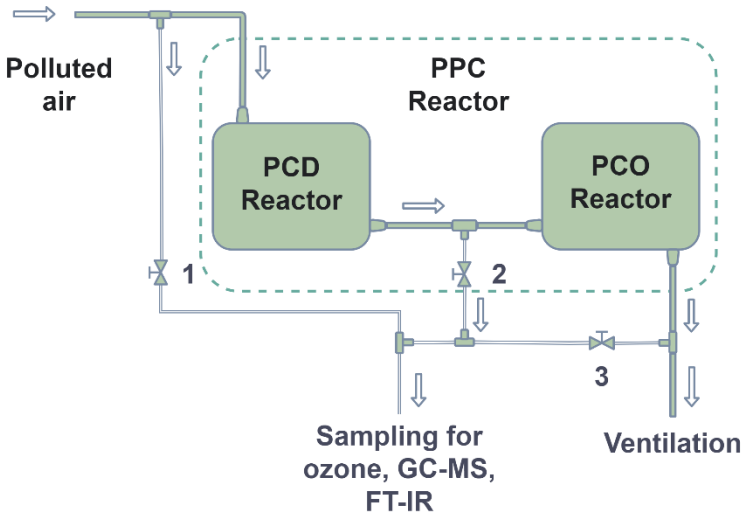

Figure 10. PPC reactor setup: 1 – valve for input air sampling, 2 - valve for PCD air sampling, 3 - valve for PCO air sampling.

2.6 Experimental procedure

The experimental setup and reactor system enabled manipulation of several operational parameters. In different experiments, the air flow rate was varied between 1 and 8 $m^3 h^{-1}$, resulting in different residence times within the reactors (Table 4). Low relative humidity (RH) was achieved by supplying compressor air and further drying it with silica gel, yielding an average RH of 2.5% in the reactors (Paper III). An RH of 35% was obtained using room air, while an elevated RH of 65% was achieved by combining room air and water circulation in the PCD sprinkler system (Paper I & III).

For standalone PCD experiments, an inlet concentration of 20±5 ppm of *m*-xylene was used (Paper I). Initial PCO experiments were conducted with 2ME concentrations ranging from 6 to 50 ppm (Paper II). The PPC reactor configuration was tested using 45±5 ppm of *m*-xylene (Paper III).

Table 4. Residence times in reactors at different air flow rates (Paper I-III).

Air flow rate, $m^3 h^{-1}$	PCD reactor, s	PCD reactor plasma zone, s	PCO reactor, s
1.0	-	-	76.7
2.0	136.6	44.1	38.3
4.0	68.3	22.1	19.2
5.0	-	-	15.3
6.0	45.5	14.7	12.8
8.0	34.2	11.0	9.6

In experiments with sprinkling in the PCD reactor, water was continuously recirculated at a constant flow rate adjustable between 3 and 18 L min^{-1} (Paper I). For PPC experiments, the water circulation rate was fixed at 9 L min^{-1} (Paper III). Distilled water with a pH of 7 was used as the circulating medium. For specific studies, the water pH was

adjusted using sulfuric acid or sodium hydroxide to decrease or increase the pH, respectively (Paper I).

All air samples were taken at least 15 minutes after the start of each experiment to ensure that steady-state conditions had been established (Paper I-III).

2.7 Analysis

The degradation performance of *m*-xylene and 2ME was assessed by comparing inlet (C_{in}) and outlet (C_{out}) concentrations in the gas stream, as defined in Eq. 19. Air samples were analyzed using either FT-IR or GC-MS, depending on the experiment.

$$degradation = \frac{C_{in} - C_{out}}{C_{in}} \quad (19)$$

Gas-phase analysis by FT-IR

For FT-IR measurements, air samples were collected in a 4 L metal body gas cell (Specac, United Kingdom) and analyzed using an FT-IR spectrometer (Interspec 200-X, Interspectrum OÜ, Estonia). Data interpretation was performed with Essential FT-IR software (Operant LLC) using the FDM HiRes VPFTIR for Quant database.

FT-IR enabled the detection of *m*-xylene, 2ME, N_2O and additional gaseous by-products. *m*-Xylene was monitored at 770–766 cm^{-1}, N_2O was monitored at 2256–2223 cm^{-1}. The optimal region for 2ME quantification was 2921–2838 cm^{-1}, minimizing spectral overlap with other species (Paper I-III).

Gas-phase analysis by GC-MS

Alternatively, air samples were collected in 20 mL vials and analyzed by GC-MS (QP2010 Plus, Shimadzu, Japan). The GC system was equipped with a Zebron (USA) ZB-WAXplus capillary column (30 m length, 0.32 mm inner diameter, 0.25 µm film thickness). The injection port was maintained at 50 °C, and the oven temperature at 30 °C. The MS operated in selected ion monitoring mode at m/z = 106 for *m*-xylene quantification.

Parallel reference measurements using FT-IR and GC-MS were used to generate calibration curves, enabling accurate quantification of the mass spectrometric signals (Paper I & III).

Analysis of aqueous-phase by-products and water-soluble species

Aqueous degradation products of *m*-xylene were extracted using a three-step liquid-liquid extraction with dichloromethane. Extracts were dried over anhydrous Na_2SO_4 and concentrated tenfold (1:10, v/v) by evaporation before GC-MS analysis.

For GC-MS analysis of liquid extracts, the injection port was maintained at 260 °C. The GC temperature program consisted of an initial hold at 80 °C for 1 min, a 10 °C min^{-1} ramp to 250 °C, and a final hold at 250 °C for 5 min. Mass spectra were recorded using electron impact ionization across m/z 40–340 at 1.666 amu s^{-1} (Paper III).

Water samples were collected from the circulating system to quantify water-soluble oxidation products. Nitrite (NO_2^-) and nitrate (NO_3^-) concentrations were measured using ion chromatography (Metrohm® 761 Compact IC) equipped with a suppressed conductivity detector and a Metrosep A Supp 5 column (150 × 4.0 mm) (Paper I).

m-Xylene concentrations in water were analyzed by high-performance liquid chromatography (HPLC, Shimadzu LC-2030D, Japan) with a PDA detector and a Luna Omega polar C18 column (150 mm, 5 µm particle size). Isocratic elution was performed using a 60:40 methanol-water mixture at 0.2 mL min^{-1} with a column temperature of

40 °C. Quantification of m-xylene at pH > 9.5 was not possible due to instability of the column's stationary phase under alkaline conditions (Paper I).

Ozone, pH, humidity and temperature monitoring

Depending on the ozone concentrations generated during operation, two ozone analyzers were used: an Anseros ozone monitor (Anseros Klaus Nonnenmacher GmbH, Germany) and a BMT 965 BT analyzer (BMT Messtechnik GmbH, Germany) (Paper I-III).

In experiments involving water sprinkling, water pH was measured with a SevenCompact pH meter (Mettler-Toledo®, USA). Humidity and temperature in the gas stream were monitored using a TPI597 digital hygrometer (Test Products International, USA) (Paper I).

3 Results and discussion

3.1 Plasma treatment and the influence of sprinkling water

Experiments with the PCD reactor were conducted to evaluate its applicability as an environmental control system, specifically, as an end-of-pipe device for pollutant degradation. A series of experiments with varying operational parameters was performed to obtain a systematic overview and deeper understanding of the prototype PCD reactor's performance (Paper I & III).

3.1.1 VOC degradation with plasma

The influence of pulse repetition frequency, and consequently pulsed power input, on *m*-xylene oxidation was studied in the water-sprinkled PCD reactor. As shown in Figure 11, increasing the input power enhanced *m*-xylene conversion, indicating a higher plasma density within the reactor. Higher plasma density implies increased formation of RONS, which are primarily responsible for VOC degradation. Khadem *et al*. (Khadem *et al*., 2019) proposed several oxidation pathways involving HO• generated in humid air. This is relevant to the water-sprinkled PCD reactor, where water likely serves as a precursor for hydrogen-containing ROS such as HO• and HO_2•, as was explained in Section 1.2.

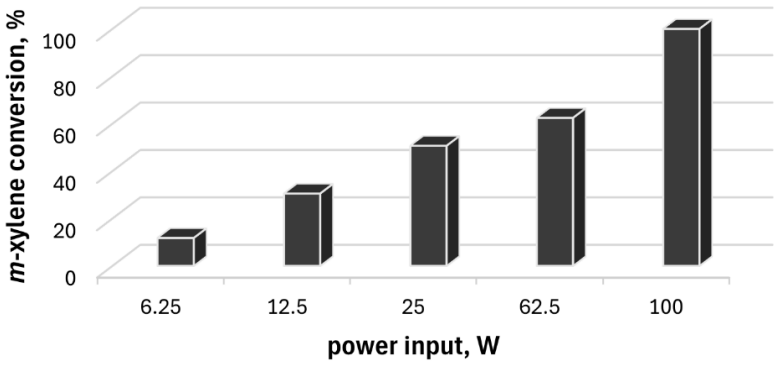

Figure 11. Oxidation of airborne m-xylene dependent on power input: m-xylene inlet concentration 20±5 ppm, air flow rate 6 m^3 h^{-1}, water circulation rate 9 L min^{-1}, pH 6.0 – 6.5, error margin in m-xylene quantification ±5%.

The impact of residence time on oxidation efficiency was evaluated by varying the air flow rate from 8.0 to 2.0 m^3 h^{-1}, corresponding to residence times between 34.1 and 136.6 s.

Figure 12 shows that the conversion efficiency at 35% RH was lower than at 2.5% RH (27 ± 3 °C). Unexpectedly, a further decrease in oxidation efficiency was observed in the water-sprinkled PCD reactor operated at 65% RH. This observation contradicts previous reports indicating that water sprinkling enhances *m*-xylene degradation by promoting the formation of surface-bound hydroxyl radicals, which act as potent oxidants (Khadem *et al*., 2019).

This discrepancy may be attributed to the influence of VOC concentration on interfacial processes. Earlier findings demonstrated that sprinkling-induced enhancement occurred at *m*-xylene concentrations around 20 ppm (Paper I), whereas this effect diminished when the concentration was doubled. It is hypothesized that water-soluble intermediates, particularly phenolic compounds, accumulate in the sprinkling water and alter the oxidant balance at the interface. These intermediates, which are rapidly oxidized during PCD treatment (Kornev *et al*., 2006), likely compete with *m*-xylene for short-lived radicals such as HO• at the gas-liquid interface. Their presence may reduce the availability of reactive species on the plasma side of the interface, thereby inhibiting further *m*-xylene degradation.

Furthermore, oxidation efficiency was consistently higher in dry air than in moderately humid air (35% RH), reinforcing the detrimental impact of humidity on plasma-induced oxidation (Preis *et al*., 2013; Ajo *et al*., 2017). The observed decline at elevated RH may result from reduced peak voltage and current in the plasma pulses, which limits the generation of oxidative species such as ozone. This humidity-dependent behaviour was also evident in the present study.

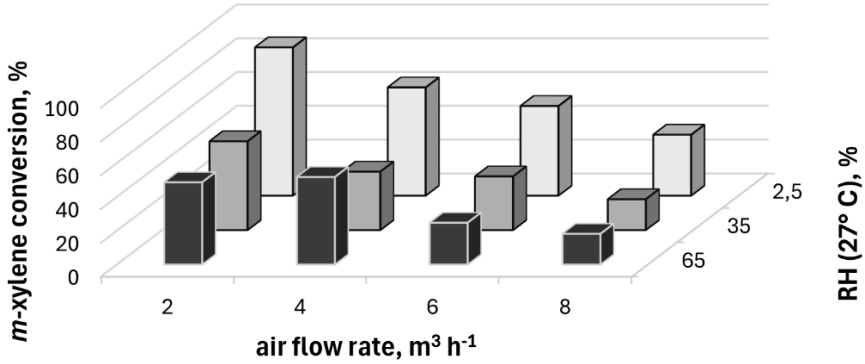

Figure 12. m-Xylene oxidation degree in the PCD reactor at varying relative humidity levels vs air flow rate at 12.5 W power input: m-xylene inlet concentration 40±5 ppm, water circulation rate 9 L min^{-1} at RH 65%, circulation water pH 6.0 – 6.5, error margin in m-xylene quantification ±5%.

3.1.2 Ozone and N_2O production during plasma treatment

Ozone yield

Unwanted by-products of plasma-based VOCs abatement include ozone and nitrogen oxides. In clean, dry air, ozone is formed via three-body collisions as described in Eq. 8. The dependence of ozone concentration on power input in the water-sprinkled plasma reactor, with and without *m*-xylene present, is shown in Figure 13. Under the studied conditions, the discharge power input exhibits an almost linear effect on ozone yield, i.e., higher power input results in higher concentrations of ozone in the outlet air stream.

The linear increase becomes clearer when considering the maximum achievable ozone concentration under equilibrium conditions in the sprinkled PCD reactor with no air flow, which may reach approximately 3.000 ppm (5 mg L^{-1}) (Preis *et al*., 2013). Thus, increasing the input power enhances ozone generation at the air flow rates applied in the experiments.

A reduced ozone concentration was observed when *m*-xylene was present. This reduction may arise from direct oxidation of the VOC by ozone or, more likely, from competition among

reactive species involved in ozone formation and *m*-xylene oxidation. Given the short residence time and the relatively slow reaction kinetics of molecular ozone, the latter explanation appears more plausible (Ridgway *et al*., 2017).

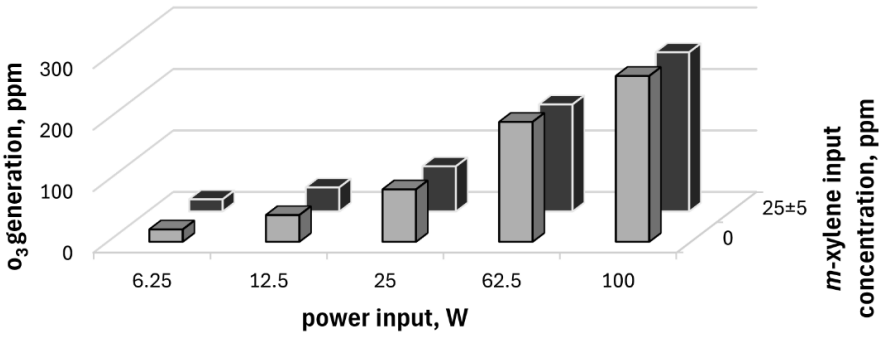

Figure 13. Ozone generation dependent on power input with m-xylene inlet concentrations of 0 and 20±5 ppm, air flow rate 6 $m^3 h^{-1}$, water circulation rate 9 L min^{-1}, pH 6.0 – 6.5, error margin ±5%.

The influence of air humidity and residence time on ozone formation is illustrated in Figure 14. Concentration of ozone followed a trend similar to that observed for *m*-xylene oxidation: ozone production increased at higher pulse repetition frequencies and longer residence times. Humidity strongly affected ozone yield, with nearly twice as much ozone produced in dry air (RH 2.5%) compared with the water-sprinkled reactor (RH 65%).

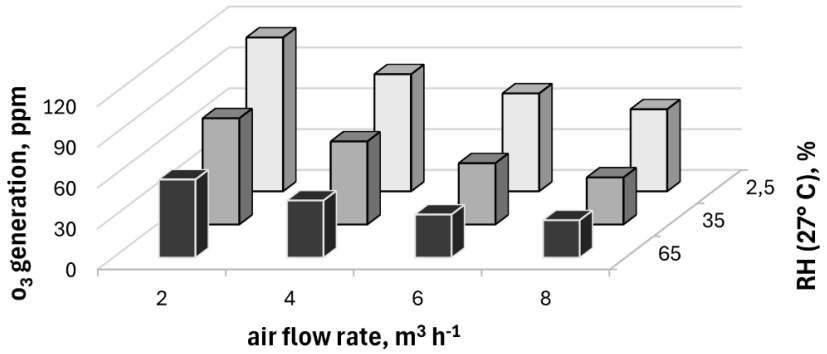

Figure 14. Ozone generation at varying relative humidity levels vs air flow rate at 12.5 W power input: m-xylene inlet concentration 40±5 ppm, water circulation rate 9 L min^{-1} at RH 65%, circulation water pH 6.0 – 6.5, error margin ±5%.

Several factors contribute to the higher ozone yield in the absence of sprinkling. Lukes *et al*. (2005) concluded that part of the discharge energy is lost when electrodes are partially covered by water droplets. Additionally, water vapor plays a crucial role in corona-discharge ozone formation, as it reduces the lifetime of atomic oxygen and thereby limits ozone production (Carey, 1992; Ono & Oda, 2003).

Nitrous oxide formation

N_2O is one of the relatively stable nitrogen oxides formed in plasma through multiple reaction pathways involving excited nitrogen species, nitrogen oxides, oxygen, and ozone (Becker *et al*., 2004). In the prototype PCD reactor, N_2O generation exhibited trends similar to ozone formation: high humidity and water sprinkling reduced the yield of nitrogen-containing gaseous compounds.

At an air flow rate of 6.0 $m^3\ h^{-1}$, an *m*-xylene concentration of 20±5 ppm, and a pulse repetition frequency of 800 pps, N_2O concentrations were 3.7 ppm at RH 65% and 7.1 ppm at RH 35%. Experiments at 2.5% RH (with doubled *m*-xylene concentration) resulted in 8.6 ppm of N_2O. The lower N_2O concentrations in the sprinkled reactor may be attributed either to hydroxyl-radical attack at the gas-liquid interface, producing nitrites detected in the aqueous phase, or to reduced formation of N_2O due to oxidation of nitrogen to NO, further to NO_2, and ultimately to NO_3.

Nitrite and nitrate yield

The formation of N_2O was observed in both dry and sprinkled PCD reactors; however, NO and NO_2 were not detected in the gas phase under either condition. The absence of NO can be attributed to its high reactivity, while NO_2 is expected to react rapidly with HO• radicals, forming nitric acid.

In the aqueous phase, NO_2 appeared only as minor intermediates, whereas NO_3 concentrations increased continuously over the course of plasma treatment (Figure 15). In the sprinkled reactor at 100 pps (12.5 W of pulsed power), the quantified NO_3 mass was approximately 50 mg, corresponding to about 11.3 mg of nitrogen bound in the aqueous phase. This value is an order of magnitude higher than the amount of nitrogen transferred as N_2O in the gas phase over 30 min (1.9 mg in dry mode and 0.9 mg in sprinkled mode). The NO_3 production energy efficiency in the sprinkled reactor was 8.0 g $kW^{-1}\ h^{-1}$, consistent with the findings of Preis *et al*. (Preis *et al*., 2014).

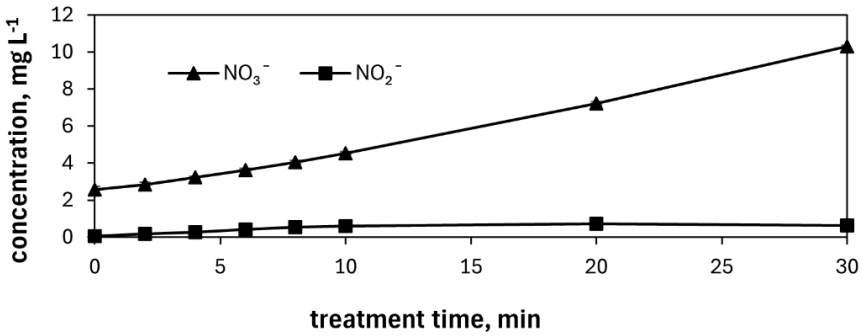

Figure 15. Aqueous nitrite and nitrate concentrations dependent on treatment time: m-xylene concentration 20±5 ppm, pulse repetition frequency 100 pps, air flow rate 6 $m^3\ h^{-1}$, water circulation rate 9 L min^{-1}, pH 6.0 – 6.5.

3.1.3 Reference experiments

The PCD reactor inherently functions as a wet scrubber, enabling the absorption of gaseous pollutants into the liquid phase (Figure 16). However, due to the low water solubility of the hydrophobic compound m-xylene, the contribution of physical absorption to overall pollutant removal is negligible. In the present study, a hydrophobic VOC was intentionally

selected to focus on chemical degradation processes and to highlight the non-selectivity and versatility of the PCD system for air purification.

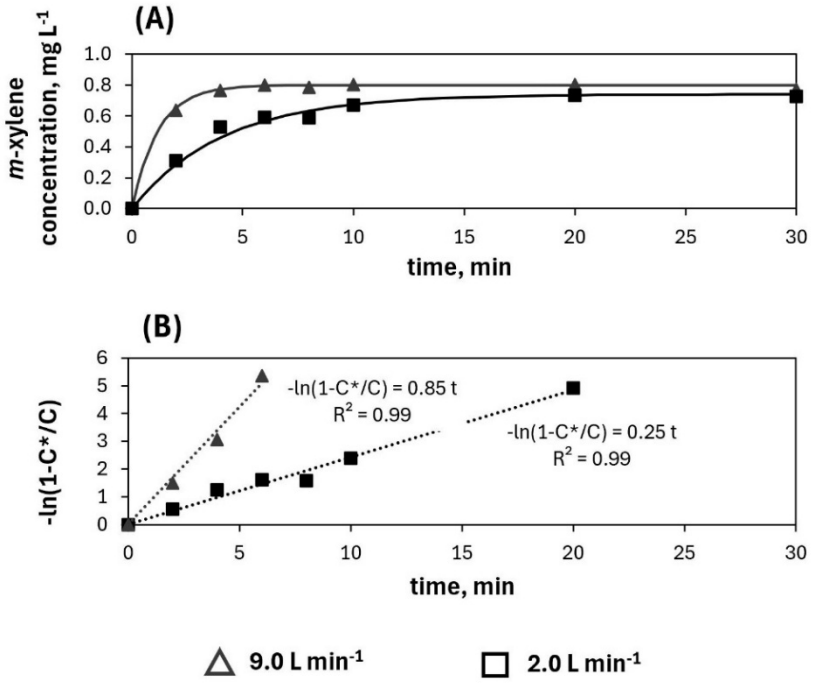

Figure 16. (A) – m-Xylene absorption by water in time at various water recirculation rates, (B) – linearized form of absorption kinetics: gaseous m-xylene input concentration 20±5 ppm, air flow rate 6 m^3 h^{-1}, pH 6.0 – 6.5.

After saturation of the recirculating water with *m*-xylene, the PCD generator was switched on, causing an almost immediate decrease in the aqueous *m*-xylene concentration. Subsequently, an equilibrium concentration was established, which depended on the applied pulsed power input (Figure 17).

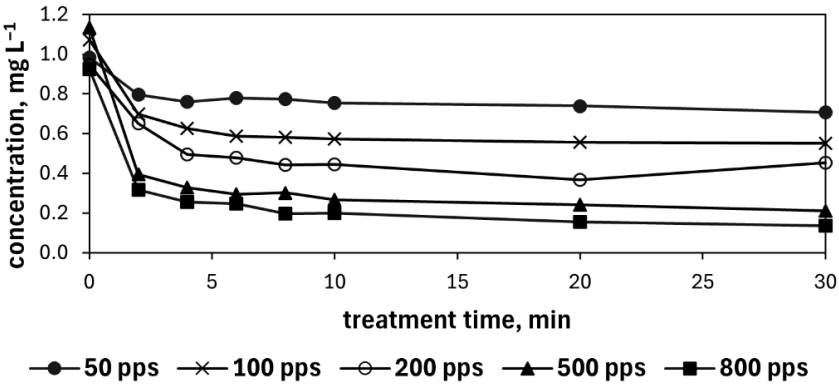

Figure 17. Aqueous m-xylene concentration as a function of experimental run time at different pulse repetition frequencies: airborne m-xylene inlet concentration 20 ± 5 ppm, air flow rate 6 m^3 h^{-1}, water circulation rate 9 L min^{-1}, pH 6.0 – 6.5.

The observed differences in equilibrium aqueous *m*-xylene concentrations at varying pulse repetition frequencies can be attributed to two main factors: i) higher power input results in lower *m*-xylene concentrations in the gas phase, thereby reducing the amount available for absorption into the water, ii) increased power input enhances plasma-induced oxidation of *m*-xylene in aqueous phase due to a higher flux of ROS at the plasma-liquid interface (Tikker *et al*., 2020).

3.1.4 By-products of m-xylene degradation

The formation of degradation by-products following plasma treatment is of critical importance and must be thoroughly assessed. For this purpose, oxidation products of *m*-xylene generated in the PCD reactor were analysed in both the treated air and the recirculating water using FT-IR and GC-MS, respectively.

In the gas phase, the concentrations of oxidation by-products remained below the detection limit of the FT-IR method, preventing their identification and quantification in the exhaust air. In contrast, several intermediate products were detected in the aqueous phase using GC-MS, including phenolic intermediates, dialdehyde compounds and 2,6-dimethylhydroquinone, among others. The by-product formation followed three basic pathways, nitration, hydroxylation with following ring opening. Waterborne oxidation intermediates were collected during experiments conducted at a power input of 62.5 W, *m*-xylene inlet concentration of 40±5 ppm, a water circulation rate of 9 L min^{-1}, a sprinkling water pH of 6.0 – 6.5, and an air flow rate of 6 m^3 h^{-1} (Figure 3 Paper III).

It should be noted that these undesired oxidation intermediates, although detected only in the aqueous phase, are likely to also form in the gas phase. However, their presence in the air effluent was not detected by FT-IR analysis. This observation suggests that the water-sprinkling system in the PCD reactor acts as an effective scrubber, capturing more hydrophilic oxidation products. In a dry reactor configuration, assuming incomplete mineralization of the target compound, such by-products would be released with the treated air, thereby increasing the treatment burden on downstream post-plasma purification systems.

3.2 Photocatalytic treatment of VOCs

Experiments with the PCO reactor were conducted to evaluate its operating parameters and its potential as a post-plasma environmental control system. Similar to the PCD reactor, a series of experiments with varying operational conditions were performed to systematically assess the performance of the prototype PCO reactor (Paper II-III).

3.2.1 VOC degradation with PCO

The PCO reactor was designed to operate under solar irradiation. The UV-A component of solar radiation at the Earth's surface does not exceed approximately 90 W m^{-2} at (Rivas *et al*., 2020). Therefore, most experiments with the PCO reactor were conducted at an irradiance of 119 W m^{-2}, which slightly exceeds realistic outdoor conditions. This elevated irradiance was chosen to enhance photocatalytic activity and to facilitate evaluation of the reactor's performance characteristics.

For the initial PCO experiments, 2ME was selected as the target pollutant. Oxidation of 2ME was performed at constant irradiance and residence time while varying the inlet concentration. As shown in Figure 18, in the absence of ozone, approximately 4±1 ppm of 2ME is degraded, irrespective of the inlet concentration. This behaviour indicates pseudo-zero order reaction kinetics, with the initial substrate concentration having no influence on the degradation rate. Similar kinetic behaviour has been reported previously (Biard *et al*., 2007; Boulinguiez *et al*., 2008).

The PCO reactor is intended to operate as a post-treatment unit following the PCD reactor; therefore, additional experiments were conducted in the presence of ozone. These experiments were designed to assess the effectiveness of the PCO reactor in treating air streams containing residual ozone after plasma processing. The results of simultaneous photocatalytic degradation of 2ME and ozone are also presented in Figure 18. In the presence of ozone, the extent of 2ME oxidation increased by up to a factor of three at the highest inlet concentration. Moreover, the dependence of pollutant removal on the initial concentration indicates that, in the presence of ozone, the PCO process no longer follows pseudo-zero order kinetics. This behaviour can be explained by the interaction between ozone and TiO_2. Under UV-A irradiation, ozone acts as an electron acceptor on the TiO_2 surface and serves as an additional source of reactive oxygen species, thereby suppressing electron-hole recombination and enhancing photocatalytic activity (Pengyi *et al*., 2003; Qi *et al*., 2007; Yu & Lee, 2007; Yuan *et al*., 2013; Krichevskaya *et al*., 2017). Reduced recombination increases the availability of photogenerated holes for the oxidation of 2ME.

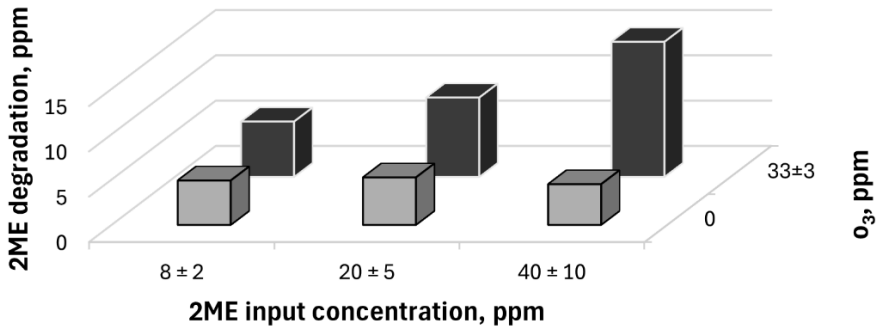

Figure 18. Photocatalytic degradation of 2ME with and without ozone dependent on 2ME concentration: ozone inlet concentration 33±3 ppm, residence time 12.8 sec, irradiance 119 W m^{-2}, error margin in 2ME quantification ±5%.

The effects of relative humidity and residence time on *m*-xylene oxidation in the PCO reactor are shown in Figure 19. Two primary trends are evident:

i) *m*-xylene conversion increased with increasing residence time (i.e., decreasing air flow rate), as also shown in Paper II (Figure 9);

ii) higher air humidity enhanced PCO performance, a phenomenon also reported by other authors (Bouazza *et al*., 2008).

The enhanced oxidation efficiency at elevated RH can be attributed to increased formation of hydroxyl radicals on the photocatalyst surface (Eq. 12). Nevertheless, *m*-xylene degradation was observed under all tested conditions, demonstrating that both relative humidity and residence time play critical roles in the design and operation of PCO systems.

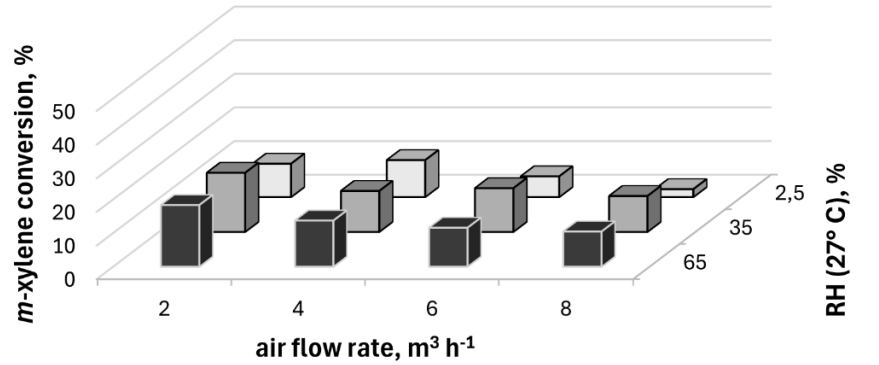

Figure 19. m-Xylene conversion in the PCO reactor as a function of relative humidity and air flow rate: m-xylene inlet concentration 40±5 ppm, irradiance (315-400 nm) 119 W m^{-2}, error margin in m-xylene quantification ±5%.

3.2.2 Photocatalytic decomposition of ozone

Ozone removal in the PCO reactor depending on residence time, with and without VOCs present, is shown in Figure 20. The air residence time, controlled by the flow rate, varied between 7 and 77 s. An increase in residence time resulted in improved ozone conversion; however, increasing the residence time by nearly an order of magnitude led to only an approximately twofold increase in ozone conversion.

In the absence of 2ME, ozone decomposition is only dependent on residence time as can be seen in the linear drop of ozone concentration over the time axes. This is in accordance with the Langmuir-Hinshelwood kinetics of heterogeneous catalysis resulting in pseudo-zero order kinetics, similar to the oxidation of 2ME in the absence of ozone and is thoroughly explained in Paper II (Eq. 1-7). In contrast, when ozone reduction occurs simultaneously with 2ME oxidation, the process exhibits apparent second-order kinetics with respect to both reactants, as their degradation rates are directly and/or indirectly affected by each other's concentrations. This observation suggests that PCO is not the sole reaction pathway in the gas mixture.

During the simultaneous degradation of 2ME and ozone, the conversion of both species increased with increasing 2ME concentration. Similar behaviour has been attributed to the formation of additional oxidative species, such as ozonides (Rivas *et al*., 2006, 2012), as well as to gas-phase degradation of ozone that influences the oxidation rate of VOCs (Zhang & Liu, 2004). The higher conversion of ozone observed in the presence of 2ME may also be explained by the formation of ozone reduction intermediates and by an overall increase in reactive organic species interacting with ozone and ozone-derived radicals, thereby promoting regeneration of active sites (electron-hole pairs) on the photocatalyst surface.

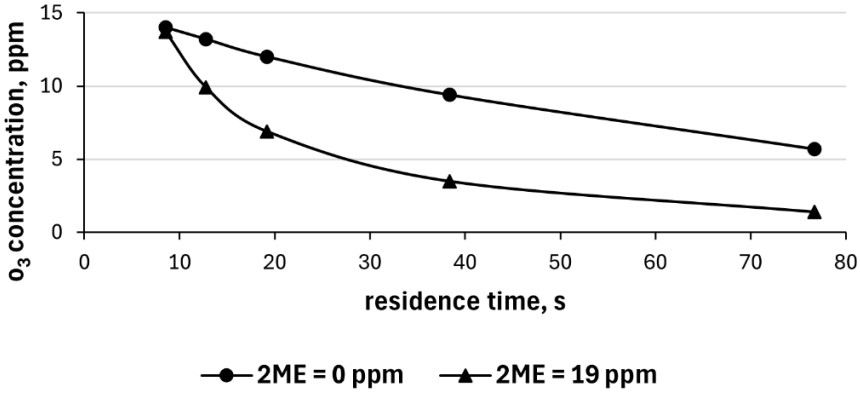

Figure 20. Photocatalytic degradation of ozone in the absence and presence of 2ME, ozone inlet concentration 26±1 ppm, irradiance 119 W m^{-2}

The influence of RH and residence time on ozone degradation in the PCO reactor is shown in Figure 21. Similar to *m*-xylene oxidation, ozone degradation in dry air exhibited poor performance. At elevated humidity, degradation of ozone was notably enhanced due to radical-driven reactions described by Eq. 20 (an extension of Eq. 13) and Eq. 21 (Huang & Li, 2011):

$$O_3 + e^- \rightarrow O_3^{\bullet -} \rightarrow O^{\bullet} + O_2 \quad (20)$$

$$O^{\bullet -}(O_3^{\bullet -}) + H_2O \rightarrow \bullet OH + OH^-(+O_2) \quad (21)$$

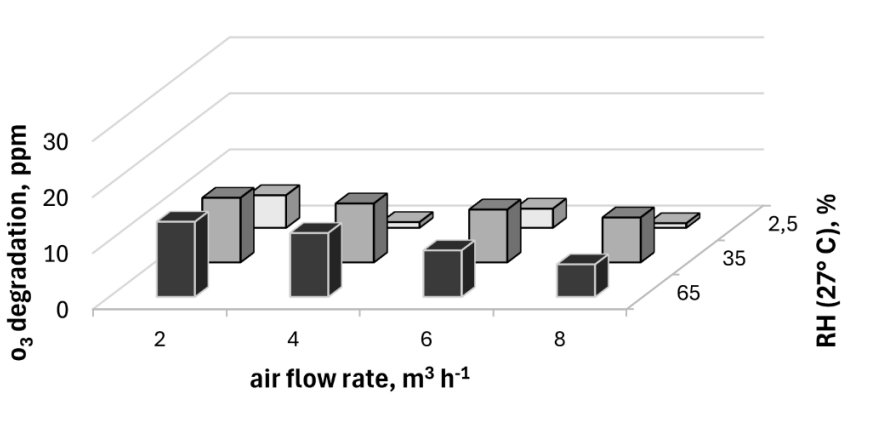

Figure 21. Ozone PCO-degradation at varying relative humidity levels vs air flow rate: ozone inlet concentrations were generated in the PCD reactor and varied with relative humidity and the air flow rate at 100 pps; irradiance (315-400 nm) 119 W m^{-2}, error margin in m-xylene quantification ±5%.

3.2.3 Nitrous oxide degradation with PCO

In addition to ozone reduction, nitrous oxide degradation in the PCO reactor was evaluated. Several studies have reported photocatalytic removal of N_2O in batch reactors over timescales of several hours (Obalová *et al*., 2013; Kočí *et al*., 2017; Tan *et al*., 2019). However, such long retention times are not compatible with the significantly shorter residence times employed in the present plug-flow PCO reactor. Within the experimental conditions applied in this study, no measurable changes in N_2O concentration were observed after treatment in the PCO reactor.

3.3 Post-plasma catalysis in a scaled-up plug-flow reactor

Experiments with the combined PPC reactor configuration were conducted to investigate the dynamics, advantages and limitations of integrating PCD with PCO. The PPC system was studied to address the apparent contradiction arising from the different optimal operating conditions of the two technologies: while the PCD achieves higher pollutant degradation efficiency in dry air, PCO requires elevated humidity to reach its full potential (Paper III).

3.3.1 VOC degradation in the PPC configuration

The results of *m*-xylene oxidation in the PPC configuration are presented in Figure 22. The figure shows *m*-xylene concentration after sequential treatment in the PCD and PCO reactors. At a power input of 12.5 W (100 pps), a noticeable improvement in overall oxidation efficiency was observed in wet air due to the contribution of the PCO stage, effectively compensating for the reduced performance of the PCD under humid conditions (Figure 12). It was previously established that PCO performs poorly under dry-air conditions, and the PPC results confirm this behaviour: at 2.5% RH, the contribution of PCO to *m*-xylene oxidation is nearly identical to that of the standalone PCD reactor. This finding highlights the combined effect of water vapor and residual ozone in promoting photocatalytic degradation of VOCs. At the maximum PCD input power of 100 W (800 pps), *m*-xylene was almost completely oxidized in the PCD reactor, leaving

only negligible VOC concentrations for subsequent treatment in the PCO stage (Figure 6 B Paper III).

In the PPC configuration, both target pollutant degradation and ozone reduction must be evaluated simultaneously. Ozone degradation in the PPC system is shown in Figure 23. A pronounced difference is observed between ozone reduction in the presence and absence of *m*-xylene (Figure 24). Figure 26 also illustrates the effect of increasing the PCD input power to 100 W (800 pps). Although ozone reduction generally increases due to the substantially higher ozone inlet concentration, a sharp decrease in ozone degradation is observed at an air flow rate of 2 $m^3 h^{-1}$. This effect is attributed to the negligible amounts of organic matter remaining in the air stream, as m-xylene oxidation in the PCD reactor was nearly complete at 100 W. These results further emphasize the importance of ozone-assisted PCO of VOCs.

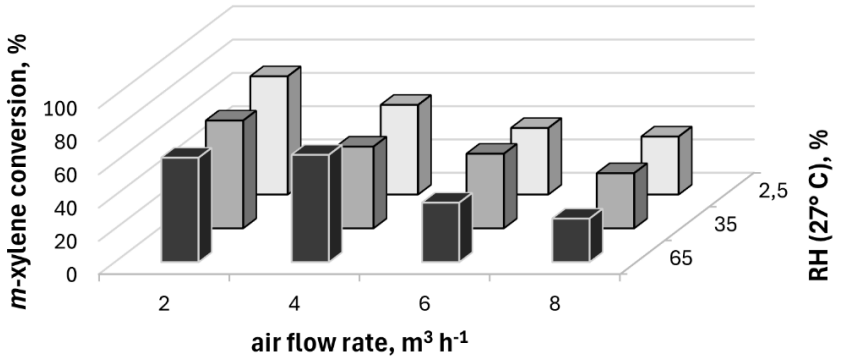

Figure 22. m-Xylene oxidation in the post-plasma catalytic configuration as a function of relative humidity and air flow rate: pulse repetition frequency 100 pps (12,5 W), m-xylene inlet concentration 40±5 ppm, water circulation rate at RH 65% of 9 L min^{-1}, sprinkling water pH 6.0 – 6.5, irradiance in PCO reactor 119 W m^{-2}.

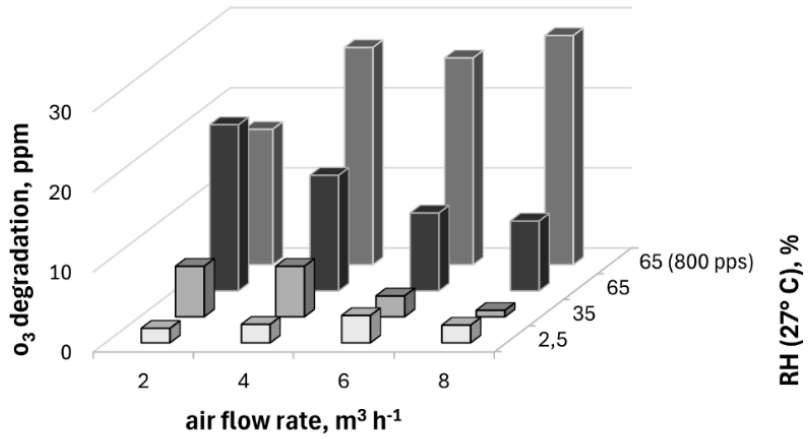

Figure 23. Ozone degradation in the PPC reactor configuration at different relative humidities, air flow rates and pulse repetition frequencies: m-xylene inlet concentration, 40±5 ppm, water circulation rate 9 L min^{-1} (only at 65% RH), water pH 6.0 – 6.5.

The importance of water scrubbing becomes even more apparent when examining the contribution of the PCO reactor to *m*-xylene degradation within the PPC configuration (Figure 24). At first glance, the degree of *m*-xylene degradation in the presence of ozone appears lower than that observed for the standalone PCO reactor (Figure 19). However, the experimental conditions are not directly comparable. In the PPC configuration, the PCO reactor treats air that has already undergone plasma treatment at 12.5 W, meaning that the photocatalyst is exposed not only to residual *m*-xylene and ozone but also to volatile plasma-treatment-generated by-products. This effect is particularly evident when comparing results obtained at 65% RH (sprinkled PCD) with those obtained under dry conditions. At high humidity, the PCO efficiency remains nearly unchanged, whereas under dry conditions it decreases to nearly zero. This behaviour can be explained by the fact that a substantial amount of *m*-xylene oxidation by-products is absorbed into the circulating water in the sprinkled PCD. In dry-air operation, the PCO reactor must oxidize not only the residual target pollutant but also all volatile by-products exiting the PCD reactor.

These findings indicate that high humidity and the presence of water play a critical role in the performance of the PPC reactor configuration and that evaluation of reactor performance based solely on target pollutant conversion is insufficient. The formation and fate of oxidation by-products must also be considered.

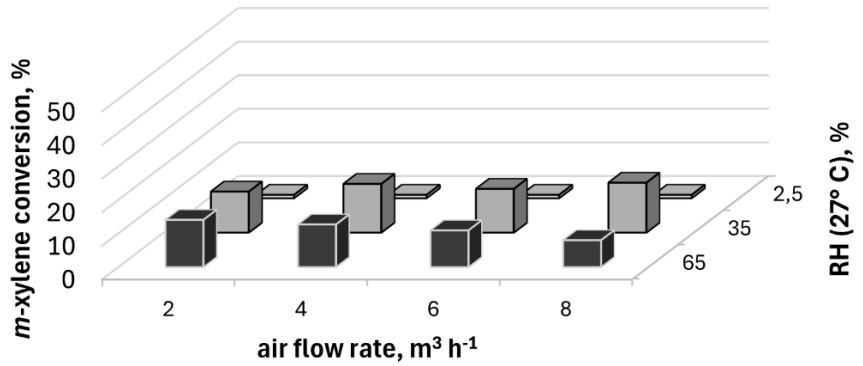

Figure 24. m-Xylene degradation in the PCO reactor within the PPC reactor configuration at different relative humidities, air flow rates and pulse repetition frequencies: m-xylene inlet concentration 40±5 ppm, water circulation rate 9 L min^{-1} (only at 65% RH), water pH 6.0 – 6.5.

3.3.2 Energy efficiency of the PPC configuration

Table 5 summarizes energy yield data for xylene oxidation reported in selected studies on plug-flow plasma reactors. The compiled results provide insight into key operational parameters, including VOC concentration and air flow rate. In the present study the highest energy efficiency was achieved at an air flow rate of 6 m^3 h^{-1}, an initial VOC concentration of 45.0±5 ppm, RH 2.5%, and a power input of 12.5 W.

The energy consumption of the PCO reactor is not included in comparison, as the PCO stage is intended to operate under solar irradiation and thus requires no external energy input. However, achieving the reported performance under real-world conditions would require drying of the air stream, leading to increased overall energy consumption. Moreover, ozone generation in dry air is an order of magnitude higher than in the

sprinkled PCD configuration, further increasing operational costs due to the additional ozone reduction required downstream.

Table 5. Comparison of airborne xylene oxidation performance in plasma reactors.

Reactor type	Xylene concentration, ppm	Gas flow rate, $m^3\ h^{-1}$	Removal, %	Energy yield, $g\ kW^{-1}h^{-1}$	Source
PCD (RH 2.5%)	45.0 ± 5.0	2.0-8.0	36.0-100.0	3.9-49.4	(Paper III)
PCD (RH 35%)	45.0 ± 5.0	2.0-8.0	18.0-100.0	3.9-29.6	
PCD (RH 65%)	45.0 ± 5.0	2.0-8.0	18.0-100.0	3.9-32.2	
PCD	20.0 ± 5.0	6.0	18.0-100.0	5.6-21.1	(Paper I)
DBD	23.0-2303.0	0.1-1.0	95.0	20.0	(Bugaev *et al.*, 1996)
DBD	0.0-500.0	0.03 – 0.09	80.0	7.1	(Lee & Chang, 2003)

Conclusions

This thesis investigated the abatement of VOCs from air using AOPs based on non-thermal plasma and photocatalysis. The research was structured around three complementary approaches: PCD with water sprinkling, PCO under UV-A irradiation, and the combination of PCD and PCO into a PPC reactor configuration. Together, these studies provide a comprehensive understanding of oxidation mechanisms, energy efficiency, synergistic effects, and the potential benefits and limitations associated with real-world application of this technology.

A prototype PCD reactor with water sprinkling was evaluated for the oxidation of *m*-xylene as a model air pollutant. The pulsed power input (6.25 – 100 W) was identified as the key factor governing the oxidation rate, while residence time also influenced reactor performance. Higher power input resulted in increased plasma density, leading to enhanced formation of RONS and, consequently, higher oxidation rates. Longer residence times further promoted reactions between pollutants and oxidative species. Other controllable parameters, such as water flow rate and water pH, had negligible effects. Air humidity in the PCD reactor exhibited a complex influence: low RH slightly improved target pollutant degradation but resulted in more than a twofold increase in O_3 and N_2O formation. The water-sprinkled PCD reactor also functioned as a partial scrubber, as oxidation by products of *m*-xylene were detected in the aqueous phase. Although no organic by-products were identified in the exhaust air, it is reasonable to assume that compounds not absorbed by water may remain in the gas stream.

An upscaled PCO reactor was investigated for the removal of 2ME, *m*-xylene, N_2O, and ozone. The reactor employed TiO_2 as the photocatalyst and was designed for outdoor operation using solar radiation or, alternatively, UV-A lamps. The performance of the PCO reactor in VOCs degradation was primarily controlled by irradiance, residence time, and air humidity. Increasing residence time and irradiation intensity improved pollutant removal efficiency. RH had the most significant impact on photocatalytic performance; low humidity conditions (RH 2.5% at 27 °C) nearly completely inhibited photocatalytic degradation.

The PCO followed pseudo-zero-order reaction kinetics during the oxidation of individual VOCs or O_3, indicating that removal efficiency was largely independent of pollutant concentration. In the presence of ozone, however, the kinetics of VOC oxidation changed, revealing the full potential of the PCO process. Simultaneous VOC oxidation and O_3 reduction were approximately doubled under these conditions. Ozone prolonged the lifetime of electron-hole pairs on the photocatalyst surface and contributed additional oxidizing species, thereby improving photocatalytic efficiency. In contrast, the PCO reactor showed no measurable effect on N_2O degradation, which was attributed to the limited residence time (max 77 s) in the plug-flow reactor.

Integration of PCD and PCO into a PPC system revealed pronounced synergistic effects strongly dependent on humidity and ozone dynamics. The PCD reactor alone performed better under dry air conditions; however, the introduction of water sprinkling, which increased RH to approximately 65%, substantially enhanced downstream photocatalytic activity. Under dry conditions, large amounts of ozone generated in the PCD reactor were only partially decomposed in the PCO reactor, while nitrous oxide concentrations remained unchanged.

Under humid conditions, ozone formation in the PCD reactor was suppressed, and residual ozone was effectively decomposed in PCO reactor due to improved electron-hole separation and enhanced formation of hydroxyl radicals on the TiO_2 surface. High air humidity was therefore identified as a critical parameter for achieving optimal synergy between plasma and photocatalysis. It not only limited the formation of undesirable by-products (O_3 and N_2O) but also compensated for the reduced *m*-xylene oxidation efficiency of the PCD reactor. Overall, the PPC process achieved a balance between high oxidation efficiency and reduced secondary pollution, representing a clear improvement over either technology operated independently.

The energy efficiency of the PCD reactor for *m*-xylene oxidation was calculated to reach up to 49.4 g kW^{-1} h^{-1}. The energy efficiency of the PCO reactor was not evaluated, as the system is intended to operate using solar radiation and, ideally without additional external energy input.

In conclusion, this study identified key operational aspects of a PPC system composed of a PCD reactor followed by a PCO reactor. The results demonstrate that while PCD provides rapid, on-demand oxidation suitable for dynamic pollution control, PCO offers a sustainable and potentially low-energy approach for continuous air purification, particularly through effective ozone removal and mitigation of oxidation by-products. Importantly, ozone reduction in the PCO reactor is enhanced in the presence of VOCs, and both high air humidity and ozone are necessary to maximize PCO efficiency. Nitrous oxide cannot be effectively degraded in a plug-flow PCO reactor under the investigated conditions. Finally, PCO is not suitable for integration into PPC systems operating under dry air conditions, as sufficient humidity is required to generate hydroxyl radicals that drive both oxidation and reduction reactions.

References

Ajo, P., Kornev, I., Preis, S. (2017). Pulsed Corona Discharge Induced Hydroxyl Radical Transfer Through the Gas-Liquid Interface. *Scientific Reports*, *7*(1). https://doi.org/10.1038/s41598-017-16333-1

Almaie, S., Vatanpour, V., Rasoulifard, M. H., Koyuncu, I. (2022). Volatile organic compounds (VOCs) removal by photocatalysts: A review. *Chemosphere*, *306*. https://doi.org/10.1016/j.chemosphere.2022.135655

Atsdr. (2021). Agency of Toxic Substances and Disease Registry. *Public Health Statement Xylene*. www.atsdr.cdc.gov/ (last access 2026, May 6).

Bagchi, G., & Waxman, D. J. (2008). Toxicity of ethylene glycol monomethyl ether: Impact on testicular gene expression. *International Journal of Andrology*, *31*(2), 269–274. https://doi.org/10.1111/j.1365-2605.2007.00846.x

Becker, K.H., Kogelschatz, U., Schoenbach, K.H., Barker, R.J., (2004). Non-Equilibrium Air Plasmas at Atmospheric Pressure, *CRC Press*, https://doi.org/10.1201/9781482269123.

Belkessa, N., Assadi, A.A., Bouzaza, A., Nguyen-Tri, P., Amrane, A., Khezami, L. (2024) A review of non-thermal plasma -catalysis: The mutual influence and sources of synergetic effect for boosting volatile organic compounds removal. *Environmental Research*, Volume 257, https://doi.org/10.1016/j.envres.2024.119333.

Biard, P. F., Bouzaza, A., & Wolbert, D. (2007). Photocatalytic degradation of two volatile fatty acids in an annular plug-flow reactor; kinetic modeling and contribution of mass transfer rate. *Environmental Science and Technology*, *41*(8), 2908–2914. https://doi.org/10.1021/es062368n

Bolden, A. L., Kwiatkowski, C. F., & Colborn, T. (2015). New look at BTEX: Are ambient levels a problem. *Environmental Science and Technology*, *49*(9), 5261–5276. https://doi.org/10.1021/es505316f

Bouazza, N., Lillo-Ródenas, M. A., & Linares-Solano, A. (2008). Photocatalytic activity of TiO2-based materials for the oxidation of propene and benzene at low concentration in presence of humidity. *Applied Catalysis B: Environmental*, *84*(3–4), 691–698. https://doi.org/10.1016/j.apcatb.2008.06.002

Boulinguiez, B., Bouzaza, A., Merabet, S., & Wolbert, D. (2008). Photocatalytic degradation of ammonia and butyric acid in plug-flow reactor: Degradation kinetic modeling with contribution of mass transfer. *Journal of Photochemistry and Photobiology A: Chemistry*, *200*(2–3), 254–261. https://doi.org/10.1016/j.jphotochem.2008.08.005

Bugaev, S. P., Kuvshinov, V. A., Sochugov, N. S., & Khryapov, P. A. (1996). Energy Characteristics of the Process of Air Scrubbing from Hydrocarbon Contaminants in a Barrier-Discharge Reactor. *Plasma Chemistry and Plasma Processing* (Vol. 16, Issue 4). https://doi.org/10.1007/BF01447014

Carey, J. H. (1992). An Introduction to Advanced Oxidation Processes (AOP) for Destruction of Organics in Wastewater. *Water Quality Research Journal*, *27*(1), 1–22. https://doi.org/10.2166/wqrj.1992.001

Channei, D., Inceesungvorn, B., Wetchakun, N., Ukritnukun, S., Nattestad, A., Chen, J., & Phanichphant, S. (2014). Photocatalytic degradation of methyl orange by CeO_2 and Fe-doped CeO_2 films under visible light irradiation. *Scientific Reports*, *4*. https://doi.org/10.1038/srep05757

Chen, J., Xie, Z., Tang, J., Zhou, J., Lu, X., & Zhao, H. (2016). Oxidation of toluene by dielectric barrier discharge with photo-catalytic electrode. *Chemical Engineering Journal*, *284*, 166–173. https://doi.org/10.1016/j.cej.2015.09.006.

Chen, K., Dong, W., Huang, Y., Wang, F., Zhou, J. L., Li, W., (2025). Photocatalysis for sustainable energy and environmental protection in construction: A review on surface engineering and emerging synthesis, *Journal of Environmental Chemical Engineering*, Volume 13, Issue 5, https://doi.org/10.1016/j.jece.2025.117529.

Chu, P.K. & Lu, X.P., (2013). Low Temperature Plasma Technology. *CRC Press*. https://doi.org/10.1201/b15153

Destrieux, A., Jangra, R., Hensel, K., Machala, Z., (2025). Review on scientific studies and commercial indoor air purification devices: Focus on plasma-catalytic technology, *Journal of Electrostatics*, Volume 137, https://doi.org/10.1016/j.elstat.2025.104153.

Directive (EU) 2016/2284 of the European Parliament and of the Council of 14 December 2016 on the Reduction of National Emissions of Certain Atmospheric Pollutants, Amending Directive 2003/35/EC and Repealing Directive 2001/81/EC (2016).

Edwards, R. D., Jurvelin, J., Koistinen, K., Saarela, K., & Jantunen, M. (2001). VOC source identification from personal and residential indoor, outdoor and workplace microenvironment samples in EXPOLIS-Helsinki, Finland. *Atmospheric Environment*, *35*, 4829–4841. https://doi.org/10.1016/S1352-2310(01)00271-0

European Chemicals Agency. (2023). *European Chemicals Agency*. Https://Echa.Europa.Eu/Substance-Information/-/Substanceinfo/100.003.377. (last access 2023, May 5).

European Chemicals Agency. (2024) *Substance Infocard (Xylene)*. Https://Echa.Europa.Eu/et/Substance-Information/-/Substanceinfo/100.014.124. (last access 2024, May 27).

Everaert, K., & Baeyens, J. (2004). Catalytic combustion of volatile organic compounds. *Journal of Hazardous Materials*, *109*(1–3), 113–139. https://doi.org/10.1016/j.jhazmat.2004.03.019

Fan, H., Jiang, T., Li, H., Wang, D., Wang, L., Zhai, J., He, D., Wang, P., & Xie, T. (2012). Effect of $BiVO_4$ crystalline phases on the photoinduced carriers behaviour and photocatalytic activity. *Journal of Physical Chemistry C*, *116*(3), 2425–2430. https://doi.org/10.1021/jp206798d

Henry, J. G., & Heinke, G. W. (1996). *Environmental science and engineering*. Hoboken: Prentice Hall.

Huang, H., & Li, W. (2011). Destruction of toluene by ozone-enhanced photocatalysis: Performance and mechanism. *Applied Catalysis B: Environmental*, *102*(3–4), 449–453. https://doi.org/10.1016/j.apcatb.2010.12.025

Meichsner, J., Schmidt, M., Schneider, R. & Wagner, H.-E. (2012). *Nonthermal Plasma Chemistry and Physics*. Boca Raton: CRC Press. https://doi.org/10.1201/b12956

Kask, M., Bolobajev, J., & Krichevskaya, M. (2020). Gas-phase photocatalytic degradation of acetone and toluene, and their mixture in the presence of ozone in continuous multi-section reactor as possible air post-treatment for exhaust from pulsed corona discharge. *Chemical Engineering Journal*, *399*. https://doi.org/10.1016/j.cej.2020.125815

Kask, M., Krichevskaya, M., Preis, S., & Bolobajev, J. (2021). Oxidation of Aqueous Toluene by Gas-Phase Pulsed Corona Discharge in Air-Water Mixtures Followed by Photocatalytic Exhaust Air Cleaning. *Catalysts*, *11*(5), 549. https://doi.org/10.3390/catal11050549

Keskkonnaamet. Republic of Estonia. *Keskkonnaotsuste infosüsteem.* https://kotkas.envir.ee/annual_reports_registry. (last access 2022, March 28).

Khadem, A., Khani, M. R., Hosseini rad, R., Shokri, B., Rashnoo, S., & Ghobadian, B. (2019). Experimental analysis of volatile organic compounds conversion by a dielectric barrier discharge reactor to study the main products: Hydrogen, CO, CO_2, NOx and hydrocarbons. *Chemical Engineering and Processing - Process Intensification*, *145*. https://doi.org/10.1016/j.cep.2019.107660

Kiely, Gerard. (1997). *Environmental engineering*. McGraw-Hill.

Kočí, K., Reli, M., Troppová, I., Šihor, M., Kupková, J., Kustrowski, P., & Praus, P. (2017). Photocatalytic decomposition of N_2O over TiO_2/g-C_3N_4 photocatalysts heterojunction. *Applied Surface Science*, *396*, 1685–1695. https://doi.org/10.1016/j.apsusc.2016.11.242

Kohtani, S., Yoshioka, E., & Miyabe, H. (2012). Photocatalytic Hydrogenation on Semiconductor Particles. In *Hydrogenation*. InTech. https://doi.org/10.5772/45732

Kornev, J., Yavorovsky, N., Preis, S., Khaskelberg, M., Isaev, U., & Chen, B.-N. (2006). Generation of Active Oxidant Species by Pulsed Dielectric Barrier Discharge in Water-Air Mixtures. *Ozone: Science & Engineering*, *28*(4), 207–215. https://doi.org/10.1080/01919510600704957

Krichevskaya, M., Preis, S., Moiseev, A., Pronina, N., & Deubener, J. (2017). Gas-phase photocatalytic oxidation of refractory VOCs mixtures: Through the net of process limitations. *Catalysis Today*, *280*, 93–98. https://doi.org/10.1016/j.cattod.2016.03.041

Lee, H. M., & Chang, M. B. (2003). Abatement of Gas-phase p-Xylene via Dielectric Barrier Discharges. *Plasma Chemistry and Plasma Processing*, *23*(3), 541–558. https://doi.org/10.1023/A:1023239122885

Lukes, P., Clupek, M., Babicky, V., Janda, V., & Sunka, P. (2005). Generation of ozone by pulsed corona discharge over water surface in hybrid gas-liquid electrical discharge reactor. *Journal of Physics D: Applied Physics*, *38*(3), 409–416. https://doi.org/10.1088/0022-3727/38/3/010

Miller, R. R., Hermann, E.-A., Young, J. T., Landry, T. D., & Calhoun, L. L. (1984). Ethylene Glycol Monomethyl Ether and Propylene Glycol Monomethyl Ether: Metabolism, Disposition, and Subchronic Inhalation Toxicity Studies. *Environmental Health Perspectives*, *57*, 233–239. doi: 10.1289/ehp.8457233.

Niaz, K., Bahadar, H., Maqbool, F., & Abdollahi, M. (2015). A review of environmental and occupational exposure to xylene and its health concerns. In *EXCLI Journal* (Vol. 14, pp. 1167–1186). Leibniz Research Centre for Working Environment and Human Factors. https://doi.org/10.17179/excli2015-623

Nijdam, S., van Veldhuizen, E., Bruggeman, P., & Ebert, U. (2012). An Introduction to Nonequilibrium Plasmas at Atmospheric Pressure. In *Plasma Chemistry and Catalysis in Gases and Liquids* (pp. 1–44). Wiley. https://doi.org/10.1002/9783527649525.ch1

Obalová, L., Reli, M., Lang, J., Matějka, V., Kukutschová, J., Lacný, Z., & Kočí, K. (2013). Photocatalytic decomposition of nitrous oxide using TiO2 and Ag-TiO_2 nanocomposite thin films. *Catalysis Today*, *209*, 170–175. https://doi.org/10.1016/j.cattod.2012.11.012

Ogata, A., Ito, D., Mizuno, K., Kushiyama, S., Gal, A., & Yamamoto, T. (2002). Effect of coexisting components on aromatic decomposition in a packed-bed plasma reactor. *Applied Catalysis A: General*, Volume 236, Issues 1–2, Pages 9-15, https://doi.org/10.1016/S0926-860X(02)00280-6

Ono, R., & Oda, T. (2003). Dynamics of ozone and OH radicals generated by pulsed corona discharge in humid-air flow reactor measured by laser spectroscopy. *Journal of Applied Physics*, *93*(10 1), 5876–5882. https://doi.org/10.1063/1.1567796

Pearson, J. K. (2019). European solvent VOC emission inventories based on industry-wide information. *Atmospheric Environment*, *204*, 118–124. https://doi.org/10.1016/j.atmosenv.2019.02.014

Pengyi, Z., Fuyan, L., Gang, Y., Qing, C., & Wanpeng, Z. (2003). A comparative study on decomposition of gaseous toluene by O3/UV, TiO2/UV and O3/TiO2/UV. *Journal of Photochemistry and Photobiology A: Chemistry*, *156*(1–3), 189–194. https://doi.org/10.1016/S1010-6030(02)00432-X

Preis, S., Kornev, I., Hatakka, H., Yavorovskiy, N., Kallas, J. (2016). *Method and device for a liquid purifying and use of device.* Patent of Finland No. 125772.

Preis, S., Panorel, I. C., Kornev, I., Hatakka, H., & Kallas, J. (2013). Pulsed corona discharge: the role of ozone and hydroxyl radical in aqueous pollutants oxidation. *Water Science and Technology*, *68*(7), 1536–1542. https://doi.org/10.2166/wst.2013.399

Preis, S., Panorel, I., Llauger Coll, S., & Kornev, I. (2014). Formation of Nitrates in Aqueous Solutions Treated with Pulsed Corona Discharge: The Impact of Organic Pollutants. *Ozone: Science and Engineering*, *36*(1), 94–99. https://doi.org/10.1080/01919512.2013.836955

Qi, H., De-Zhi, S., & Guo-Qing, C. (2007). Formaldehyde degradation by UV/TiO_2/O_3 process using continuous flow mode. *Journal of Environmental Sciences*, *19*, 1136–1140. https://doi.org/10.1016/S1001-0742(07)60185-5

Ren, H., Koshy, P., Chen, W. F., Qi, S., & Sorrell, C. C. (2017). Photocatalytic materials and technologies for air purification. *Journal of Hazardous Materials*, *325*, 340–366. https://doi.org/10.1016/j.jhazmat.2016.08.072

Ridgway, H.F., Mohan, B., Cui, X., Chua, K.J., Islam, M.R. (2017). Molecular dynamics simulation of gas-phase ozone reactions with sabinene and benzene. *Journal of Molecular Graphics and Modelling*. 74, 241–250. https://doi.org/10.1016/j.jmgm.2017.04.020.

Rivas, F. J., Beltrán, F. J., & Encinas, A. (2012). Removal of emergent contaminants: Integration of ozone and photocatalysis. *Journal of Environmental Management*, *100*, 10–15. https://doi.org/10.1016/j.jenvman.2012.01.025

Rivas, F. J., Beltrán, F. J., Gimeno, O., & Carbajo, M. (2006). Fluorene oxidation by coupling of ozone, radiation, and semiconductors: A mathematical approach to the kinetics. *Industrial and Engineering Chemistry Research*, *45*(1), 166–174. https://doi.org/10.1021/ie050781i

Rivas, M., Calaf, G. M., Laroze, D., Rojas, E., Mendez, J., Honeyman, J., & Araya, M. C. (2020). Solar ultraviolet A radiation and nonmelanoma skin cancer in Arica, Chile. *Journal of Photochemistry and Photobiology B: Biology*, *212*, 112047. https://doi.org/10.1016/j.jphotobiol.2020.112047

Sax Irving N. (1984). Dangerous Properties of Idustrial Materials (Sixth Edition). Van Nostrand Reinhold Company Inc.

Schiorlin, M., Marotta, E., Rea, M., & Paradisi, C. (2009). Comparison of toluene removal in air at atmospheric conditions by different corona discharges. *Environmental Science and Technology*, *43*(24), 9386–9392. https://doi.org/10.1021/es9021816

Schlink, U., Thiem, A., Kohajda, T., Richter, M., & Strebel, K. (2010). Quantile regression of indoor air concentrations of volatile organic compounds (VOC). *Science of the Total Environment*, *408*(18), 3840–3851. https://doi.org/10.1016/j.scitotenv.2009.12.002

Sharma, G., & Kumar, A. (2021). *Photocatalysis: advanced materials and reaction engineering*. Materials Research Forum LLC.

Sujatha, G., Shanthakumar, S., & Chiampo, F. (2020). UV light-irradiated photocatalytic degradation of coffee processing wastewater using tio2 as a catalyst. *Environments - MDPI*, *7*(6), 1–13. https://doi.org/10.3390/environments7060047

Tan, J., Cheng, H., Liu, J., Sun, J., Li, Y., Wang, H., Liu, J., & Zhao, Z. (2019). Room-Temperature Photocatalytic Decomposition of N 2 O over Nanobelt-Like Bi_2MoO_6. *ChemistrySelect*, *4*(18), 5338–5344. https://doi.org/10.1002/slct.201900323

Tikker, P., Kornev, I., & Preis, S. (2020). Oxidation energy efficiency in water treatment with gas-phase pulsed corona discharge as a function of spray density. *Journal of Electrostatics*, *106*. https://doi.org/10.1016/j.elstat.2020.103466

Wang, H. L., Nie, L., Li, J., Wang, Y. F., Wang, G., Wang, J. H., & Hao, Z. P. (2013). Characterization and assessment of volatile organic compounds (VOCs) emissions from typical industries. *Chinese Science Bulletin*, *58*(7), 724–730. https://doi.org/10.1007/s11434-012-5345-2

Yu, K. P., & Lee, G. W. M. (2007). Decomposition of gas-phase toluene by the combination of ozone and photocatalytic oxidation process (TiO_2/UV, TiO_2/UV/O_3, and UV/O_3). *Applied Catalysis B: Environmental*, *75*(1–2), 29–38. https://doi.org/10.1016/j.apcatb.2007.03.006

Yuan, J., Huang, X., Chen, M., Shi, J., & Shangguan, W. (2013). Ozone-assisted photocatalytic degradation of gaseous acetaldehyde on TiO_2/M-ZSM-5 (M = Zn, Cu, Mn). *Catalysis Today*, *201*(1), 182–188. https://doi.org/10.1016/j.cattod.2012.06.003

Zhang, P., & Liu, J. (2004). Photocatalytic degradation of trace hexane in the gas phase with and without ozone addition: Kinetic study. *Journal of Photochemistry and Photobiology A: Chemistry*, *167*(2–3), 87–94. https://doi.org/10.1016/j.jphotochem.2004.05.015

Zhang, Y., Wang, Y., Xie, R., Huang, H., Leung, M. K. H., Li, J., & Leung, D. Y. C. (2022). Photocatalytic Oxidation for Volatile Organic Compounds Elimination: From Fundamental Research to Practical Applications. *Environmental Science and Technology*, *56*(23), 16582–16601. https://doi.org/10.1021/acs.est.2c05444

Zhang, Y., Zhu, Y., Tao, S., Zhang, Z., Chen, M., Jiang, Z., & Shangguan, W. (2022). Plasma-coupled catalysis in VOCs removal and CO2 conversion: Efficiency enhancement and synergistic mechanism. In *Catalysis Communications* (Vol. 172). Elsevier B.V. https://doi.org/10.1016/j.catcom.2022.106535

Zoveidavianpoor, M., Samsuri, A., & Shadizadeh, S. R. (2012). Health, Safety, and Environmental Challenges of Xylene in Upstream Petroleum Industry. *Energy & Environment*. 23. 1339-1352. 10.1260/0958-305X.23.8.1339.

Acknowledgements

I would like to acknowledge the Estonian Ministry of Education and Research for supporting the research through the Centre of Excellence in Circular Economy for Strategic Mineral and Carbon Resources (01.01.2024–31.12.2030, TK228). Furthermore, I want to acknowledge the Institutional Development Program of Tallinn University of Technology for 2016–2022, project 2014-2020.4.01.16-0032 from EU Regional Development Fund for support.

I also want to express my sincere gratitude to Prof. M. Krichevskaya for continued support and help in every aspect of the work. Prof. S.Preis for refined academic insight that helped to improve every published article. Dr. J. Bolobajev for upholding the highest standards of scientific research making no compromises in quality or quantity.

Abstract

Development of a Pulsed Corona Discharge–Photocatalytic Oxidation System for Environmental Air Treatment

Volatile organic compounds (VOCs) used in manufacturing processes are often toxic and harmful to the environment. Industries producing paints, adhesives, and cleaning agents rely on a wide range of organic solvents that negatively affect air quality. To mitigate these impacts, EU Directive 2016/2284 was introduced, obliging Member States to reduce VOC emissions by 40% by the year 2030.

Various air emission control technologies are currently applied for VOC removal in industry, including absorption, adsorption, thermal catalysis, and incineration. However, advanced oxidation processes (AOPs) remain rarely implemented despite their potential to offer energy-efficient alternatives for future applications.

This study focuses on the development and performance evaluation of a state-of-the-art hybrid air treatment system combining pulsed corona discharge (PCD) plasma with photocatalytic oxidation (PCO) for efficient degradation of VOCs. A prototype 75.9 L plug-flow PCD reactor with a power input range of 6.25-100 W and an internal water-sprinkling system was employed as the primary treatment stage. For post-plasma treatment, a 21.3 L flat-bed PCO reactor was constructed and equipped with up to twenty 15 W UV-A lamps. Photocatalytic coatings were prepared by spraying TiO_2 on glass substrates, which were subsequently installed inside the reactor.

Initial experiments evaluated the performance of each reactor independently. The PCO reactor was tested using 20 ppm of 2-methoxyethanol (2ME) under varying irradiance levels and residence times ranging from 7 to 77 s, both in the presence and absence of ozone as a co-oxidant. The results showed that ozone significantly enhanced the photocatalytic degradation of 2ME. Notably, ozone degradation within the PCO reactor was approximately doubled in the presence of an organic pollutant.

The PCD reactor was examined separately across a range of power inputs and under both dry and humid conditions, the latter achieved through water sprinkling at flow rates between 3 and 18 L min^{-1}. The introduction of water into the plasma for enhanced air treatment was investigated for the first time. *m*-xylene (20±5 ppm), a relatively resistant aromatic VOC, was selected as target pollutant. The influence of water pH on the formation of reactive oxygen and nitrogen species (ROS and RNS respectively) was also examined. Key performance indicators, including *m*-xylene conversion, ozone generation, and N_2O formation, were quantified. The results indicated that water sprinkling has only a minor effect on *m*-xylene degradation but substantially altered ozone and N_2O formation pathways.

Subsequently, the combined system consisting of a PCD reactor followed by a PCO reactor (post-plasma catalysis) was evaluated under integrated operating conditions using *m*-xylene (40±5 ppm) as the target pollutant. Experiments were conducted under three relative humidity (RH) regimes: dry air (RH 2.5%), moderately humid air (RH 35%), and high humidity (RH 65%), the latter achieved by activating the water-sprinkling system within the PCD reactor. Dry air conditions favoured higher *m*-xylene oxidation efficiency, but resulted in increased ozone formation, raising concerns regarding secondary pollution. In contrast, humid conditions, especially with water-assisted PCD operation, suppressed ozone formation but slightly reduced VOC conversion. Under dry air conditions, the PCO reactor exhibited negligible activity toward *m*-xylene and ozone

degradation. At high humidity, however, photocatalytic performance was enhanced, compensating for the reduced efficiency of the water-sprinkled PCD reactor and improving ozone removal.

Throughout the study, Fourier-transform infrared (FT-IR) spectroscopy and gas chromatography–mass spectrometry (GC-MS) were used to quantify target pollutants and by-products, while continuous ozone monitoring was performed using an ozone analyser. The results confirm the complementary behaviour of PCD and PCO reactors, demonstrating that the hybrid configuration provides a viable platform for VOC abatement in real-world air purification applications. The findings highlight the critical roles of humidity, power input, and residence time in controlling pollutant degradation. Furthermore, the results indicate that post-plasma photocatalytic treatment is effective only when coupled with water-assisted PCD operation. Alternative post-plasma catalytic approaches and the use of more active photocatalysts are identified as promising pathways for further improving post-plasma catalysis performance.

Lühikokkuvõte

Impulss-koroonalahenduse ja fotokatalüütilise oksüdatsiooni kombineeritud tehnoloogia arendamine õhu puhastamiseks

Tööstuses kasutatavad lenduvad orgaanilised ühendid (LOÜ-d) on sageli toksilised ja keskkonnale kahjulikud. Värvide, liimide ja puhastusvahendite tootmisel kasutatakse mitmesuguseid orgaanilisi lahusteid, mis mõjutavad negatiivselt õhukvaliteeti. LOÜ-de heitmete vähendamise edendamiseks on vastu võetud Euroopa Liidu direktiiv 2016/2284, mis kohustab liikmesriike vähendama LOÜ-de heitmeid 40% võrra aastaks 2030.

LOÜ-de eemaldamiseks rakendatakse mitmesuguseid õhusaaste kontrolli süsteeme, mis põhinevad absorptsiooni-, adsorptsiooni-, termilise katalüüsi- ja põletamisprotsessidel. Süvaoksüdatsiooniprotsessid on tööstuses veel haruldased, kuid need võivad tulevikus osutuda energiatõhusateks alternatiivideks.

Käesolev uuring keskendub hübriidse töötlussüsteemi arendamisele ja selle jõudluse hindamisele, mis ühendab impulss-koronalahenduse (IKL) fotokatalüütilise oksüdatsiooniga (FKO), et saavutada lenduvate orgaaniliste ühendite tõhus lagundamine. Põhireaktorina kasutati 75,9-liitrise läbivooluga IKL-reaktorit võimsusvahemikus 6,25–100 W, mis oli varustatud sisseehitatud veepihustussüsteemiga. Järeltöötluseks konstrueeriti 21,3-liitrine tasapinnaline FKO-reaktor, milles kasutati UV-A lampe TiO_2 fotokatalüsaatori aktiveerimiseks. Fotokatalüütiline kattekiht valmistati TiO_2/etanooli suspensiooni pihustamisel klaaspinnale, mis seejärel paigaldati reaktorisse.

Esialgsetes katsetes hinnati mõlema reaktori jõudlust eraldi. FKO-reaktorit testiti 2-metoksüetanooli (2ME) lagundamisel kontsentratsioonil 20 ppm. Katsed viidi läbi erinevate UV-kiirguse intensiivsuste ja saasteaine viibeaegade juures (7– 77 s) ning lisaks juhiti reaktorisse osooni. Osooni lisamise mõju hinnati 2ME lagunemise efektiivsuse alusel. Tulemused näitasid, et osooni olemasolu soodustas 2ME fotokatalüütilist lagundamist. Veelgi olulisem on, et orgaanilise saasteaine juuresolekul kahekordistus osooni lagunemine FKO-reaktoris.

IKL-reaktorit uuriti eraldi erinevatel võimsustasemetel ning nii kuiva kui ka niiske õhu tingimustes. Töödeldav saastunud õhk niisutati reaktorisse integreeritud veepihustussüsteemi abil. Käesolevas uuringus uuriti esmakordselt vee lisamist plasmasse õhu töötlemise tõhustamiseks. Õhu saasteainena kasutati *m*-ksüleeni kontsentratsioonil 20±5 ppm. Samuti varieeriti vee pH-d, et uurida selle mõju reaktiivsete hapniku- ja lämmastikuühendite tekkele. Peamisteks hinnatavateks näitajateks olid *m*-ksüleeni konversioon, osooni teke ja N_2O moodustumine. Uuringu tulemused näitasid, et veepihustus avaldas *m*-ksüleeni lagundamisele vaid väikest mõju, kuid vähendas samal ajal märkimisväärselt osooni ja dilämmastikoksiidi teket.

Seejärel hinnati kombineeritud süsteemi toimivust, milles IKL-reaktoris toimunud õhupuhastusele järgnes FKO. Õhu saasteainena kasutati *m*-ksüleeni (40±5 ppm). Katseid viidi läbi kolme suhtelise õhuniiskuse tingimustes: kuiv õhk (RH 2,5%), mõõdukalt niiske õhk (RH 35%) ja kõrge niiskusega õhk (RH 65%). Viimane saavutati veepihustusel IKL-reaktorisse. Katsete tulemused näitasid, et kuivas süsteemis saavutati suurem *m*-ksüleeni oksüdatsioonitõhusus, kuid sellega kaasnes ka suurenenud osooni teke. Osoon on teadaolevalt õhusaasteaine ning selle moodustumine põhjustab sekundaarset õhusaastumist. Niisketes tingimustes, eriti veepihustusega IKL-reaktori kasutamisel, vähenes osooni teke, kuid LOÜ-de lagundamise määr vähenes mõnevõrra. Kuiva õhu korral oli *m*-ksüleeni ja osooni lagundamine madal, kuid kõrge suhtelise õhuniiskuse juures

paranes oluliselt FKO efektiivsus kompenseerides madalamat LOÜ-de eemaldust veepihustusega IKL-is.

Uurimistöös määrati sihtsaasteainete ja kõrvalproduktide kontsentratsioonid. Saadud andmed viitavad IKL- ja FKO-reaktorite teineteist täiendavale toimimisele ning näitavad, et hübriidsüsteem võib olla perspektiivne platvorm LOÜ-de oksüdatsiooniks reaalsetes õhupuhastusrakendustes. Tulemused rõhutavad niiskuse, plasma intensiivsuse ja viibeaegade reguleerimise olulisust, kuna need parameetrid määravad nii saasteainete lagunemise kui ka sekundaarsete produktide tekke. Uuringute käigus ilmnes, et plasmajärgne töötlus FKO-ga oli efektiivne eeskätt koos veepihustusega IKL-reaktoriga. Alternatiivsed meetodid FKO asemel ja aktiivsemate fotokatalüsaatorite kasutamine võivad pakkuda uusi võimalusi plasmajärgse katalüüsi jõudluse parandamiseks.

Appendix 1

Paper I

K. Altof, M. Krichevskaya, S. Preis, J. Bolobajev. (2024). Oxidation of Airborne *m*-Xylene in Pulsed Corona Discharge: Impact of Water Sprinkling, *ChemEngineering*, 8, 99. https://doi.org/10.3390/chemengineering8050099

chemengineering

MDPI

Article

Oxidation of Airborne *m*-Xylene in Pulsed Corona Discharge: Impact of Water Sprinkling

Kristen Altof *, Marina Krichevskaya, Sergei Preis and Juri Bolobajev *

Laboratory of Environmental Technology, Department of Materials and Environmental Technology, Tallinn University of Technology, 5 Ehitajate Tee, 19086 Tallinn, Estonia; marina.kritsevskaja@taltech.ee (M.K.); sergei.preis@taltech.ee (S.P.)

* Correspondence: kristen.altof@taltech.ee (K.A.); juri.bolobajev@taltech.ee (J.B.)

Abstract: Plasma from electric discharges can be used in the abatement of volatile organic compounds (VOCs). The application of gas-phase pulsed corona discharge (PCD) in air–water mixtures provides favorable conditions for the oxidation of VOCs at unsurpassed energy efficiency. This research investigates the impact of water sprinkling on PCD performance in the oxidation of *m*-xylene as a model compound. Experimental research into the plasma treatment of continuous air flow was undertaken using the PCD reactor in dry and water-sprinkled modes. Water sprinkling more than doubled the *m*-xylene oxidation rate, which can be attributed to abundant OH-radicals produced at the plasma–water interface. Water sprinkling substantially reduced the formation of nitrous oxide, which is considered to be a secondary pollutant in the outlet air. Ozone is considered a by-product helping the subsequent photocatalytic oxidation of potential residues and photocatalyst maintenance. The use of water-sprinkled PCD is a promising approach to energy-efficient abatement of VOCs.

Keywords: AOP; plug flow plasma reactor; water sprinkled plasma; air purification; nitrous oxide; non-thermal plasma; ozone; VOCs; ROS

Citation: Altof, K.; Krichevskaya, M.; Preis, S.; Bolobajev, J. Oxidation of Airborne *m*-Xylene in Pulsed Corona Discharge: Impact of Water Sprinkling. *ChemEngineering* **2024**, *8*, 99. https://doi.org/10.3390/chemengineering8050099

Academic Editor: Alírio E. Rodrigues

Received: 6 August 2024
Revised: 17 September 2024
Accepted: 24 September 2024
Published: 1 October 2024

1. Introduction

Volatile organic compounds (VOCs) of toxic character both indoors and outdoors present an increasingly relevant health hazard to be addressed for proper elimination [1]. Countries in the European Union have obligated themselves to reduce the emissions of non-methane VOCs by 40% by 2030 [2]. The problem is solved by a variety of methods, requiring systematic analysis for a feasible choice. Of the two categories of VOC-treatment technologies, i.e., recovering VOCs when they are utilized and in situ destruction of VOCs, the latter is focused on air purification [3]. Technologies for destroying VOCs include thermal and catalytic incineration, biological oxidative filtering, and advanced oxidation processes (AOPs), including non-thermal plasma treatment. Incineration uses supplemental fuel that produces significant amounts of CO_2, while catalytic incineration is vulnerable to sulfur, phosphorus, and halogens deactivating the catalysts. Non-thermal plasmas are innovative solutions that can tackle the issue at hand. A concentration–flow rate disposition for air treatment methods was given by Revah and Morgan-Sagastume [4]. There is some overlap of plasma treatment with adsorption and bio-filtration, with plasma treatment substantially less costly than adsorption and far more compact than biological filtration.

Sustainable and environmentally friendly VOC control may be provided by AOPs, including pulsed corona discharge (PCD) as a non-thermal plasma treatment [5–7]. Amongst AOPs, PCD is particularly attractive for its potential in degrading VOCs in an energy-efficient way: in a study on the removal of pollutants in water, PCD has shown outstanding performance [8,9]. Plasma technology has also been studied for air purification [10,11], showing that PCD also as the most energy-efficient AOP for the oxidation of airborne benzene and toluene [5,12]. The remarkable results of PCD applications are linked to the

formation of reactive oxygen species (ROS), mostly hydroxyl radicals, predominantly on the surface of the water sprinkled into the plasma zone [13,14]. It has also been stated that increased humidity plays a crucial role in gas phase oxidation of VOCs with plasma technology, which improves radical production and the overall effectiveness of the process [6,15]. In air treatment, most of the studies with plasma technology have been conducted with dry or ambient air. To fill the knowledge gap and take full advantage of ROS, a new prototype plug flow PCD reactor with water sprinkling was built and tested for the oxidation of VOCs. *m*-Xylene was used as a model pollutant in a continuous airstream treated at various pulse repetition frequencies, with and without water sprinkling. By choosing *m*-xylene for experiments, the authors addressed the need for the removal of chemicals of aromatic structure that are often considered to be carcinogenic, mutagenic and neurotoxic. This also applies for *m*-xylene, which is widely used as a solvent in many industries, resulting in emissions into the environment [16–18]. The U.S. Department of Labor Occupational Safety and Health Administration set an exposure limit for xylene (all isomers) at a maximum of 100 ppm for an 8 h standard workday. In Europe, the exposure limit is 50 ppm [19]. Yet some scientists suggest that the exposure limits are too high [20]. With sprinkling, *m*-xylene conversion in both gas and aqueous phases was studied to understand the effect of ROS formed at the water surface. In addition, ozone and N_2O by-products of air molecule interactions occurring in a plasma environment were quantified.

2. Materials and Methods

2.1. Chemicals

Analytical grade *m*-xylene (C8H10, 99+% from Thermo Scientific Chemicals, Waltham, MA, USA) was used as the model pollutant. For high-performance liquid chromatography (HPLC), methanol (CH3OH, ≥99.9% from Honeywell International Inc., Charlotte, NC, USA) and Milli-Q water obtained from a Millipore ultrapure water UV system (Simplicity®, EMD Millipore Corporation, Burlington, MA, USA), were used as eluents. Distilled water was used in PCD experiments with sprinkling. For pH regulation, sulfuric acid (H_2SO_4, 96%, Lach:Ner, Neratovice, Czech Republic) and sodium hydroxide (NaOH, puriss p.a., STANCHEM Sp. Z o.o, Niemce, Poland) were used.

2.2. PCD Reactor

The schematics of the PCD reactor (Flowrox Oy, Lappeenranta, Finland) can be seen in Figure 1. The PCD reactor with a total volume of 75.9 L consists of an inter-electrode zone (1275 mm × 550 mm × 35 mm) and two side boxes, in which high-voltage electrodes are attached to tension devices. The electrode system consists of two vertical grounded electrode plates and horizontal high-voltage electrode wires between them. The perforated plate (565 mm × 97 mm) with 24 holes (3 mm in diameter) on top of the reactor ensures the uniform distribution of water droplets and jets across the plasma zone. The 12.7 L water storage tank was filled with 5.0 L of distilled water with adjusted pH. For water circulation, a magnet drive water circulation pump (Iwaki Co. Ltd., Tokyo, Japan) was used. The pump feeds water to the top of the reactor onto a perforated plate. The plate is 565 mm × 97 mm in size and has 24 holes with a diameter of 3 mm. As the water passes through the holes it showers down to the water tank, passing through the plasma zone that is 0.011 m^3 in volume. The application of high voltage pulses between electrodes generated low-temperature gas-phase plasma of PCD in air. The amplitude of voltage and current and the duration of each pulse were 18 kV, 380 A and 100 ns, respectively. The pulse repetition frequency applied in the experiments varied between 25 and 800 pulses per second (pps) corresponding to the power delivered to the reactor of 3.0 to 100 W, respectively.

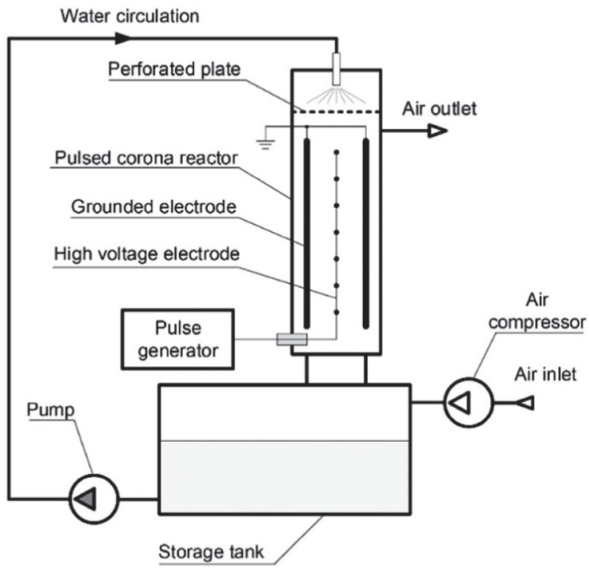

Figure 1. Pulsed corona discharge reactor schematics [12].

2.3. Experimental Procedure

The pollutant was dosed into the air stream by means of liquid *m*-xylene evaporation from a bubble column (400–600 mL). To regulate the concentration of the pollutant, the bubble column was connected to the main flow in a bypass mode (Figure S1 in the Supplementary Materials) [21]. This arrangement provided a steady air stream of 6.0 m^3 h^{-1}, where the pollutant concentration could be varied from 10 to 50 ppm. The assessment of pollutant degradation performance was made by measuring input (Cin) and output (Cout) concentrations of *m*-xylene in the air stream. Air samples were collected using a 4 L metal body gas cell (Specac, Orpington, UK) and subjected to FT-IR spectrometry analysis (Interspec 200-X, Interspectrum OÜ, Tõravere, Estonia) for the presence of *m*-xylene and other compounds in the air. *m*-Xylene was measured at a bandwidth between 770 and 766 cm^{-1}, and N_2O at a bandwidth between 2256 and 2223 cm^{-1}, which had the least interference from other substances while a distinctive spike on the specter was still visible (Figure S2). The FT-IR data interpretation was accomplished using Essential FTIR v.2.00.045 (Operant LCC) software with FDM HiRes VPFTIR for the Quant database. All air samples were withdrawn at least 15 min after the experiment started to ensure a steady state in all experimental parameters.

The aqueous concentrations of nitrites and nitrates were measured using ion chromatograph (Metrohm®, 761CompactIC, Metrohm AG, Herisau, Switzerland) equipped with a suppressed conductivity detector and analytical ion separation column (Metrosep A Supp 5, 150 mm × 4.0 mm inner diameter, Metrohm AG, Herisau, Switzerland).

In PCD experiments with water sprinkling, water was continuously recirculated at a flow rate of 3 to 18 L min^{-1}, and regulated by adjusting the recirculation pump rotation frequency. Aqueous samples were withdrawn from the reactor and analyzed for *m*-xylene concentration using HPLC (Shimadzu LC-2030D, Shimadzu Corporation, Kyoto, Japan) equipped with a PDA detector and a Luna Omega column (150 mm, polar C18, p.s. = 5 μm). Isocratic elution was applied using 60% methanol and 40% water at the flowrate of 0.2 mL min−1. The column temperature was kept at 40 °C. Quantification of aqueous *m*-xylene was impossible in water samples at pH exceeding 9.5 due to the tolerance limit of the stationary phase of HPLC columns. Time-consuming manipulations with samples containing *m*-xylene for the pH adjustment were also impossible for the quick evaporation of volatile *m*-xylene. Gaseous ozone concentration was measured in

the reactor's outflow air using an ozone analyzer (Anseros Klaus Nonnenmacher GmbH, Tübingen, Germany). The pH of sprinkled water was measured by using SevenCompact pH-meter (Mettler-Toledo® Solutions, Columbus, OH, USA).

3. Results and Discussion

3.1. PCD Oxidation of Airborne m-Xylene

The pulse repetition frequency and, consequently, the input power affected the *m*-xylene oxidation rate in both the water-sprinkled and dry PCD reactor. Figure 2 presents the difference in *m*-xylene conversion depending on the pulse repetition frequency. It is evident that the sprinkling of water into the plasma environment induced the oxidative degradation of *m*-xylene. The difference is explained by different ROS formation in dry and humid air. Khadem et al. [22] suggested different oxidation pathways, pointing to the formation of hydroxyl radicals $OH^{\bullet}$ in humid air. The radical plays a crucial role as the most powerful oxidant, with a redox potential as high as 2.8 V [15,23,24]. One can presume that water serves as the source of hydrogen-containing ROS ($HO^{\bullet}$, $HO_2^{\bullet}$), which contribute to the radical-mediated oxidation.

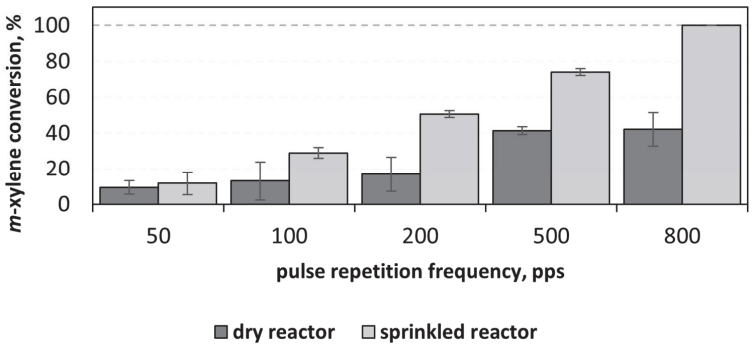

Figure 2. Oxidation of airborne *m*-xylene dependent on pulse repetition frequency: *m*-xylene input concentration 20 ± 5 ppm, air flow rate 6 m^3 h^{-1}, water circulation rate 9 L min^{-1}, pH 6.0–6.5.

3.2. m-Xylene Absorption and Oxidation in Water

Water sprinkling in the PCD reactor provides physical absorption of *m*-xylene dissolved in water. The absorption experiments were conducted by purging air containing *m*-xylene through the sprinkled PCD reactor with frequent sampling for the first 5 to 20 min of the experiment. The content of *m*-xylene was determined in the water samples. In the absence of pollutant oxidation, the liquid phase is saturated with *m*-xylene (Figure 3A) in accordance with Henry's law, in which an aqueous concentration of the VOC at the saturation point is proportional to its partial pressure in the reactor chamber (Equation (1)):

$$C_L^* = k_H \cdot P_i \quad (1)$$

where k_H and P_i are Henry's constant and *m*-xylene partial pressure, respectively.

The driving force of mass transfer is the concentration gradient between two phases (Equation (2)):

$$\frac{dC_L}{dt} = k_L a(C_L^* - C_L) \quad (2)$$

where $k_L a$, C_L, and C_L^* are the mass transfer coefficient, and the aqueous *m*-xylene concentrations at time *t* and at the saturation point, respectively. Because of continuous gas inflow and the low solubility of *m*-xylene in water (146 mg L^{-1} at 25 °C), the VOC's partial pressure remains constant during absorption, providing constant C_L^*. As a result, the differential Equation (2) can be solved with boundary conditions: $t = 0$ to t and corresponding

$C_L = 0$ to C_L^*. This allows the linearized form of the dependence of the aqueous concentration on time (Equation (3)) occurring during absorbance (Figure 3B) to be obtained:

$$-ln\left(1 - \frac{C_L^*}{C_L}\right) = k_L a \cdot t \quad (3)$$

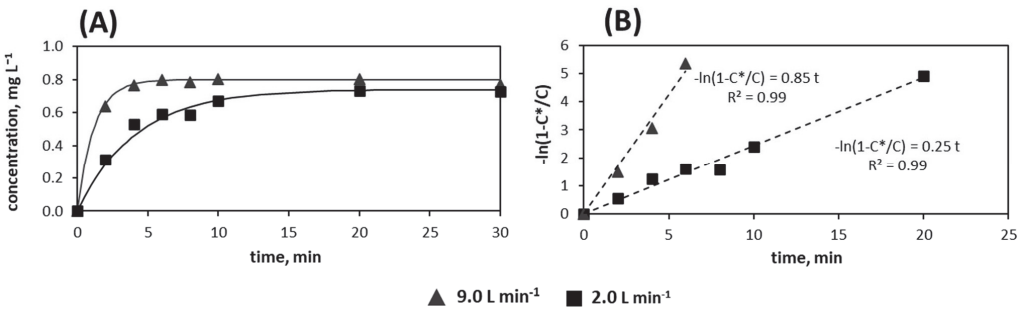

Figure 3. (**A**) *m*-Xylene absorption by water in time at various water recirculation rates, (**B**) linearized form of absorption kinetics: gaseous *m*-xylene input concentration 20 ± 5 ppm, air flow rate 6 m^3 h^{-1}, pH 6.0–6.5.

The slopes of the linear paths characterize mass transfer coefficients $k_L a$, which were found to be 0.85 and 0.24 at flowrates of 9.0 and 2.0 L min^{-1}, respectively. One can see that the water recirculation rate affects the absorption kinetics through the specific surface area *a* incorporated in the $k_L a$ coefficient (Equation (3)), which depends on the number of droplets per unit of time delivered through the perforated plate, and the size of droplets. In turn, the liquid-film mass transfer coefficient k_L is mostly compound-specific, and thus, depends on the turbulence of the gas–liquid mixture, which is intensified with the flow rate.

In such a design, the PCD reactor acts as a wet scrubber, absorbing gaseous pollutants in liquid. It is reasonable to assume that vapors of hydrophilic compounds such as formaldehyde, methoxyethanol, low-molecular alcohols etc., would be susceptible to absorption, and thus, favorable for such an application. However, the present study was ultimately focused on a hydrophobic compound to stress out the non-selectivity and versatility of PCD in the chemical degradation of recalcitrant pollutants in air.

After saturation of the recirculating water with *m*-xylene, the PCD generator was switched on, decreasing the concentration of the aqueous VOC, and reaching an equilibrium concentration dependent on the pulsed power input (Figure 4).

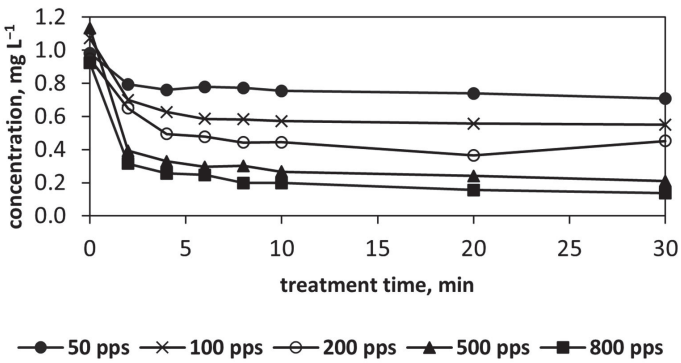

Figure 4. Aqueous *m*-xylene concentration vs. experimental run time dependent on the pulse repetition frequency: airborne *m*-xylene input concentration 20 ± 5 ppm, air flow rate 6 m^3 h^{-1}, water circulation rate 9 L min^{-1}, pH 6.0–6.5.

The different equilibrium states of *m*-xylene in water dependent on the pulse repetition frequency can be explained from two reinforcing points of view: (i) higher power input oxidizes more of *m*-xylene in the gas phase, reducing the amount of *m*-xylene absorbed by water; and (ii) at a higher power input, more *m*-xylene is also oxidized in water by the increased amount of ROS at the plasma–liquid interface [25].

3.3. Ozone Generation in PCD Reactor

The dependence of ozone gaseous concentration on the pulse repetition frequency in the plasma reactor is given in Figure 5. Ozone concentration in the air outflow was measured in the absence and presence of *m*-xylene vapors with and without water sprinkling 7 to 10 min after the start of the experiment. Ozone concentration remained stable within 15 to 20 min of measurements.

In a plasma environment, air oxygen is prone to ionization, forming ozone. One can see that the discharge power input almost linearly affects the ozone yield, i.e., higher pulse frequency results in higher concentrations of ozone in the air outflow. The linear growth in ozone production is explained by the difference between the ozone concentration and its maximum achievable concentration at the equilibrium state in the sprinkled PCD reactor with no air flow, reaching about 3000 ppm (5 mg L^{-1}) [26]. Increased pulsed power input naturally improves ozone production at the air flow rate applied in the experiments.

Greater ozone yield in the absence of sprinkling is explained by the discharge energy lost, since electrodes are partly covered by water droplets, as was concluded by Lukes et al. [27] and developed by Kornev et al. in research with conductive liquids. They also suggested how to construct the PCD reactor with minimal losses [28]. Another reason for reduced ozone output is the higher concentration of water vapor in the reactor. Water vapor plays a crucial role in ozone formation in corona discharge [29], reducing the lifetime of atomic oxygen and, therefore, ozone production [24].

The presence of *m*-xylene in the gas mixture also reduced ozone production, which can be explained either by ozone directly oxidizing the VOC, or, more likely, by competitive reactions of active species in ozone formation and *m*-xylene oxidation: the short residence time and relatively slow reactions of molecular ozone makes the second explanation more plausible.

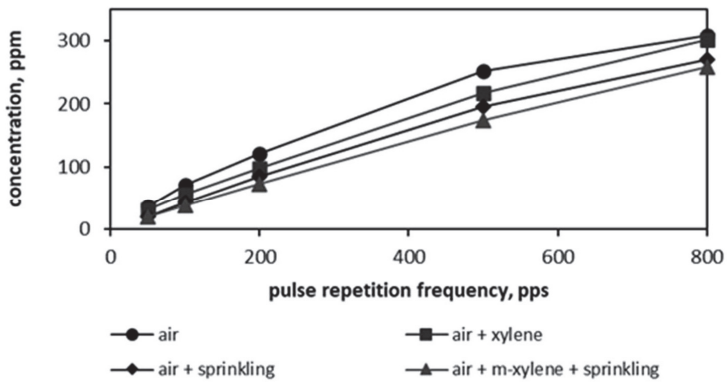

Figure 5. Airborne ozone concentration dependent on water sprinkling and presence of *m*-xylene vapors vs. pulse repetition frequency: airborne *m*-xylene concentration 20 ± 5 ppm, air flow rate 6 m^3 h^{-1}, water circulation rate 9 L min^{-1}, pH 6.0–6.5.

3.4. m-Xylene Oxidation: Impact of Water Circulation Rate

The impact of the water circulation rate, i.e., the gas–liquid interface area linearly growing with the flow rate, on aqueous *m*-xylene oxidation is illustrated in Figure 6, showing that at 100 pps, the substrate concentration is practically independent at the

experimental flow rates from 3 to 18 L min^{-1}. This concentration corresponds with the *m*-xylene conversion rate observed for the pulse repetition frequency of 100 pps, comprising about 40% (Figure 4). This observation leads us to conclude that within the studied sprinkling range, the VOC was oxidized at a constant rate determined by the amount of ROS generated by the pulsed power input. In other words, the oxidation rate is limited by the input power spread over a bigger or smaller area of the contact surface without any impact on the overall oxidation rate. This agrees with the hydroxyl radicals predominantly formed at the gas–liquid interface, as described by Ajo et al. [30] and studied by Onga et al. [31]. Thus, the intense water circulation only promotes the absorption rate of target vapors (Figure 3), but not the PCD oxidation rate.

The ozone generation rate slightly decreased with increasing sprinkling intensity (Figure S3). This is most likely linked to the loss of discharge energy, which was increased by more intense watering of the electrodes, as described above.

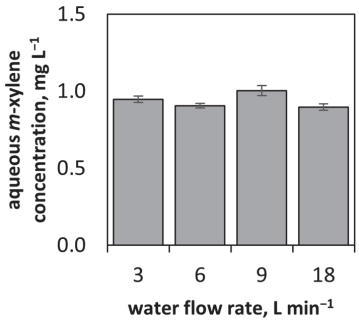

Figure 6. *m*-Xylene concentration in water dependent on water flow rate with airborne xylene input concentration 20 ± 5 ppm, air flow rate 6 m3 h^{-1}, pulse repetition frequency 100 pps, pH 6.0–6.5.

3.5. m-Xylene Oxidation: Impact of Airborne m-Xylene Concentration

The effect of *m*-xylene input concentration on its removal rate was studied within the interval of 10 to 45 ppm at 100 pps. At *m*-xylene input concentrations of 35 and 45 ppm, the net degradation, i.e., the difference between influent and effluent concentrations of *m*-xylene, approached its maximum of about 10 ppm, showing no more growth in the VOC removal. This points to the limit in the amount of ROS available at this input power of 12.5 W. This observation is supported by the higher aqueous concentration of *m*-xylene at its higher content in air, i.e., the gaseous VOC concentration continued to grow (Figure 7).

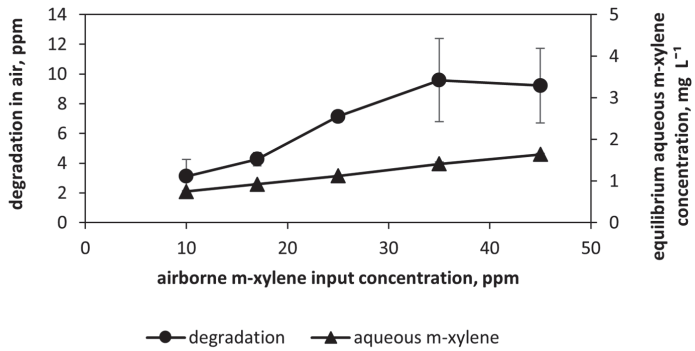

Figure 7. Dependents on *m*-xylene input concentration: air flow rate 6 m^3 h^{-1}, water circulation rate 9 L min^{-1}, pulse repetition frequency 100 pps, pH 6.0–6.5.

Ozone concentration moderately decreased by 12% with higher *m*-xylene input concentrations, which supports the assumption made earlier–ozone plays minor role in *m*-xylene oxidation. Small decrease in ozone concentration may be explained either by direct reaction of the VOC with ozone, or by competitive reactions of short-living ROS forming ozone with *m*-xylene. Some ozone reacted with higher concentrations of aqueous *m*-xylene, which may also explain the minor loss.

3.6. m-Xylene Oxidation: Impact of Sprinkling Water pH

The formation of hydroxyl radicals from aqueous ozone in alkaline media may contribute to *m*-xylene oxidation and ozone decomposition in water [32]. Changes in airborne m-xylene conversion, however, were too subtle, indicating no practical effect of alkaline sprinkling, showing only a 3% increase in m-xylene oxidation with water pH 2 compared to pH 7 and pH 12 (Figure S4). This observation is evidence of the minor role of aqueous *m*-xylene oxidation with dissolved ozone.

With respect to ozone concentration in the gas phase, alkaline sprinkling water caused no change, although modest degradation was observed in the presence of m-xylene, where ozone generation was decreased to 31.5 ppm at pH 12 compared to 36.0 ppm at pH 7 (Figure S5). Apparently, some decomposition of ozone took place in the presence of the dissolved VOC in alkaline solution, although a slight improvement in gaseous m-xylene conversion is evidence of the minor role of slowly-reacting ozone in oxidation.

In all experiments, the presence of *m*-xylene in the airstream results in a decreased gaseous ozone output. As observed in this study, ozone is a rather slow oxidant in the gas phase, requiring long residence times and taking several hours to oxidize aromatic molecules [33], thus excluding gas-phase ozone from ROS from contributing to oxidation. The small amount of alkaline sprinkling in *m*-xylene oxidation also indicated the minor role of dissolved ozone, although it made the aqueous ozone decomposition slightly faster. These observations show that the gas-phase oxidation of *m*-xylene with short-living ROS in PCD plasma is predominant.

3.7. Nitrogen Oxidation

In air pollution control with electric discharges, secondary pollutants, ozone and nitrogen oxides must be considered for process safety and possible down-flow arrangements [21]. In a plasma environment, excitation and ionization of airborne nitrogen produce active species, radicals and ions, including $N^{\bullet}$, $N_2^{\bullet}$ and N_2^{+}, which are able to react with oxygen, forming nitrogen oxides [34,35]. In this study, the formation of N_2O was detected in both dry and sprinkled PCD reactors. The discharge at pulse repetition frequencies below 200 pps produces insignificant amounts of N_2O, rendering the issue moot. Other nitrogen oxides, NO and NO_2, were detected neither in the dry nor in the sprinkled gas phase: the absence of NO is easily explained by its fast-reactive character, whereas the absence of NO_2 is caused by further reaction with OH-radical forming nitric acid in ambient air at relative humidity of 30–40% at 20 °C. In both wet and dry conditions, N_2O concentration followed a linear growth with growing pulse repetition frequency, yet water sprinkling substantially reduced the N_2O concentration (Figure 8). As it is low enough even at the highest pulsed energy input, the nitrous oxide concentration decreased more than two-fold, reaching 3 ppm at 800 pps in the air–water mixtures. This is evidence of its more effective oxidation to nitric oxides of a higher oxidation state at the air–water interface, and that it is a gathering place for short-living ROS.

Nitrous oxide experiences either a hydroxyl-radical attack at the gas–liquid interface, producing nitrites identified in the aqueous phase (Figure 9) and reducing the N_2O concentration in treated air (Figure 8); or the formation of nitrous oxide may be reduced in water-sprinkled PCD due to straightforward oxidation of nitrogen to NO and further to NO_2 and, ultimately, to nitrate, thus providing lower concentrations of N_2O. Nitrites are formed as intermediates determined in the aqueous phase in low concentrations, whereas nitrates tend to grow continuously (Figure 9).

The amount of nitrates quantified in the sprinkled reactor at 100 pps, i.e., 12.5 W of pulsed power, equals approximately 50 mg, meaning the amount of nitrogen bond in the aqueous phase was around 11.3 mg, which is an order of magnitude higher than the amount of nitrogen carried in the N_2O form with air flow for 30 min—1.9 and 0.9 mg N in the dry and the sprinkled reactor, respectively. The nitrate production energy efficiency observed in the sprinkled reactor experiments comprises 8.0 g kW^{-1} h^{-1}, which is an agreement with data obtained earlier by Preis et al. [36]. The energy efficiency of N_2O production in the dry reactor reaches a maximum of 0.94 g kW^{-1} h^{-1} at 7.5 ppm in outlet air (Figure 10), i.e., an order of magnitude smaller than nitrate production. Considering the downstream removal of N_2O, studies of photocatalytic oxidation may be promising for further research [37].

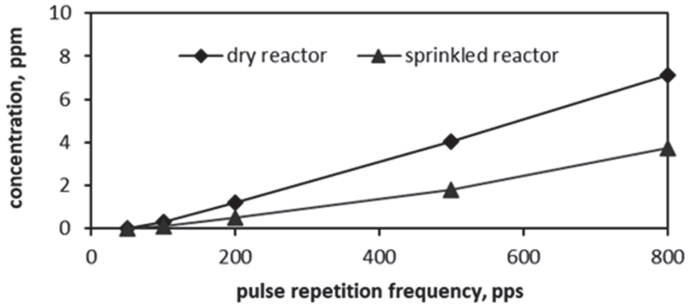

Figure 8. Airborne N_2O concentration in air in dry and water-sprinkled PCD reactors dependent on the pulse repetition frequency: *m*-xylene input concentration 20 ± 5 ppm, air flow rate 6 m^3 h^{-1}, water circulation rate 9 L min^{-1}, pH 6.0–6.5.

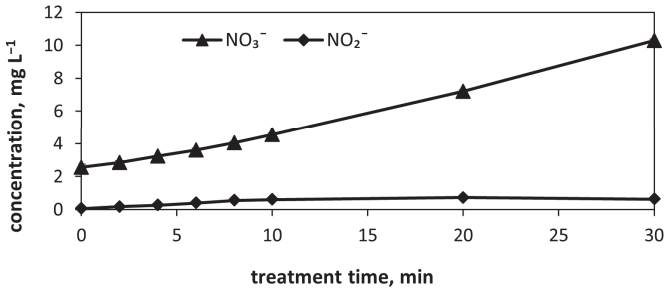

Figure 9. Aqueous nitrite and nitrate concentrations dependent on treatment time: *m*-xylene concentration 20 ± 5 ppm, pulse repetition frequency 100 pps, air flow rate 6 m^3 h^{-1}, water circulation rate 9 L min^{-1}, pH 6.0–6.5.

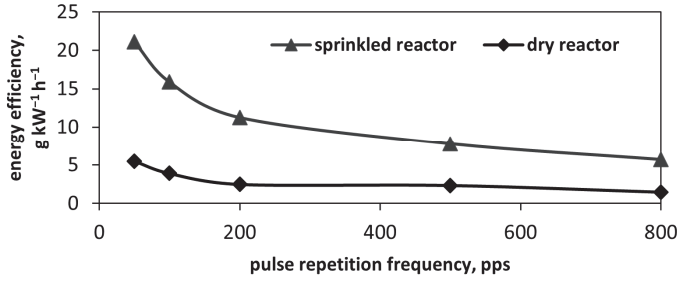

Figure 10. Energy efficiency of *m*-xylene degradation in air with and without sprinkling dependent on pulse repetition frequency: *m*-xylene concentration 20 ± 5 ppm, air flow rate 6 m^3 h^{-1}, water circulation rate 9 L min^{-1}, pH 6.0–6.5.

3.8. Energy Efficiency of m-Xylene Oxidation

The energy efficiency of airborne *m*-xylene oxidation was calculated for both dry and water-sprinkled PCD (Figure 10). The energy efficiency was calculated using Equation (4):

$$E = \frac{\Delta C \cdot Q}{P} \quad (4)$$

where E—energy efficiency, g kW^{-1} h^{-1}, ΔC—the difference between *m*-xylene concentrations in inlet and outlet air streams, g m^{-3}, Q—air volumetric flow rate, m^3 h^{-1}, P—pulsed power input, kW. One can see a significant difference in energy efficiency, with oxidation in the sprinkled reactor surpassing that in dry conditions by four to six times at 50 and 800 pps, respectively. This indicates the crucial role of water in accelerating *m*-xylene oxidation, and shows the advantageous character of pulsed discharge techniques in providing safe oxidation of airborne pollutants in air–water mixtures that is impossible for DC and AC coronas.

The fact that the energy efficiency of *m*-xylene oxidation depends on the pulse repetition frequency deserves to be discussed. Concerning oxidation of *m*-xylene in the dry reactor, maximum energy efficiency was achieved at 50 pps, equaling 5.5 g kW^{-1} h^{-1}. Other studies reported similar results: Shang et al. [38] used positive DC corona degrading benzene with energy yields of up to 3.6 g kW^{-1} h^{-1} at the initial benzene concentration of 100 ppm, degrading to 86.5%. Jiang et al. [11] degraded nearly 70% of benzene at its 400 ppm initial concentration, reaching an energy yield of 8.5 g kW^{-1} h^{-1}. This was attributed to the starting concentration, which was twenty times higher than the one used in this study. Kask et al. [12] treated 1.2 mg L^{-1} (323.8 ppm) of toluene in a batch process PCD reactor and reached an energy efficiency of 29.6 g kW^{-1} h^{-1} with 32 W input power and 40% degradation. In the water-sprinkled continuous flow PCD, the energy efficiency at 50 pps was 21.1 g kW^{-1} h^{-1}, which was the highest energy efficiency achieved in this study.

Efficiency in *m*-xylene oxidation, however, dropped to 5.7 g kW^{-1} h^{-1} at 800 pps. Explanations given for similar observations in PCD oxidation of aqueous pollutants relied on the role of long-living ozone, realizing its oxidation potential in the time between pulses—longer pauses give ozone time to dissolve in treated water, and to contribute to oxidation. In this study, however, molecular ozone played a minor role in the oxidation of *m*-xylene, whether gaseous or aqueous. The higher efficiency of low pulse repetition frequency is explained by the short-living ROS synthesis and utilization in plasma, proceeding in competition between VOC vapor oxidation reactions, and ozone synthesis and decomposition: the higher the ozone concentration at a higher pulse repetition frequency, which requires energy for synthesis and decomposition, the smaller the fraction of the pulse energy available for direct oxidation of the VOC. Rare pulses thus utilize more energy in *m*-xylene oxidation at low ozone concentration (Figure 5) instead of wasting it in ozone synthesis and decomposition at higher frequencies and, consequently, higher ozone concentrations. In other words, the tendency of lower pulse repetition rates to be more energy-efficient remains analogous with the oxidation of aqueous pollutants, although due to different mechanism of action. In the gas phase, the intense power input results in higher concentrations of synthesized molecular ozone, which, being less reactive with the VOC in both phases, wastes a part of the pulsed energy for synthesis and decomposition, reducing the overall efficiency of VOC oxidation.

4. Conclusions

A prototype PCD reactor with water sprinkling was tested in *m*-xylene oxidation as a model pollutant of air flow. Water sprinkling increased the oxidation efficiency of the VOC by four to six times compared to PCD in dry air, indicating that oxidation reactions are significantly accelerated at the plasma–water interface. The pulsed power input acted as the key factor in the oxidation rate and its energy efficiency: it proceeded faster at a high pulse repetition rate; i.e., at a higher power input, oxidation demonstrated an energy yield more than three times higher than at a lower frequency, which sets up an optimization task in practical applications.

The difference in *m*-xylene oxidation efficiency at different power inputs is explained by the competitive reactions of short-living reactive oxygen species in plasma, when the target pollutant and long-living ozone are present at higher concentrations and at higher pulsed power inputs. Ozone itself showed a poor oxidation ability towards the target VOC.

The *m*-xylene oxidation energy efficiency appeared to be comparable to those observed for benzene and toluene, thus confirming its unequalled character in relation to other AOPs.

The variation on other process parameters provided a better understanding of the oxidation pattern, inlet concentration of airborne *m*-xylene, water flow rates, and sprinkled water pH. The increased airborne concentration of *m*-xylene resulted in faster degradation of the VOC. However, it reached a certain limit in the oxidation rate; e.g., a maximum of 10 ppm was degraded at a pulse repetition frequency of 100 pps, providing pulsed power input of 12.5 W. The higher oxidation rates achieved with higher power inputs are accompanied, however, by lower energy yields, thus offering an optimization task for engineering solutions. The sprinkling water flow rate and its pH had a negligible effect on the degradation of gas-phase *m*-xylene, conveniently minimizing the expense in these process parameters.

Secondary pollutants, ozone and N_2O are inevitably formed in PCD treatment of air. Water-sprinkling reduced the formation of nitrous oxide approximately twofold, whereas ozone formation was only slightly affected by water sprinkling in the absence or presence of the target VOC. Ultimately, nitric oxides end up as nitrates absorbed by the sprinkling water. The N_2O residues are likely removable downstream in photocatalytic oxidation.

This research shows that water sprinkling in a PCD reactor significantly contributes to the efficiency of VOC oxidation in a continuous flow mode. Further research is needed on degrading other classes of pollutants, including water-soluble hydrophilic compounds. This study of the conductivity of sprinkling water caused by the accumulation of nitrates and its performance is necessary for practical adoption of the technology.

Supplementary Materials: The following supporting information can be downloaded at: https://www.mdpi.com/article/10.3390/chemengineering8050099/s1, Figure S1: Flow chart of experimental setup: 1—main flow control valve, 2—main flow rotameter, 3—*m*-xylene bubble column, 4—rotameter and control valve for the bypass air flow saturated with *m*-xylene, 5—stopcock valve for *m*-xylene bypass flow, 6—control valve for air inflow sampling, 7—control valve for air outflow sampling, 8—sampling line rotameter, Figure S2. FT-IR specter of gas sample, post PCD treatment (sprinkled). *m*-Xylene input concentration 20 ± 5 ppm, air flow rate 6 m^3 h^{-1}, pulse repetition frequency 200 pps, pH 6.0–6.5. Red line—standard for 20 ppm of N_2O, black line—standard for 50 ppm *m*-xylene, green line—air sample. Figure S3: Airborne ozone concentration dependent on sprinkling water flow rate in absence and presence of *m*-xylene vapors: airborne *m*-xylene input concentration 20 ± 5 ppm, air flow rate 6 m^3 h^{-1}, pulse repetition frequency 100 pps, pH 6.0–6.5, Figure S4: Airborne *m*-xylene conversion dependent on sprinkling water pH: gaseous *m*-xylene input concentration 20 ± 5 ppm, air flow rate 6 m^3 h^{-1}, pulse repetition frequency 100 pps, sprinkling water flow rate 9 L min^{-1}, Figure S5: Airborne ozone concentration dependent on sprinkling water pH in absence and presence of *m*-xylene vapors: airborne *m*-xylene concentration 20 ± 5 ppm, air flow rate 6 m^3 h^{-1}, pulse repetition frequency 100 pps, water flow rate 9 L $min^{-1.}$

Author Contributions: Conceptualization, K.A., M.K., S.P. and J.B.; methodology, K.A., M.K., S.P. and J.B.; validation, K.A., M.K., S.P. and J.B.; formal analysis, K.A., M.K., S.P. and J.B.; data curation, K.A. and J.B.; writing—original draft preparation, K.A., M.K., S.P. and J.B.; supervision, M.K., S.P. and J.B. All authors have read and agreed to the published version of the manuscript.

Funding: This work was funded by the Ministry of Education and Research through Centre of Excellence in Circular Economy for Strategic Mineral and Carbon Resources (1 January 2024–31 December 2030, TK228).

Data Availability Statement: Experimental data will be made public on request.

Acknowledgments: We thank Kristjan Rikas for assistance in the laboratory and for supporting the experimental data acquisition.

Conflicts of Interest: The authors declare no conflicts of interest.

References

1. Pearson, J.K. European solvent VOC emission inventories based on industry-wide information. *Atmos. Environ.* **2019**, *204*, 118–124. [CrossRef]
2. European Parliament and of the Council of the European Union. Directive (EU) 2016/2284 of the European Parliament and of the Council of 14 December 2016 on the reduction of national emissions of certain atmospheric pollutants, amending Directive 2003/35/EC and repealing Directive 2001/81/EC. *Off. J. Eur. Union.* **2016**. Available online: https://eur-lex.europa.eu/eli/dir/2016/2284/oj (accessed on 15 September 2024).
3. Hirota, K.; Sakai, H.; Washio, M.; Kojima, T. Application of Electron Beams for the Treatment of VOC Streams. *Ind. Eng. Chem. Res.* **2004**, *43*, 1185–1191. [CrossRef]
4. Revah, S.; Morgan-Sagastume, J.M. *Biotechnology for Odor and Air Pollution Control*; Springer: Berlin/Heidelberg, Germany, 2005. [CrossRef]
5. Kornev, I.; Preis, S. Aqueous Benzene Oxidation in Low-Temperature Plasma of Pulsed Corona Discharge. *J. Adv. Oxid. Technol.* **2016**, *19*, 284–289. [CrossRef]
6. Du, C.; Gong, X.; Lin, Y. Decomposition of volatile organic compounds using corona discharge plasma technology. *J. Air Waste Manag. Assoc.* **2019**, *69*, 879–899. [CrossRef]
7. Hezami, L.; Nguyen-Tri, P.; Saoud, W.A.; Bouzaza, A.; El Jery, A.; Nguyen, D.D.; Gupta, V.K.; Assadi, A.A. Assadi, Recent progress in air treatment with combined photocatalytic/plasma processes: A review. *J. Environ. Manag.* **2021**, *299*, 113588. [CrossRef]
8. Onga, L.; Kattel-Salusoo, E.; Preis, S.; Dulova, N. Degradation of anti-inflammatory drug dexamethasone by pulsed corona discharge: The effect of peroxycompounds addition. *J. Environ. Chem. Eng.* **2022**, *10*, 108042. [CrossRef]
9. Tikker, P.; Nikitin, D.; Preis, S. Oxidation of aqueous bisphenols A and S by pulsed corona discharge: Impacts of process control parameters and oxidation products identification. *Chem. Eng. J.* **2022**, *438*, 135602. [CrossRef]
10. Sobacchi, M.G.; Saveliev, A.V.; Fridman, A.A.; Gutsol, A.F.; Kennedy, L.A. Experimental Assessment of Pulsed Corona Discharge for Treatment of VOC Emissions. *Plasma Chem. Plasma Process.* **2003**, *23*, 347–370. [CrossRef]
11. Jiang, N.; Lu, N.; Shang, K.; Li, J.; Wu, Y. Innovative approach for benzene degradation using hybrid surface/packed-bed discharge plasmas. *Environ. Sci. Technol.* **2013**, *47*, 9898–9903. [CrossRef]
12. Kask, M.; Krichevskaya, M.; Preis, S.; Bolobajev, J. Oxidation of Aqueous Toluene by Gas-Phase Pulsed Corona Discharge in Air-Water Mixtures Followed by Photocatalytic Exhaust Air Cleaning. *Catalysts* **2021**, *11*, 549. [CrossRef]
13. Bruggeman, P.J.; Kushner, M.J.; Locke, B.R.; Gardeniers, J.G.E.; Graham, W.G.; Graves, D.B.; Hofman-Caris, R.C.H.M.; Maric, D.; Reid, J.P.; Ceriani, E.; et al. Plasma-liquid interactions: A review and roadmap. *Plasma Sources Sci. Technol.* **2016**, *25*, 053002. [CrossRef]
14. Sato, M.; Ohgiyama, T.; Clements, J.S. Formation of chemical species and their effects on microorganisms using a pulsed high voltage discharge in water. In Proceedings of the 1994 IEEE Industry Applications Society Annual Meeting, Denver, CO, USA, 2–6 October 1994. [CrossRef]
15. Schiorlin, M.; Marotta, E.; Rea, M.; Paradisi, C. Comparison of toluene removal in air at atmospheric conditions by different corona discharges. *Environ. Sci. Technol.* **2009**, *43*, 9386–9392. [CrossRef] [PubMed]
16. Zoveidavianpoor, M.; Samsuri, A.; Shadizadeh, S.R. Safety, and Environmental Challenges of Xylene in Upstream Petroleum Industry. *Energy Environ.* **2012**, *23*, 1339–1352. [CrossRef]
17. Agency for Toxic Substances and Disease Registry. Public Health Statement Xylene. 2007. Available online: www.atsdr.cdc.gov/ (accessed on 28 July 2024).
18. Niaz, K.; Bahadar, H.; Maqbool, F.; Abdollahi, M. A review of environmental and occupational exposure to xylene and its health concerns. *EXCLI J.* **2015**, *14*, 1167–1186. [CrossRef]
19. European Chemicals Agency, Substance Infocard (Xylene). 2024. Available online: https://Echa.Europa.Eu/et/Substance-Information/-/Substanceinfo/100.014.124 (accessed on 28 July 2024).
20. Bolden, A.L.; Kwiatkowski, C.F.; Colborn, T. New look at BTEX: Are ambient levels a problem. *Environ. Sci. Technol.* **2015**, *49*, 5261–5276. [CrossRef]
21. Altof, K.; Krichevskaya, M.; Preis, S.; Tähemaa, T.; Bolobajev, J. Ozone-assisted degradation of 2-methoxyethanol in a prototype plug flow photocatalytic reactor. *Chem. Eng. J.* **2024**, *481*, 148488. [CrossRef]
22. Khadem, A.; Khani, M.R.; Rad, R.H.; Shokri, B.; Rashnoo, S.; Ghobadian, B. Experimental analysis of volatile organic compounds conversion by a dielectric barrier discharge reactor to study the main products: Hydrogen, CO, CO_2, NO_x and hydrocarbons. *Chem. Eng. Process. Process Intensif.* **2019**, *145*, 107660. [CrossRef]
23. Chen, J.; Xie, Z.; Tang, J.; Zhou, J.; Lu, X.; Zhao, H. Oxidation of toluene by dielectric barrier discharge with photo-catalytic electrode. *Chem. Eng. J.* **2016**, *284*, 166–173. [CrossRef]
24. Carey, J.H. An Introduction to Advanced Oxidation Processes (AOP) for Destruction of Organics in Wastewater. *Water Qual. Res. J.* **1992**, *27*, 103466. [CrossRef]
25. Tikker, P.; Kornev, I.; Preis, S. Oxidation energy efficiency in water treatment with gas-phase pulsed corona discharge as a function of spray density. *J. Electrost.* **2020**, *106*, 103466. [CrossRef]
26. Preis, S.; Panorel, I.C.; Kornev, I.; Hatakka, H.; Kallas, J. Pulsed corona discharge: The role of ozone and hydroxyl radical in aqueous pollutants oxidation. *Water Sci. Technol.* **2013**, *68*, 1536–1542. [CrossRef] [PubMed]

27. Lukes, P.; Clupek, M.; Babicky, V.; Janda, V.; Sunka, P. Generation of ozone by pulsed corona discharge over water surface in hybrid gas-liquid electrical discharge reactor. *J. Phys. D Appl. Phys.* **2005**, *38*, 409–416. [CrossRef]
28. Kornev, I.; Saprykin, F.; Preis, S. Stability and energy efficiency of pulsed corona discharge in treatment of dispersed high-conductivity aqueous solutions. *J. Electrost.* **2017**, *89*, 42–50. [CrossRef]
29. Ono, R.; Oda, T. Dynamics of ozone and OH radicals generated by pulsed corona discharge in humid-air flow reactor measured by laser spectroscopy. *J. Appl. Phys.* **2003**, *93*, 5876–5882. [CrossRef]
30. Ajo, P.; Kornev, I.; Preis, S. Pulsed Corona Discharge Induced Hydroxyl Radical Transfer Through the Gas-Liquid Interface. *Sci. Rep.* **2017**, *7*, 16152. [CrossRef]
31. Onga, L.; Kattel-Salusoo, E.; Trapido, M.; Preis, S. Oxidation of Aqueous Dexamethasone Solution by Gas-Phased Pulsed Corona Discharge. *Water* **2022**, *14*, 467. [CrossRef]
32. Gottschalk, C.; Libra, J.A.; Saupe, A. *Ozonation of Water and Waste Water*; Wiley-VCH: Weinheim, Germany, 2009. [CrossRef]
33. Ridgway, H.F.; Mohan, B.; Cui, X.; Chua, K.J.; Islam, M.R. Molecular dynamics simulation of gas-phase ozone reactions with sabinene and benzene. *J. Mol. Graph. Model.* **2017**, *74*, 241–250. [CrossRef]
34. Fan, X.; Kang, S.; Li, J.; Zhu, T. Formation of Nitrogen Oxides (N_2O, NO, and NO_2) in Typical Plasma and Plasma-Catalytic Processes for Air Pollution Control. *Water Air Soil Pollut.* **2018**, *229*, 351. [CrossRef]
35. Sakakura, T.; Murakami, N.; Takatsuji, Y.; Morimoto, M.; Haruyama, T. Contribution of Discharge Excited Atomic N, N_2*, and N_2^+ to a Plasma/Liquid Interfacial Reaction as Suggested by Quantitative Analysis. *ChemPhysChem* **2019**, *20*, 1467–1474. [CrossRef]
36. Preis, S.; Panorel, I.; Coll, S.L.; Kornev, I. Formation of Nitrates in Aqueous Solutions Treated with Pulsed Corona Discharge: The Impact of Organic Pollutants. *Ozone Sci. Eng.* **2014**, *36*, 94–99. [CrossRef]
37. Kočí, K.; Krejčíková, S.; Šolcová, O.; Obalová, L. Photocatalytic decomposition of N_2O on Ag-TiO_2. *Catal. Today* **2012**, *191*, 134–137. [CrossRef]
38. Shang, K.; Wang, X.; Zhou, X.; Wang, N. Diagnosis of electron temperature in Ar/O_2 mixed gas and destruction of toluene/benzene by positive dc discharge plasma. *J. Electrost.* **2009**, *67*, 746–750. [CrossRef]

Supplementary Material

Oxidation of Airborne *m*-Xylene in Pulsed Corona Discharge: Impact of Water Sprinkling

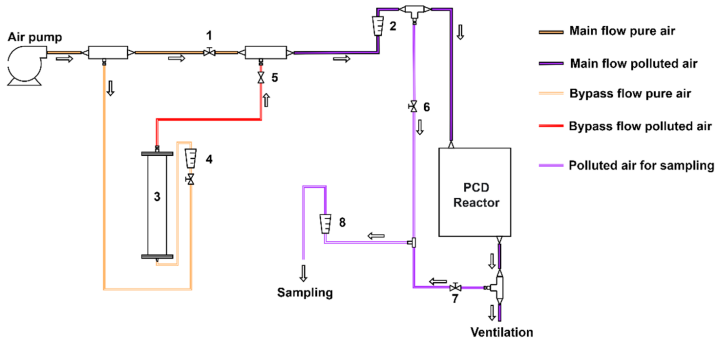

Figure S1. Flow chart of experimental setup: 1—main flow control valve, 2—main flow rotameter, 3—*m*-xylene bubble column, 4—rotameter and control valve for the bypass air flow saturated with *m*-xylene, 5—stopcock valve for *m*-xylene bypass flow, 6—control valve for air inflow sampling, 7—control valve for air outflow sampling, 8—sampling line rotameter

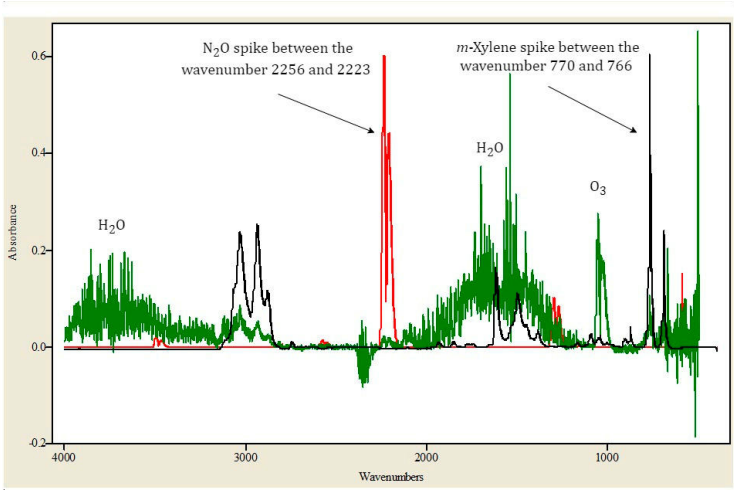

Figure S2. FT-IR specter of gas sample, post PCD treatment (sprinkled). *m*-Xylene input concentration 20 ± 5 ppm, air flow rate 6 $m^3 h^{-1}$, pulse repetition frequency 200 pps, pH 6.0-6.5. Red line—standard for 20 ppm of N_2O, black line—standard for 50 ppm *m*-xylene, green line—air sample.

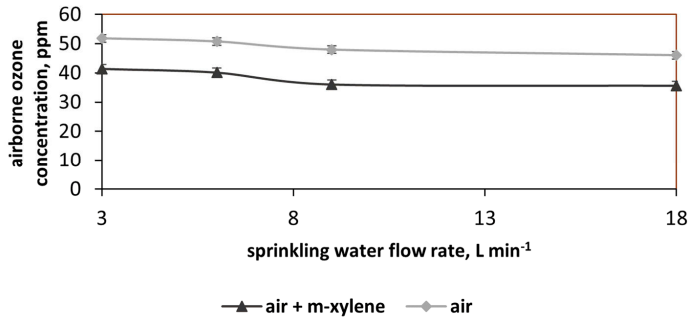

Figure S3. Airborne ozone concentration dependent on sprinkling water flow rate in the absence and presence of m-xylene vapors: airborne m-xylene input concentration 20 ± 5 ppm, air flow rate 6 m^3 h^{-1}, pulse repetition frequency 100 pps, pH 6.0-6.5.

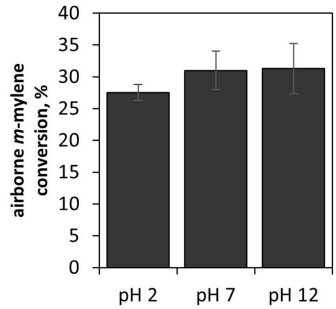

Figure S4. Airborne m-xylene conversion dependent on sprinkling water pH: gaseous m-xylene input concentration 20 ± 5 ppm, air flow rate 6 m^3 h^{-1}, pulse repetition frequency 100 pps, sprinkling water flow rate 9 L min^{-1}

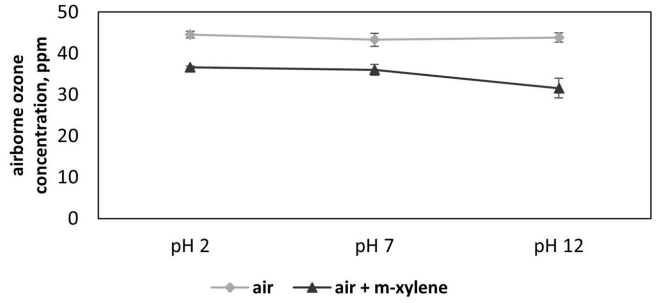

Figure S5. Airborne ozone concentration dependent on sprinkling water pH in the absence and presence of *m*-xylene vapors: airborne *m*-xylene concentration 20 ± 5 ppm, air flow rate 6 m^3 h^{-1}, pulse repetition frequency 100 pps, water flow rate 9 L min^{-1}

Appendix 2

Paper II

K. Altof, M. Krichevskaya, S. Preis, T. Tähemaa, J. Bolobajev. (2024). Ozone-assisted degradation of 2-methoxyethanol in a prototype plug flow photocatalytic reactor, *Chemical Engineering Journal*, 481. https://doi.org/10.1016/j.cej.2023.148488

Chemical Engineering Journal 481 (2024) 148488

Contents lists available at ScienceDirect

Chemical Engineering Journal

journal homepage: www.elsevier.com/locate/cej

Ozone-assisted degradation of 2-methoxyethanol in a prototype plug flow photocatalytic reactor

Kristen Altof [a,*], Marina Krichevskaya [a], Sergei Preis [a], Toivo Tähemaa [b], Juri Bolobajev [a,*]

[a] Laboratory of Environmental Technology, Department of Materials and Environmental Technology, Tallinn University of Technology, Ehitajate tee 5, Tallinn, Estonia
[b] Department of Mechanical and Industrial Engineering, Tallinn University of Technology, Ehitajate tee 5, Tallinn, Estonia

ARTICLE INFO

Keywords:
VOCs
Methyl cellosolve
Advanced oxidation process
Air treatment
Scale up
Photocatalysis

ABSTRACT

Airborne volatile organic compounds (VOCs) present an increasingly relevant health hazard addressed by the EU directive 2016/2284 requiring 40-% reduction in emissions of non-methane VOCs by 2030 in comparison to 2005. Advanced oxidation processes (AOPs) provide a solution for the VOC problem in industry. Among AOPs, pulsed corona discharge (PCD) and photocatalytic oxidation (PCO) are of particular interest in their synergy complementing each other's strengths in energy-efficient manner. In the present study, air polluted with 2-methoxyethanol (2ME) was treated by using a prototype 21.3 L photocatalytic reactor for the pollutant degradation at its variable concentrations (6–50 ppm), irradiances (65–119 W m^{-2}) and residence times (12–77 sec). Further combination of PCO reactor with forthcoming PCD requires studies in ozone photocatalytic degradation as a standalone byproduct and in combination with 2ME. The analysis of variable conditions resulted in singling out the PCO major restrictive parameters, also demonstrating the degradation enhancement, when both 2ME and ozone were present in air. The PCO treatment combined with ozone resulted in degradation of 2ME and ozone for 40 % and 95 %, respectively.

1. Introduction

Volatile organic compounds (VOCs) of toxic character in- and outdoors present an increasingly relevant health hazard to be addressed for proper elimination. It has been found that the indoor air pollutants originate from cleaning products, dwelling construction materials, kitchen activities and furniture, whereas outdoor sources include traffic and neighboring industries [1–4]. Keeping in mind that VOCs are generally hazardous, the countries of the European Union took an obligation to reduce the emissions of non-methane volatile organic compounds (NMVOCs) for 40 % by 2030 as stated in the directive (EU) 2016/2284 of the European Parliament and council states [5]. This puts the European Union under pressure to apply innovative technologies reducing the NMVOCs emissions to achieve the ambitious goal.

Industrial air pollutant emissions reported by Estonia in 2020 to the EU Environmental Board reached 1,260 tons of VOCs [6], demonstrating the industrial exhaust as a relevant source of atmospheric pollution. Wood fabrication and furniture production industries stick out with using solvents and paint bases, e.g., 2-ethoxyethanol (2EE). Twenty-two Estonian enterprises declared emissions of 2EE in a total amount of 13.7 t. Considering the ever-growing demand in goods, the problem with air pollution with VOCs is bound to worsen.

Various exhaust air treatment strategies have been developed to reduce air pollution [7,8] including filtration systems using adsorbents with traditional drawbacks of VOCs transfer to the solid phase at a limited capacity. To truly rid the air from pollutants, these must be degraded to less harmful substances, ideally to carbon dioxide and water.

Oxidation approaches used for air purification include advanced oxidation processes (AOPs) - ozonation, photocatalytic oxidation (PCO), and electric discharge plasma [9–11]. Among them, pulsed corona discharge (PCD) [12,13] and photocatalytic oxidation (PCO) [14] deserve particular attention for showing promising results in degrading VOCs at high energy efficiency, demonstrating the best performance when used in combination [15]. This explains the keen interest to test the performance of combined PCD and PCO in a twostep combination for air purification.

Pulsed corona discharge technology studied for oxidation of waterborne organic pollutants has been showing remarkable energy efficiency [16,17]. One of the main problems of PCD application in air treatment, however, is residual ozone, a side product of air ionization considered as the secondary air pollution. Photocatalytic processes are known to

* Corresponding authors.
E-mail addresses: kristen.altof@taltech.ee (K. Altof), juri.bolobajev@taltech.ee (J. Bolobajev).

https://doi.org/10.1016/j.cej.2023.148488
Received 1 September 2023; Received in revised form 30 November 2023; Accepted 30 December 2023
Available online 31 December 2023

degrade ozone thus solving the problem, usefully extending the photocatalyst lifetime [18–21]. Further understanding the PCO mechanism in simultaneous VOCs and ozone abatement with spreading the knowledge to a wide spectrum of volatiles is a pre-requisite for the progress in the combined PCD/PCO applications.

A prototype PCO reactor was built and tested with ozone and 2-methoxyethanol (2ME) in combinations. 2ME was chosen as a more hazardous model VOC rather than similar glycol ether 2EE for both substances being used in solvents and carriers in paints [22], with the occupational exposure limit of 1 ppm [23–25]. The refractory character of 2ME brings to front the experimental effort targeting the abatement of a recalcitrant VOC in a pilot-size PCO reactor thus making a good step forward in the technology implementation. This gives incentive to study the energy efficient AOP technologies helping to avoid health problems and damage to the biosphere caused by 2ME emissions applying a larger scale reactor. In the study, the 2ME industrial pollution was simulated with the PCO in a reactor varying light intensity, the pollutant and ozone concentrations at high levels, and the air flow rates in a wide span of values.

2. Materials and methods

2.1. Chemicals and reagents

Analytical grade 2ME ($C_3H_8O_2 \geq 99$ %) was purchased from Fisher Chemicals (USA) and used without further treatment. Ozone was generated onsite from air using 10G Lab Ozone Generator (A2Z Ozone, USA). Titanium dioxide P25 was purchased from Evonik Industries AG (Germany) and ethanol ($C_2H_5OH \geq 99$ %) - from Sigma-Aldrich (USA).

2.2. Air pollution

The 2ME vaporization setup was operated in continuous mode (Fig. 1). For the generation of polluted air, 2ME was vaporized using a bubble column 3. The Eco Air Pump PA200 (Jecod Co. Ltd., People's Republic of China) with flow rate varying from 1 to 6 $m^3\ h^{-1}$ fed air through the main line to the reactors. A bypass controlled by valve 5 directed a 1/400 to 1/100 vol part of the main air flow through a bubble column 3 (H = 700 mm; d_i = 50 mm) filled with liquid 2ME (750 ml). As the air passed through the column, it became saturated with vapor and was mixed with the main flow through the valve 7 and subsequently directed to the PCO reactor. Ozone was generated onsite in the ozone generator with the flow controlled by valve 6 and mixed with the main air flow. The VOC concentration was regulated and maintained with air/bypass flow ratio. All experiments were performed at the room temperature, 22 °C, atmospheric pressure, and relative humidity of 30 ± 3 % RH at 22 °C.

2.3. Reactor

The plug flow PCO reactor is flat bedded with a transparent cover (2 mm polyethylene terephthalate, PET) sealing in the gas passing through a maze-like chamber where glass plates covered with TiO_2 lay on the chamber floor as shown in Fig. 2. Entering the PCO reactor, polluted air flows through a series of chambers coming into contact with the surface of the photocatalyst. The internal size of the reactor is, mm: L = 996, W = 534, and H = 40, with a total volume of 21.3 L. The reactor is divided into five sections sized 4.26 L with stainless-steel plates with holes in the end of each section providing diagonal air flow along the sections. The air flow rates in the reactor were varied from 1.0 to 6.0 $m^3\ h^{-1}$ corresponding to the residence times from 77 to 16 s, respectively; the

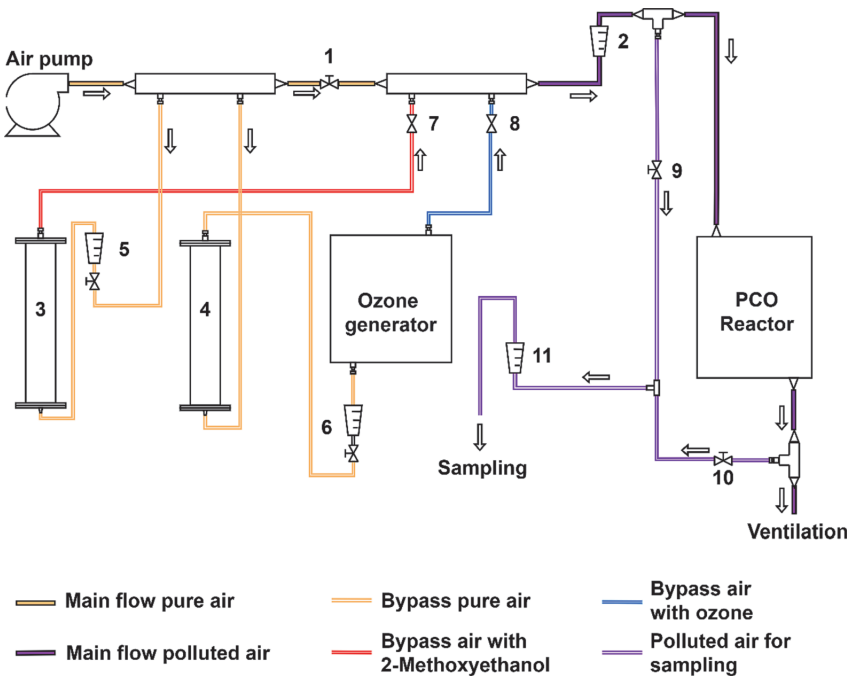

Fig. 1. Experimental setup: 1 – main flow control valve, 2 - main flow rotameter, 3 – 2ME column, 4 – air dryer filled with silica gel for the generation of ozone, 5 – rotameter and control valve for the 2ME-saturation bypass, 6 – rotameter and control valve for ozone generator, 7 – shut off valve for 2ME bypass, 8 - shut off valve for ozone generator, 9 – control valve for main airflow sampling before the PCO reactor, 10 - control valve for main airflow sampling after the PCO reactor, 11 – sampling line rotameter.

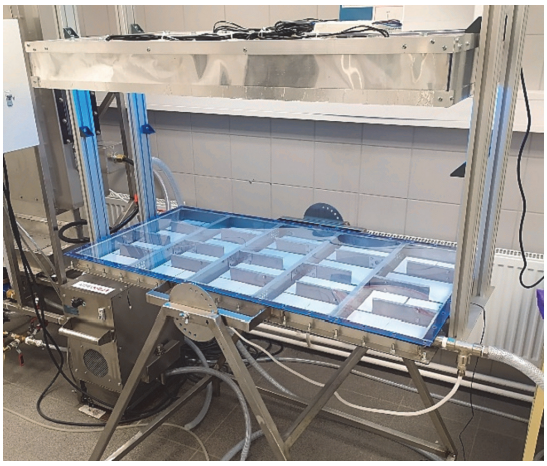

Fig. 2. Photocatalytic oxidation reactor (The picture is for illustration purpose only; for experiments the lamps were lowered to 7 cm above the reactor).

average air velocity at the reactor inlet was 0.2 – 1.3 m s^{-1}, and 0.003 – 0.2 m s^{-1} in the reactor section. To assure the turbulent contact of polluted air with the surface of the catalyst, three additional stainless-steel partition walls were placed across the channels providing the zigzag trajectory of the gas flow along the section. In order to check the airflow distribution in the reactor, a software simulation was performed with SolidWorks (Fig. 3) demonstrating flow trajectory within the reactor chambers. The experimental runs for PCO of 2ME and decomposition of ozone were carried out with and without the partition walls in each section. No difference in the reactor's ability to degrade pollutants, however, was detected at the average flow rate of 5.0 m^3 h^{-1} confirming sufficient turbulence of air passing through the reactor with no additional mass transfer intensification.

2.4. Experimental procedure

Prior to each experimental run, polluted air was fed to the reactor in a continuous mode for at least 30 min in the absence of light to saturate the catalyst with the pollutant and exclude adsorption from the overall pollutant's removal. Initial gaseous samples were collected after the air had passed through the dark reactor ensuring the adsorption equilibrium. After that, the UV-A TL-D 15 W lamps (Philips, Germany) were switched on and air samples were withdrawn until the outlet 2ME concentration stabilized. The 2ME concentrations and the formation of gaseous byproducts were registered with FT-IR spectroscopy using Interspec 200-X spectroscope (Interspectrum OÜ, Estonia) and analyzed with Essential FTIR (Operant LCC) software with (FDM, HiRes VPFTIR for Quant) database. The 2ME content in the air was measured using a 20 m metal body gas cell (Specac, United Kingdom) at a bandwidth between 2921 and 2838 cm^{-1} having the least interference from other substances. Gaseous ozone content was measured with ozone analyzer (Anseros Klaus Nonnenmacher GmbH, Germany).

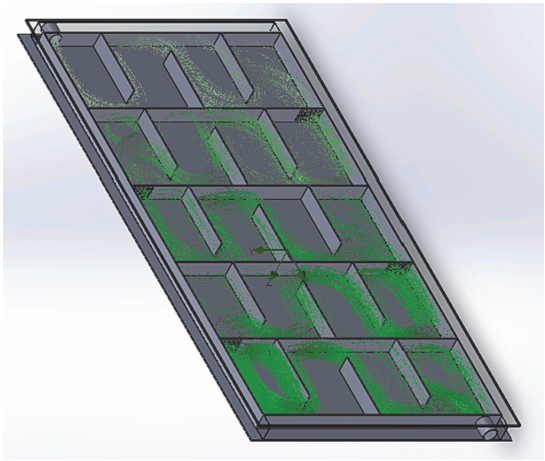

Fig. 3. Air flow trajectories simulated in photocatalytic oxidation reactor at the gas flow of 5.0 m^3 h^{-1}.

2.5. Preparation of photocatalytic coating

Powdery P25 titanium dioxide AEROXIDE® TiO_2 P25 from Evonik ≥ 99.5 % TiO_2 [26], crystalline with predominantly anatase structure (rutile fraction 13.4 ± 7 wt%), was used as photocatalytic material. TiO_2 was coated on 115 x 90 x 2 mm glass plates by spraying as described by Kask et al. [18] and shown in Fig. 4. Forty glass plates covered with 1.53 ± 0.11 mg cm^{-2} TiO_2 were fitted into the reactor, making the overall catalyst surface area equal to 4,140 cm^2. The thickness of the photocatalytic coating was measured using the surface profiler TENCOR P-10 showing a range of 1 μm. The image of the coating with specific weight of 1.4 mg cm^{-2} TiO_2 P25 was obtained by the field emission scanning electron microscopy (FE SEM, Dual-Beam Helios Nanolab 600, FEI) and is presented in supplementary material (Figure S1). The UV-A radiation was provided by twenty TL-D 15 W lamps positioned at 7.0 cm above the catalyst surface (Fig. 5). The intensity of light was regulated by the number of switched-on lamps in sets of five distributed evenly along the reactor.

Spectrometry parameters of UV-A radiation within 315 – 400 nm were measured using a USB 2000 + UV–VIS spectrometer (Ocean Optics, USA). The dependence of the average irradiance at the photocatalyst surface on the nominal power is seen in Fig. 6, ranging from 29 to 119 W m^{-2} provided by the number of lamps from 5 to 20, respectively.

Fig. 4. Glass plates covered with TiO_2 by spraying.

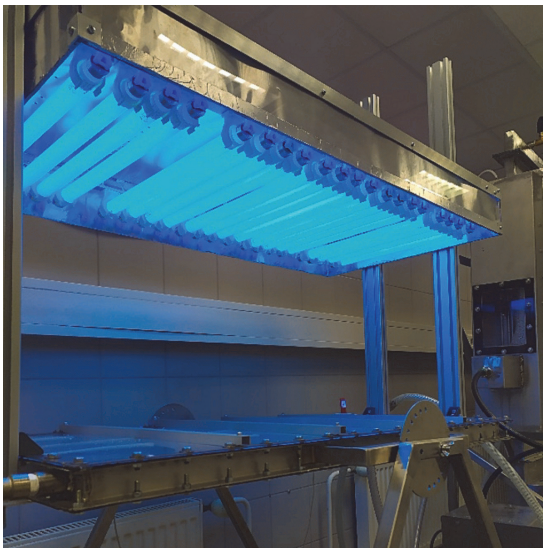

Fig. 5. UV-A lamps above the PCO reactor (The picture is for illustration purpose only; for experiments the lamps were lowered to 7 cm above the reactor).

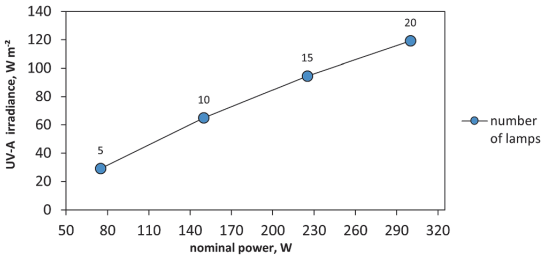

Fig. 6. Irradiance of the photocatalyst vs nominal power consumed by the UV-A lamps.

2.6. Reference experiments

To exclude the possible role of photolysis induced by UV-A, the experiments were conducted in the absence of photocatalyst. Air mixtures containing 2ME and ozone at various concentrations were led through the reactor under UV-A radiation. No changes in 2ME concentration with or without ozone were observed. Small, below 10 % conversion of ozone was detected with the residence time as long as 77 sec. The effect of ozone photolysis was thus found to be neglectable in the current study. Even though it has been suggested that ozone degradation in gas phase could play a role in the oxidation rate of VOCs [19] no changes of 2ME concentration in the presence of ozone and the absence of photocatalyst could be detected. Thus, it leads to the conclusion that gas phase oxidation is negligible at the residence times applied in the experiments, as was also observed in other studies [18,27,28].

3. Results and discussion

3.1. Photocatalytic degradation of ozone

In anticipation of combining the PCD and PCO reactors to a two-step air purification system, ozone with its important role in oxidation of VOCs and the maintenance of the photocatalyst activity was studied for its photocatalytic conversion. Degradation of ozone in air with variations in irradiance and residence time may be seen in Fig. 7. The photocatalyst irradiance has a clear effect on conversion as quadrupling the energy input from 29 to 119 W m^{-2} increases the conversion of ozone by the factor of 1.5–1.9. Small impact of irradiance is consistent with the kinetic regime of ozone decomposition at the photocatalyst surface with the rate limited by chemical reaction. The air residence time controlled by the flow rate varied between 7 and 77 sec at the flow rates between 166 and 17 L min^{-1}, respectively, and also showed conversion reasonably improved with extended contact: the residence time increased almost tenfold provides only doubled ozone conversion confirming the kinetic limitation of the reaction with excess amounts of ozone.

The role of residence time in the photocatalytic degradation of substrate could be explained in terms of the mass balance for ideal plug flow reactor. With respect to a substrate, the mass-balance is written in general word statement Eq. (1) with corresponding mathematical expression Eq. (2) as follows:

$$\text{Accumulation} = \text{inflow} - \text{outflow} + \text{generation} \tag{1}$$

$$\frac{\partial C}{\partial t}\Delta V = QC|_{L} - QC|_{L+\Delta L} + r_c \Delta V, \tag{2}$$

where ΔV, Q, C, L, and r_c are differential volume element in reactor section, volumetric flow, concentration of substrate in air, flow path, and reaction rate for heterogeneous photocatalysis, respectively.

Eq. (2) undergoes a series of transformations, which are omitted here for the sake of brevity. The transformations end up by taking the limit as ΔL approaches zero, where A is the surface area of the reactor Eq. (3):

$$\frac{\partial C}{\partial t} = -\frac{Q}{A}\frac{\partial C}{\partial L} + r_c \tag{3}$$

With respect to r_c, the most common decay model observed in PCO is Langmuir-Hinshelwood (LH) kinetics of heterogeneous catalysis, Eq. (4) [29–33]:

$$r_c = -\frac{k_r K C}{1 + KC} \tag{4}$$

where k_r, K, and C are limiting rate constant of reaction, adsorption equilibrium constant, and substrate concentration, respectively. Considering the steady-state conditions ($\partial C/\partial t = 0$) and LH reaction rate Eq. (4), the equation Eq. (5) for a plug flow reactor becomes as follows:

$$\frac{Q}{A}\frac{dC}{dL} = -\frac{k_r K C}{1 + KC} \tag{5}$$

Under condition $KC \ll 1$, Eq. (5) could be approximated to the first order kinetics. The zero order is observed at surface saturation when $KC \gg 1$, i.e., zero order suggests occupation of all reaction sites by substrate, and the LH reaction rate approximates to a constant (k_{obs}), Eq. (6),

$$\frac{Q}{A}\frac{dC}{dL} = -k_{obs} \tag{6}$$

Integrating Eq. (6) between the limits C = C_0 and C = C and corresponding L = 0 and L = L yields the linear dependence between residence time and concentration of substrate Eq. (7):

$$C = C_0 - \frac{A}{Q} \bullet L \bullet k_{obs} = C_0 - \tau \bullet k_{obs} \tag{7}$$

A pseudo-zero order reaction with the substrate initial concentration having no influence on the reaction kinetics has also been observed earlier in similar flow reactors [34,35]. With respect to ozone degradation, it is evident that linear paths (Fig. 7) have cross-sections with Y-axis significantly below the initial concentration (C_{in} = 22.6 ppm), which is inconsistent with Eq. (7). Besides, clear deviations from the

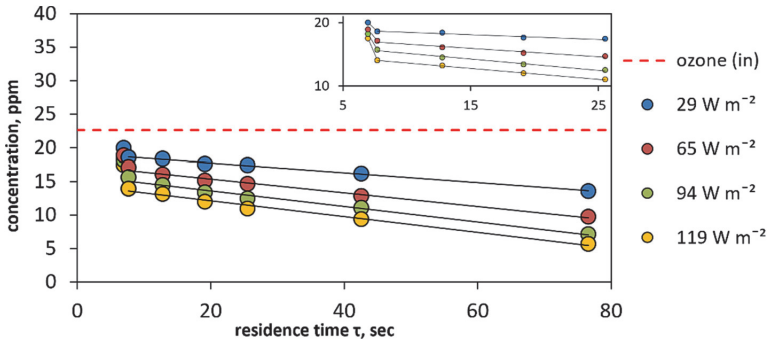

Fig. 7. Photocatalytic degradation of ozone dependent on UV-A irradiance and residence time: initial concentration of ozone (in) 22.6 ppm, inset – ozone degradation at residence time from 7 to 26 sec.

linearity are seen at residence time of 7 sec (Fig. 7, see inset). The reason could lay in a diffusion-controlled process at short residence times, where the reaction rate is limited by the substrate transport to the active sites of the photocatalyst.

3.2. Photocatalytic degradation of 2ME

The effects of 2ME inlet concentration and irradiance on the PCO rate were studied. The results obtained at the residence time of 12.8 sec are seen in Fig. 8. The irradiance doubled from 65 to 119 W m^{-2} resulted in only slight change in degradation rate confirming the diffusion-controlled process. It is reasonable to presume that solar light, the UV-A component of which does not exceed 90 W m^{-2} at the Earth's surface [36], will not substantially improve the PCO performance if compared with the studied light irradiances.

2ME degraded in the PCO reactor for about 4 ± 1 ppm within the tested residence time regardless of its input concentration thus following the pseudo-zero order kinetic model. It has also been stated that at very high light intensities, the experimental data are approximated to the zero-order kinetics with respect to the light intensity because of diffusion limitation for the transport of reagent molecules to the photocatalyst surface [37]. The substrate degradation rate becomes invariant to the UV-A irradiance.

The effect of residence time on PCO of 2ME with its initial concentration 20 ± 2 ppm at the highest irradiance of 119 W m^{-2} is seen in Fig. 9. The residence time varied between 12.8 and 77.0 sec was provided with the air flow rate from 6.0 to 1.0 m^3 h^{-1}, respectively, showing a moderate effect on oxidation performance: conversions of 2ME varied from 3.6 to 4.9 ppm at residence times of 12.8 and 77.0 sec,

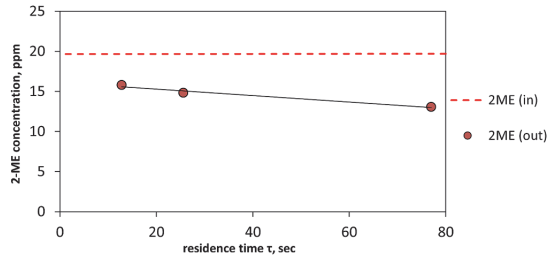

Fig. 9. Photocatalytic degradation of 2ME dependent on the air residence time: 2ME inlet concentration 19.7 ± 0.2 ppm, irradiance 119 W m^{-2}.

respectively. Thus, the contact time increased more than six times provides degradation of 2ME accelerated for only about 36 %, indicating equilibrium established at the photocatalyst surface densely occupied with the VOC molecules attributable to the high pollutant concentrations. Weak dependence of oxidation rate on residence time is consistent with the LH description of descendent rate curve approximating a constant manifesting the kinetic regime of chemisorption Eq. (6). Higher conversions may be achieved by increasing the residence time on account of substantially decreased flow rate or increased reactor size.

3.3. Photocatalytic degradation of 2 ME in ozonized air

The results of simultaneous photocatalytic degradation of 2ME and

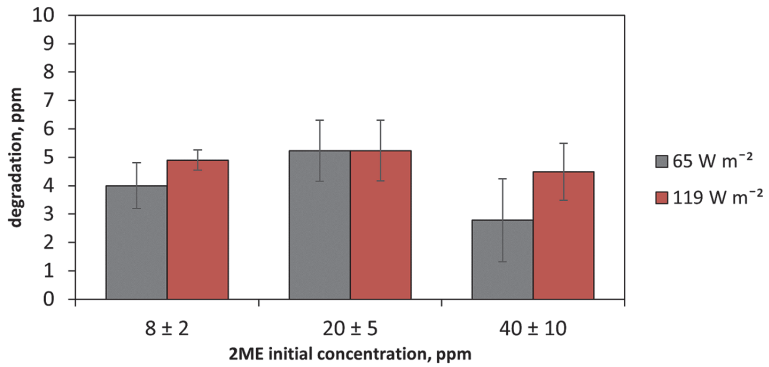

Fig. 8. Photocatalytic degradation of 2ME dependent on its inlet concentration and photocatalyst irradiance at the residence time 12.8 sec.

ozone are shown in Fig. 10. The experimental conditions were chosen imitating PCD and PCO combined action, in which ozone concentration remains more or less constant determined by the air flow rate and discharge parameters, whereas the VOC concentration may vary dependent on external parameters at the point of air pollution. In the study, the inlet ozone concentration was kept at 33 ± 3 ppm, and concentrations of 2ME were chosen as 8 ± 2, 20 ± 5, and 40 ± 10 ppm at maximum available irradiance and rather short residence time. One can see a significant difference in 2ME oxidation rates promoted with ozone compared to unassisted PCO: maximum 2ME degradation observed in non-assisted PCO did not exceed 5 ppm regardless of its inlet concentration, whereas the one achieved in PCO with ozone tripled the number at the highest 2ME concentration. Ozone mixed with 2ME at the highest content of the latter also decomposed faster showing 80 % conversion (Fig. 7 and Fig. 10): similar ozone conversion rates in absence of 2ME may only be seen at residence time of 77 sec.

In simultaneous degradation of 2ME and ozone, one can see the conversion of both increased with growing concentration of 2ME. This phenomenon was observed and explained earlier by formation of additional oxidative species, e.g., ozonides [38,39]. Characteristic for unsaturated and aromatic hydrocarbons oxidized by ozone with formation of unstable ozonides, these are less probable to form when the 2ME molecule reacts having no moieties attractive for the electrophilic attacks and possibilities for ozonide formation or peroxo bridging. This makes ozonides formation mechanism less relevant to the observed oxidation acceleration. Another study pointed out that ozone degradation in gas phase could play a role in the oxidation rate of VOCs [19]. Yet photolysis of ozone was found to be neglectable in the current study. It has also been stated that ozone can prohibit the recombination of electron-hole pairs on the surface of TiO_2 [40,41]. Possible pathways of oxidants formation in a PCO reactor in presence of ozone were summarized by Huang et al (2011) [42]. In the presence of TiO_2 under UV-A irradiation, ozone acts as an electron acceptor and as a source of reactive oxygen species maintaining the photocatalyst activity [18,27,28,43]. The recombination of electron-hole pairs on TiO_2 surface is slowed down freeing up electron holes for the oxidation of 2ME. The higher conversion rate of ozone in the presence of 2ME could be explained by the formation of intermediates and overall higher concentration of organic material reacting with ozone and ozone-derived radicals freeing up even more active sites on the catalyst surface.

The impact of residence time on 2ME conversion in the presence of ozone can be seen in Fig. 11. A gaseous mixture of 2ME with ozone at constant inlet concentrations of 24 ± 1 and 26 ± 1 ppm, respectively, was treated in the PCO reactor with residence times varied between 77.0 and 12.8 sec, i.e., flow rates between 1.0 and 6.0 $m^3\ h^{-1}$, respectively.

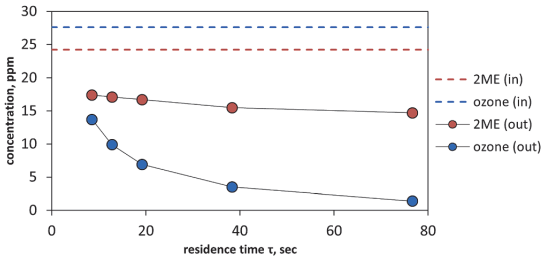

Fig. 11. Photocatalytic degradation of 2ME and ozone in their mixture with inlet concentrations 19 ± 1 and 26 ± 1 ppm, respectively, irradiance 119 W m^{-2}.

Irradiance was kept constant at the highest available level of 119 W m^{-2}.

Conversions of 2ME and ozone seem to follow a pattern of deeper ones at longer residence times. The maximum conversion of 2ME at 77 sec residence time reached 40 %, i.e., 9.5 ppm oxidized out of inlet 24 ± 1 ppm. At the same time, over 95 % of ozone was converted resulting in the highest VOC removal in the current study. This confirms the assumptions of residence time and ozone having the strongest impact on the reactors performance in VOCs removal. Besides, noteworthy is the degradations of 2ME and ozone not following the pseudo zero-order reaction rate when combined. The linearization result suggests a second order reaction kinetics in respect to both reactants with their degradation being directly and/or indirectly affected by each other's concentration, thus suggesting PCO not being the only oxidation pathway in presence of ozone.

3.4. Degradation byproducts of 2ME and ozone

Ideally, the ultimate target of PCO reactors following the PCD ones is complete mineralization of VOCs rendering mute the question of byproducts. Yet as the complete mineralization of 2ME is not observed, the question of byproducts requires analysis. Three byproducts were detected in the gas phase, formic acid, methyl formate, and formaldehyde, having the two formers registered in nearly every experiment except for PCO at 65 W m^{-2} irradiance. Formic acid and methyl formate reached their maximum concentrations, 10 and 15 ppm, respectively, in experiments, where 2ME at its inlet concentration of 40 ± 10 ppm was degraded in the presence of ozone regardless of irradiance (Supplementary material, Fig S1). Formaldehyde could only be detected at 2ME degradation in the presence of ozone, reaching its concentration up to

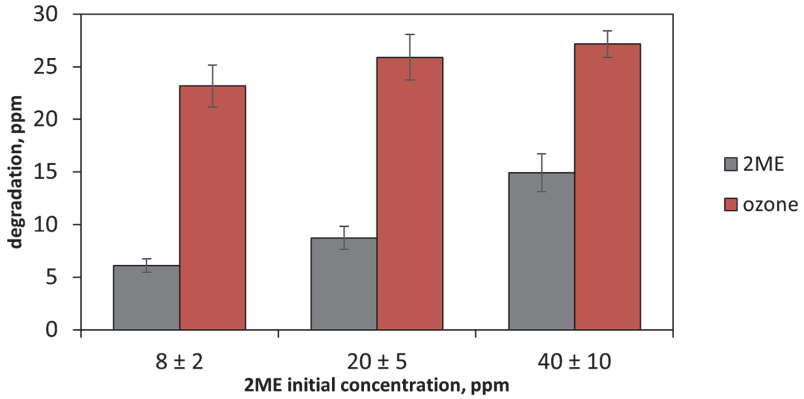

Fig. 10. Photocatalytic degradation of 2ME and ozone in their mixtures dependent on 2ME concentration: ozone inlet concentration 33 ± 3 ppm, residence time 12.8 sec, irradiance 119 W m^{-2}.

12 ppm (Supplementary material, Fig S2).

Figure S2 (Supplementary material) shows the amount of intermediate products unaffected by the increased residence time. Since the amount of degraded 2ME increases with residence time, but the content of intermediates in gaseous phase changes negligibly, an outrunning degradation of intermediates is seen. Thus, further increase in the residence time in a reactor or extending of the reactors' line should lead to the decomposition of intermediate products.

The simplified outline of 2ME PCO is suggested in Fig. 12. The degradation of 2ME employing HO• and $\bullet O_2^-$ as probable oxidation species generated by photocatalysis involves primarily hydrogen atom abstraction, ether bond cleavage, addition, hydroxylation, and decarboxylation reactions. The present degradation pathway has priori predictions and was based on the mechanisms of the gas-phase reactions of HO• with ethers, alcohols, aldehydes, and carboxylic acids published by Atkinson [44].

Hydroxyl radical attack of hydroxyl group of 2ME (1) is associated with H atom abstraction at C-H adjacent to hydroxyl group producing the corresponding radical. The radical reacts with atmospheric oxygen (2) to yield 2-methoxyacetaldehyde and HO_2•. The following series of reactions including hydrogen abstraction followed by HO• addition (3) leads to the formation of 2-methoxyacetic acid, which undergoes the decarboxylation transformation (4) producing carbon dioxide and dimethylether. The HO• attack proceeds via H atom abstraction from C-H bond of ether (5) producing methoxymethyl radical. The formation of methyl formate from this radical is well described by Atkinson (1986). Instead of ether bond decomposition, the reaction with reactive oxygen species dominates (6) yielding methyl formate. The formation of more toxic intermediate compounds formaldehyde and formic acid is associated with either 2ME ether bond cleavage or further decomposition of methyl formate.

All formed intermediate products can be successfully mineralized, which requires a targeted study of operating conditions for the practical application of a specific reactor modification. It would be necessary to determine the maximum concentrations of VOCs and the minimum residence time at which nearly complete mineralization of the initial pollutants can be achieved.

4. Conclusions

An upscaled PCO reactor was tested in removal of 2ME and ozone from air being considered as a simulation of PCD and PCO reactors combined in a sequence. The reactor operates continuously and can be used outdoors using the solar radiation to breach the band gap of TiO_2, thus providing an energy-efficient way to remove VOCs and ozone from the airstreams. However, the results of the present research show the reactor being effective only at rather long retention times (77 s) and low pollutant concentrations (<10 ppm). For higher pollutant's concentration exceeding 10 ppm, the PCO reactor is presumed to function effectively in a tandem with PCD partially oxidizing pollutants and providing ozone. Gaseous intermediate products of 2ME degradation were also studied. Formaldehyde, formic acid and methyl format could be detected. Considering the toxicity of mentioned by-products it is crucial that in future studies the operating parameters for PCO reactors will be optimized to completely oxidize all intermediate products.

The PCO reactor's performance in degrading 2ME is controlled by irradiance, increasing the UV-A irradiance from 65 to 119 W m^{-2} resulted in slight change. Residence time plays an important role in PCO as degradation of 20 ppm 2ME varied from 3.5 to 5.0 ppm at residence times of 12.8 and 77.0 sec, respectively. At rather high 2ME concentrations exceeding 10 ppm, PCO turned out to follow the pseudo-zero-order reaction kinetics, i.e., the efficacy of pollutant removal appears invariant to its concentration.

In this perspective, the performance of standalone PCO reactor could be improved in three ways. Firstly, the activity of photocatalyst needs improvement, i.e., the state-of-the-art materials or coating techniques would accelerate PCO. Photocatalytic materials activated by a broader light spectrum than anatase TiO_2 could prove useful using more energy from the light sources. Secondly, increasing the photocatalyst surface should also result in faster PCO [18], e.g., the inner walls and the cover of the reactor could be coated with the photocatalyst. This question deserves studies for unclear effect of indirect illumination or the coated cover screening-off the light.

Thirdly, residence time is a key factor in photocatalytic oxidation. Therefore, increasing the residence time by increasing the reactor size or connecting multiple reactors in series can improve the overall efficiency of the process as studies have shown before [18,45]. It should be noted that an increase in the reactor size should go along with an increase in the surface area of the photocatalytic coating.

However, the true potential of the PCO reactor is revealed when used with ozone as a complementary oxidant nearly doubling 2ME degradation from 5.0 to 9.5 ppm. Ozone extends the lifetime of electron-hole pairs on the photocatalyst surface, adding also extra oxidant species improving the effectiveness of the PCO reactor. This potential is to be disclosed in upcoming research of PCO reactor paired with PCD plasma. It is also important to stress that the PCO should not be used for merely degrading ozone as pure ozone degradation follows the zeroth order reaction kinetics and is only influenced by residence time. The PCO reactor should be used with ozone and small amounts of VOCs which reveals second order reaction kinetic with the ability to degrade 95 % of ozone and accelerate oxidation of residual VOCs.

CRediT authorship contribution statement

Kristen Altof: Conceptualization, Data curation, Formal analysis, Investigation, Methodology, Validation, Visualization, Writing – original draft, Writing – review & editing. **Marina Krichevskaya:** Conceptualization, Data curation, Formal analysis, Methodology, Supervision, Validation, Visualization, Writing – original draft, Writing – review & editing. **Sergei Preis:** Formal analysis, Funding acquisition, Investigation, Project administration, Resources, Writing – original draft, Writing – review & editing. **Toivo Tähemaa:** Formal analysis, Resources, Writing – review & editing. **Juri Bolobajev:** Conceptualization, Data curation, Formal analysis, Investigation, Methodology, Supervision, Validation, Visualization, Writing – original draft, Writing – review & editing.

Declaration of competing interest

The authors declare that they have no known competing financial interests or personal relationships that could have appeared to influence the work reported in this paper.

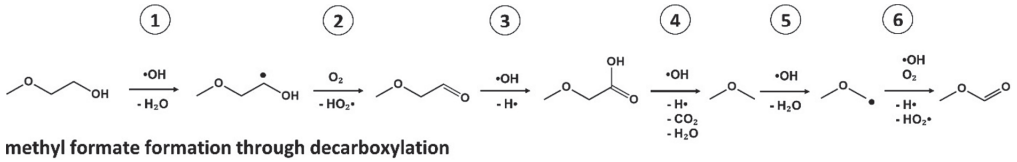

Fig. 12. Rationale of gaseous 2ME degradation induced by reactive oxygen species.

Data availability

Data will be made available on request.

Acknowledgements

This work was supported by the Institutional Development Program of Tallinn University of Technology for 2016–2022, project 2014-2020.4.01.16-0032 from EU Regional Development Fund.

Appendix A. Supplementary data

Supplementary data to this article can be found online at https://doi.org/10.1016/j.cej.2023.148488.

References

[1] U. Schlink, A. Thiem, T. Kohajda, M. Richter, K. Strebel, Quantile regression of indoor air concentrations of volatile organic compounds (VOC), Sci. Total Environ. 408 (2010) 3840–3851, https://doi.org/10.1016/j.scitotenv.2009.12.002.
[2] R.D. Edwards, J. Jurvelin, K. Koistinen, K. Saarela, M. Jantunen, VOC source identification from personal and residential indoor, outdoor and workplace microenvironment samples in EXPOLIS-Helsinki, Finland, Atmos Environ. 35 (2001) 4829–4841.
[3] H.L. Wang, L. Nie, J. Li, Y.F. Wang, G. Wang, J.H. Wang, Z.P. Hao, Characterization and assessment of volatile organic compounds (VOCs) emissions from typical industries, Chin. Sci. Bull. 58 (2013) 724–730, https://doi.org/10.1007/s11434-012-5345-2.
[4] J.K. Pearson, European solvent VOC emission inventories based on industry-wide information, Atmos Environ. 204 (2019) 118–124, https://doi.org/10.1016/j.atmosenv.2019.02.014.
[5] European Parliament and of the Council of the European Union, Directive (EU) 2016/2284 of the European Parliament and of the Council of 14 December 2016 on the reduction of national emissions of certain atmospheric pollutants, amending Directive 2003/35/EC and repealing Directive 2001/81/EC, 2016.
[6] E.B. Republic of Estonia, https://kotkas.envir.ee/annual_reports_registry, Keskkonnaotsuste infosüsteem, (2022).
[7] Joint Research Centre Directorate B – Growth and Innovation Circular Economy and Industrial Leadership Unit European IPPC Bureau, Best Available Techniques (BAT) Reference Document for Common Waste Gas Management and Treatment Systems in the Chemical Sector, Brussels, 2019.
[8] W. Zou, B. Gao, Y.S. Ok, L. Dong, Integrated adsorption and photocatalytic degradation of volatile organic compounds (VOCs) using carbon-based nanocomposites: a critical review, Chemosphere 218 (2019) 845–859, https://doi.org/10.1016/j.chemosphere.2018.11.175.
[9] S. Almaie, V. Vatanpour, M.H. Rasoulifard, I. Koyuncu, Volatile organic compounds (VOCs) removal by photocatalysts: a review, Chemosphere 306 (2022), https://doi.org/10.1016/j.chemosphere.2022.135655.
[10] Y. Zhang, Y. Wang, R. Xie, H. Huang, M.K.H. Leung, J. Li, D.Y.C. Leung, Photocatalytic oxidation for volatile organic compounds elimination: from fundamental research to practical applications, Environ Sci Technol. 56 (2022) 16582–16601, https://doi.org/10.1021/acs.est.2c05444.
[11] Y. Huang, S.S.H. Ho, R. Niu, L. Xu, Y. Lu, J. Cao, S. Lee, Removal of indoor volatile organic compounds via photocatalytic oxidation: a short review and prospect, Molecules 21 (2016), https://doi.org/10.3390/molecules21010056.
[12] C. Du, X. Gong, Y. Lin, Decomposition of volatile organic compounds using corona discharge plasma technology, J Air Waste Manage Assoc. 69 (2019) 879–899, https://doi.org/10.1080/10962247.2019.1582441.
[13] I. Kornev, S. Preis, Aqueous benzene oxidation in low-temperature plasma of pulsed corona discharge, Journal of Advanced Oxidation Technologies. 19 (2016).
[14] M. Kask, Combination of Advanced Oxidation Methods for the Energy-Efficient Abatement of Aqueous and Gaseous Hazardous Pollutants, Doctoral Thesis, Tallinn University of Technology, 2021.
[15] L. Khezami, P. Nguyen-Tri, W.A. Saoud, A. Bouzaza, A. El Jery, D. Duc Nguyen, V. K. Gupta, A.A. Assadi, Recent progress in air treatment with combined photocatalytic/plasma processes: a review, J Environ Manage. 299 (2021), https://doi.org/10.1016/j.jenvman.2021.113588.
[16] L. Onga, E. Kattel-Salusoo, S. Preis, N. Dulova, Degradation of anti-inflammatory drug dexamethasone by pulsed corona discharge: the effect of peroxycompounds addition, J Environ Chem Eng. 10 (2022), https://doi.org/10.1016/j.jece.2022.108042.
[17] P. Tikker, D. Nikitin, S. Preis, Oxidation of aqueous bisphenols A and S by pulsed corona discharge: Impacts of process control parameters and oxidation products identification, Chem. Eng. J. 438 (2022), https://doi.org/10.1016/j.cej.2022.135602.
[18] M. Kask, J. Bolobajev, M. Krichevskaya, Gas-phase photocatalytic degradation of acetone and toluene, and their mixture in the presence of ozone in continuous multi-section reactor as possible air post-treatment for exhaust from pulsed corona discharge, Chem. Eng. J. 399 (2020), https://doi.org/10.1016/j.cej.2020.125815.
[19] P. Zhang, J. Liu, Photocatalytic degradation of trace hexane in the gas phase with and without ozone addition: kinetic study, J Photochem Photobiol A Chem. 167 (2004) 87–94, https://doi.org/10.1016/j.jphotochem.2004.05.015.
[20] J. Kim, P. Zhang, J. Li, J. Wang, P. Fu, Photocatalytic degradation of gaseous toluene and ozone under UV254+185 nm irradiation using a Pd-deposited TiO_2 film, Chem. Eng. J. 252 (2014) 337–345, https://doi.org/10.1016/j.cej.2014.05.015.
[21] P. Fu, P. Zhang, J. Li, Photocatalytic degradation of low concentration formaldehyde and simultaneous elimination of ozone by-product using palladium modified TiO_2 films under UV254+185nm irradiation, Appl Catal b. 105 (2011) 220–228, https://doi.org/10.1016/j.apcatb.2011.04.021.
[22] I.N. Sax, Dangerous Properties of Idustrial Materials, Sixth Edition, Van Nostrand Reinhold Company Inc., New York, 1984.
[23] The European Chemicals Agency, European Chemicals Agency, Https://Echa.Europa.Eu/Substance-Information/-/Substanceinfo/100.003.377. (2023).
[24] R.R. Miller, E.-A. Hermann, J.T. Young, T.D. Landry, L.L. Calhoun, Ethylene glycol monomethyl ether and propylene glycol monomethyl ether: metabolism, disposition, and subchronic inhalation toxicity studies, Environ Health Perspect. 57 (1984) 233–239.
[25] G. Bagchi, D.J. Waxman, Toxicity of ethylene glycol monomethyl ether: Impact on testicular gene expression, Int J Androl. 31 (2008) 269–274, https://doi.org/10.1111/j.1365-2605.2007.00846.x.
[26] Evonik Industries AG, AEROXIDE® TiO_2 P 25, Https://Www.Silica-Specialist.Com/En/Product/PR_52000356. (2023).
[27] Z. Pengyi, L. Fuyan, Y. Gang, C. Qing, Z. Wanpeng, A comparative study on decomposition of gaseous toluene by O_3/UV, TiO_2/UV and O_3/TiO_2/UV, J Photochem Photobiol A Chem. 156 (2003) 189–194, https://doi.org/10.1016/S1010-6030(02)00432-X.
[28] M. Krichevskaya, S. Preis, A. Moiseev, N. Pronina, J. Deubener, Gas-phase photocatalytic oxidation of refractory VOCs mixtures: through the net of process limitations, Catal Today. 280 (2017) 93–98, https://doi.org/10.1016/j.cattod.2016.03.041.
[29] I. Konstantinou, Photocatalytic transformation of pesticides in aqueous titanium dioxide suspensions using artificial and solar light: intermediates and degradation pathways, Appl Catal b. 42 (2003) 319–335, https://doi.org/10.1016/S0926-3373(02)00266-7.
[30] V. Iliev, D. Tomova, L. Bilyarska, A. Eliyas, L. Petrov, Photocatalytic properties of TiO_2 modified with platinum and silver nanoparticles in the degradation of oxalic acid in aqueous solution, Appl Catal b. 63 (2006) 266–271, https://doi.org/10.1016/j.apcatb.2005.10.014.
[31] S. Alofi, C. O'Rourke, A. Mills, Kinetics of stearic acid destruction on TiO_2 'self-cleaning' films revisited, Photochem. Photobiol. Sci. 21 (2022) 2061–2069, https://doi.org/10.1007/s43630-022-00278-0.
[32] J. Bolobajev, M. Kask, K. Kreek, M. Kulp, M. Koel, A. Goi, Metal-doped organic aerogels for photocatalytic degradation of trimethoprim, Chem. Eng. J. 357 (2019) 120–128, https://doi.org/10.1016/j.cej.2018.09.127.
[33] J. Alvarez-Ramirez, R. Femat, M. Meraz, C. Ibarra-Valdez, Some remarks on the Langmuir-Hinshelwood kinetics, J Math Chem. 54 (2016) 375–392, https://doi.org/10.1007/s10910-015-0566-7.
[34] P.F. Biard, A. Bouzaza, D. Wolbert, Photocatalytic degradation of two volatile fatty acids in an annular plug-flow reactor; kinetic modeling and contribution of mass transfer rate, Environ Sci Technol. 41 (2007) 2908–2914, https://doi.org/10.1021/es062368n.
[35] B. Boulinguiez, A. Bouzaza, S. Merabet, D. Wolbert, Photocatalytic degradation of ammonia and butyric acid in plug-flow reactor: degradation kinetic modeling with contribution of mass transfer, J Photochem Photobiol A Chem. 200 (2008) 254–261, https://doi.org/10.1016/j.jphotochem.2008.08.005.
[36] M. Rivas, G.M. Calaf, D. Laroze, E. Rojas, J. Mendez, J. Honeyman, M.C. Araya, Solar ultraviolet A radiation and nonmelanoma skin cancer in Arica, Chile, J Photochem Photobiol b. 212 (2020) 112047, https://doi.org/10.1016/j.jphotobiol.2020.112047.
[37] E. Pelizzetti, M. Schiavello, Photochemical Conversion and Storage of Solar Energy, Springer Netherlands, Dordrecht, 1991. https://doi.org/10.1007/978-94-011-3396-8.
[38] F.J. Rivas, F.J. Beltrán, A. Encinas, Removal of emergent contaminants: Integration of ozone and photocatalysis, J Environ Manage. 100 (2012) 10–15, https://doi.org/10.1016/j.jenvman.2012.01.025.
[39] F.J. Rivas, F.J. Beltrán, O. Gimeno, M. Carbajo, Fluorene oxidation by coupling of ozone, radiation, and semiconductors: a mathematical approach to the kinetics, Ind Eng Chem Res. 45 (2006) 166–174, https://doi.org/10.1021/ie050781i.
[40] H. Qi, S. De-Zhi, C. Guo-Qing, Formaldehyde degradation by UV/TiO_2/O_3 process using continuous flow mode, J. Environ. Sci. 19 (2007) 1136–1140.
[41] K.P. Yu, G.W.M. Lee, Decomposition of gas-phase toluene by the combination of ozone and photocatalytic oxidation process (TiO_2/UV, TiO_2/UV/O_3, and UV/O_3), Appl Catal b. 75 (2007) 29–38, https://doi.org/10.1016/j.apcatb.2007.03.006.
[42] H. Huang, W. Li, Destruction of toluene by ozone-enhanced photocatalysis: Performance and mechanism, Appl Catal b. 102 (2011) 449–453, https://doi.org/10.1016/j.apcatb.2010.12.025.

[43] J. Yuan, X. Huang, M. Chen, J. Shi, W. Shangguan, Ozone-assisted photocatalytic degradation of gaseous acetaldehyde on TiO_2/M-ZSM-5 (M = Zn, Cu, Mn), Catal Today. 201 (2013) 182–188, https://doi.org/10.1016/j.cattod.2012.06.003.
[44] R. Atkinson, Kinetics and mechanisms of the gas-phase reactions of the hydroxyl radical with organic compounds under atmospheric conditions, Chem Rev. 86 (1986) 69–201, https://doi.org/10.1021/cr00071a004.
[45] J. Sydorenko, A. Mere, M. Krunks, M. Krichevskaya, I.O. Acik, Transparent TiO_2 thin films with high photocatalytic activity for indoor air purification, RSC Adv. 12 (2022) 35531–35542, https://doi.org/10.1039/d2ra06488j.

Supplemental materials to manuscript Ozone-assisted degradation of 2-methoxyethanol in a prototype plug flow photocatalytic reactor.

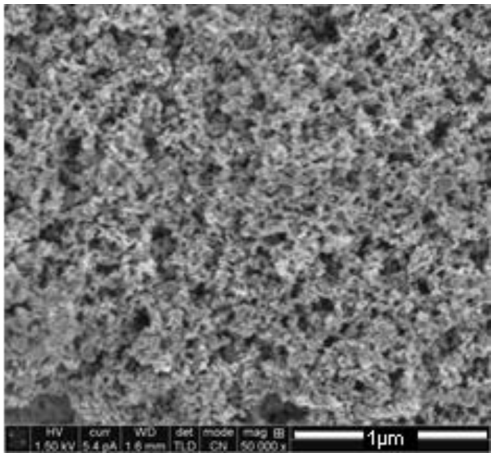

Figure S1. TiO_2 P25 coating on glass with specific weight of 1.4 mg cm^{-2} TiO_2 P25 by field emission scanning electron microscopy (FE SEM, Dual-Beam Helios Nanolab 600, FEI)

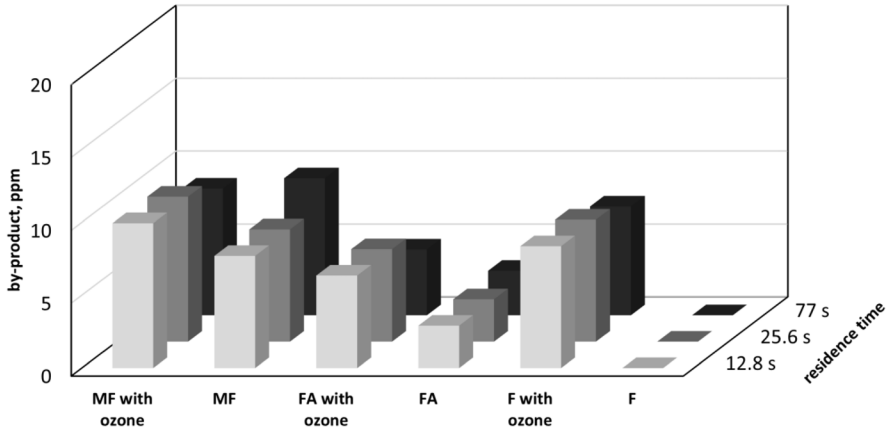

Figure S2. By-products (MF – methyl format, FA – formic acid, F - formaldehyde) at the reactor's outlet dependent on residence time with and without ozone: 2ME and ozone inlet concentrations were 20±5 ppm and 25±5 ppm, respectively

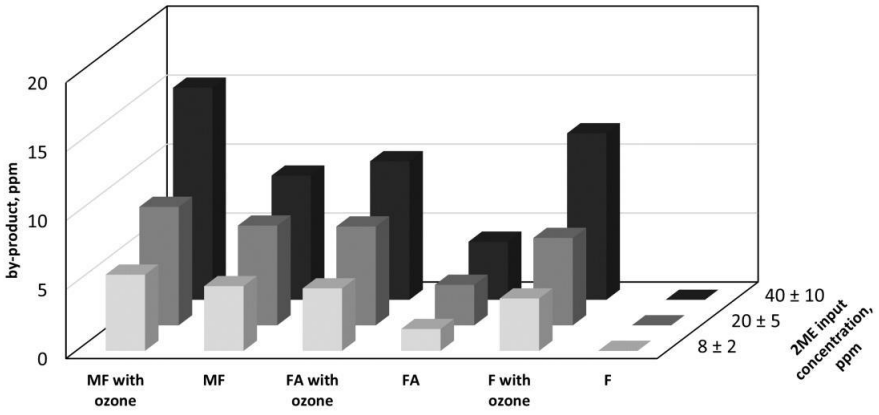

Figure S3. By-products (MF – methyl format, FA – formic acid, F - formaldehyde) at the reactor's outlet dependent on 2ME inlet concentration with and without ozone: residence time 12.8 seconds and ozone inlet concentration 25±5 ppm

Appendix 3

Paper III

K. Altof, M. Krichevskaya, S. Preis, J. Bolobajev. (2025). Advanced oxidation of airborne *m*-xylene in combination of pulsed corona discharge and post-plasma photocatalysis, *Journal of Electrostatics*, 138, 104184. https://doi.org/10.1016/j.elstat.2025.104184

Journal of Electrostatics 138 (2025) 104184

Contents lists available at ScienceDirect

Journal of Electrostatics

journal homepage: www.elsevier.com/locate/elstat

Advanced oxidation of airborne *m*-xylene in combination of pulsed corona discharge and post-plasma photocatalysis

Kristen Altof *, Marina Krichevskaya, Sergei Preis, Juri Bolobajev **

Laboratory of Environmental Technology, Department of Materials and Environmental Technology, Tallinn University of Technology, Ehitajate tee 5, Tallinn, Estonia

ARTICLE INFO

Keywords:
Advanced oxidation processes
Air purification
Nitrous oxide
Non-methane volatile organic compounds
PPC
Non-thermal plasma
Ozone
VOCs
Water
TiO_2

ABSTRACT

This study investigates the efficiency of a plug flow post-plasma catalysis air purification system for the removal of *m*-xylene (40 ± 5 ppm) from air. The treatment system consists of a pulsed corona discharge (PCD) reactor followed by a photocatalytic oxidation (PCO) reactor, arranged in series to enhance pollutant degradation. Experiments were conducted under varying conditions, including air flow rates from 2 to 10 $m^3\ h^{-1}$, and relative humidity levels of 2.5 % (dry air), 35 % (humid air), and 65 % (sprinkler-assisted humidification within the PCD reactor). In addition, the pulse frequency of the PCD reactor varied between 100 and 800 pulses per second, allowing evaluation of its influence on treatment performance. The study provides insight into how operational parameters affect the degradation efficiency of *m*-xylene in a continuous-flow system. The results highlight the synergistic potential of post-plasma photocatalysis for air purification and potential shortcomings like ozone, nitrogen oxides and by-product formation.

1. Introduction

Volatile organic compounds (VOCs) used in manufacturing are often toxic and harmful to the environment [1,2]. Manufacturing paints, glues and cleaners use a variety of organic solvents that have a negative effect on air quality, especially in urban areas [3]. The EU Directive 2016/2284 was put into effect to encourage the reduction of VOC emissions [4], challenging governments and industries, since displacement of VOCs and solvents is not technically feasible for existing production methods. Solving the problem thus requires technical solutions purifying the exhaust air contaminated with VOCs. Various technologies including filtration, adsorption, incineration, catalytic oxidation, and cold plasma oxidation are being used and studied [5,6]. All these technologies remove target pollutants, yet they all come with their own drawbacks [7]. Cold plasma could be an energy efficient solution for environmental management [8]. One of the most significant drawbacks in plasma applications is the formation of ozone [9]. Ozone may be decomposed i) thermally, ii) being used in VOCs oxidation catalyzed by metal oxides [10], or iii) in photocatalytic oxidation [11].

Oxidation of VOC molecules in a pulsed corona discharge (PCD) reactor is initiated by high energy impact of a charged particle. Dependent on the plasma conditions, the molecule excitation, ionization and attachments follow resulting in degradation of the molecular structure [12]. In dry air, oxygen and nitrogen form reactive oxygen and nitrogen species (RONS), e. g., O, O^+, O_2^+, N_2^+, and N^+ reacting with the target pollutant. In humid air, water molecules are involved producing hydrogen containing oxidative species, including H_2O_2, $OH^\bullet$, $HO_2^\bullet$ participating in oxidation of VOCs [9,13–15].

Photocatalytic oxidation (PCO) of target pollutants in air follows various pathways due to reactions with formed radicals containing oxygen and hydrogen [16]. Equations (1)–(3) illustrate fundamental principles, wherein TiO_2, upon excitation by light, generates electron-hole pairs (Equation (1)). Subsequently, oxygen and water interacting with these electron-hole pairs lead to the formation of reactive radicals (Equations (2) and (3)), which facilitate the oxidation of target pollutants.

$$TiO_2 + h\nu \rightarrow TiO_2(h^+) + e^- \quad (1)$$

$$O_2 + e^- \rightarrow O_2^{\cdot -} \quad (2)$$

$$H_2O + h^+ \rightarrow \cdot OH + H^+ \quad (3)$$

High energy efficiency, safety in electric discharge application, and the quality of treatment comprise the triune goal of the approach.

* Corresponding author.
** Corresponding author.
E-mail addresses: kristen.altof@taltech.ee (K. Altof), juri.bolobajev@taltech.ee (J. Bolobajev).

https://doi.org/10.1016/j.elstat.2025.104184
Received 9 May 2025; Received in revised form 5 September 2025; Accepted 22 September 2025
Available online 29 September 2025

Oxidation in low-temperature plasma of electric discharges has no economically justified alternative amongst energy-efficient technologies, suffering, however, from disadvantage of residual ozone in treated air, and sensitivity towards air humidity destabilizing electric discharge. The review by Li et al. also indicates inadequate utilization of intermediate products as the non-thermal plasma disadvantage [17]. The high efficiency of PCD in gas-liquid mixtures involving radicals formed at the surface of water droplets was proved earlier for plasma air treatment containing VOCs [18,19]. The stability of PCD in presence of sprinkled water is backed up by the configuration of the voltage pulse where the pulse shape is preserved along all pulse repetition frequencies applied as observed earlier [20]. The disadvantage of residual ozone is converted to advantage of ozone utilization in photocatalysis improving oxidation of VOC residues and maintaining the activity of photocatalyst as proved earlier [11,21]. Combining gas-liquid plasma treatment with photocatalysis may thus provide a promising solution. For example, in-plasma and post-plasma catalysis (PPC) with high oxidation efficiency of electric discharge plasma and low-maintenance high-yield catalysis have been studied [22]. The authors undertook an attempt to improve energy efficiency in combination of gas-liquid PCD with post-plasma photocatalysis.

Carcinogenic, mutagenic and neurotoxic *m*-xylene has an 8-h exposure limit of 50 ppm in the EU, although scientists advise it lower [23, 24]. Despite the potential hazard, *m*-xylene is widely used in industry [25–27]. Here, the results of *m*-xylene oxidation in an upscaled plug flow PPC are discussed. Pulsed corona discharge with water sprinkling coupled in a sequence with a flatbed PCO reactor showed promising results earlier [7,28]. The role of water sprinkling accelerating VOCs oxidation was studied earlier by the authors [19]. The enhancement of oxidation is due to reactive oxygen species (ROS) formed mainly on water droplets in the plasma zone [29–31], thus making water sprinkler an important attribute of PCD reactor efficient in air treatment [19,21]. In the present research, attention was paid to the impacts of air relative humidity and residence time at 40 ± 5 ppm VOC concentrations. The residual ozone, known to be a drawback of PCD in air treatment, is countered with a PCO reactor, where ozone supports oxidation [11]. In this study, the feasibility of PPC combination was tested in experiments with PCD and PCO separately and in a PPC sequence varying air flow rate, pulse repetition frequency, and air humidity while following the target pollutant oxidation and ozone concentrations.

2. Materials and methods

2.1. Chemicals

Analytical grade *m*-xylene (C_8H_{10}, 99+% from Thermo Scientific Chemicals, USA) was used as VOC. Distilled water was used in PCD experiments with sprinkling. Dichloromethane (CH_2Cl_2, 99+% from Honeywell Riedel-de Haën™, Germany) was used to extract *m*-xylene oxidation byproducts from water samples. Drying of extracts was accomplished using anhydrous sodium sulfate ($Na_2SO_4 \geq 99.8$ % from LachNer, Czech Republik). Titanium dioxide P25 was purchased from Evonik Industries AG (Germany) and ethanol ($C_2H_5OH \geq 99$ %) - from Sigma-Aldrich (USA). Silica gel ($SiO_2 > 98$ %) was purchased from Keemiakaubandus AS (Estonia).

2.2. Reactors

The experimental PPC setup is outlined in Fig. 1. The PCD reactor (Flowrox Oy, Finland) has a total volume of 75.9 L with an inter-electrode zone (1275 × 550 × 35 mm, 24.5 L) and a 12.7-L storage tank. A wire with 0.6 mm diameter and length of 12 m was used as a high voltage electrode. The distance between the high-voltage electrodes and grounded plates was 17 mm, the distance between high-voltage electrodes was 30 mm. The high voltage horizontal strings were concluded between two vertical ground plates. The water tank was filled with 5.0 L

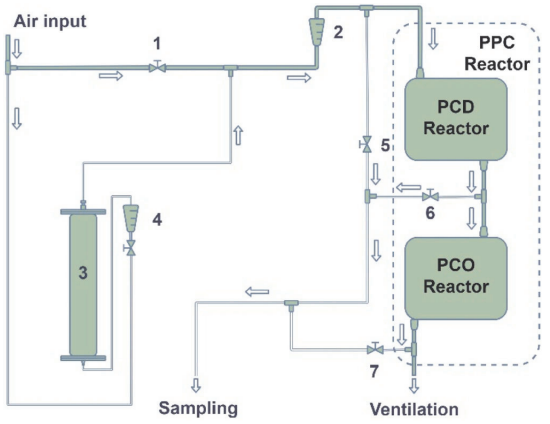

Fig. 1. Experimental PPC setup: 1 – main flow control valve, 2 - main flow rotameter, 3 – *m*-xylene bubble column, 4 – *m*-xylene dosing line rotameter and control valve, 5 – inlet air sampling valve, 6 – PCD outlet air sampling valve, 7 - PCO outlet air sampling valve.

of distilled water used for sprinkling [19]. The pulse repetition frequency applied in the experiments was 100 and 800 pulses per second (pps) corresponding to the power delivered to the reactor of 12.5 and 100 W.

The PCO reactor is flat bedded with a transparent cover and fitted with glass plates covered with TiO_2. Powdery P25 titanium dioxide AEROXIDE® TiO_2 P25 (≥99.5 %, Evonik Industries AG, Germany), crystalline with a predominantly anatase structure (rutile fraction 14 ± 1 wt%), was used as the photocatalytic material. TiO_2 was coated on 115x90 × 2 mm glass plates by spraying as described by Kask et al. [21]. The total volume of the reactor is 21.3 L (996 × 534 × 40 mm) [11]. UV-A TL-D 15W lamps (Philips, Germany) were used for the photocatalyst irradiation.

The VOC was dosed to the air stream by means of liquid *m*-xylene evaporation from a bubble column (400–600 mL). To control the VOC's concentration, the bubble column was connected to the main flow in a bypass mode.

Levels of relative air humidity (RH) used in the study comprised 2.5 %, 35 %, and around 65 % at 27 ± 3 °C. The lowest number was achieved by drying the air from the compressed air supply mains from its initial 7 % by passing through a silica gel column. The room air having RH at about 35 % was used by using Eco Air Pump PA200 (Jecod Co. 94 Ltd., People's Republic of China). High humidity of about 65 % was reached when the PCD reactor was sprinkled with water at its circulation rate of 9.0 L min^{-1}.

2.3. Experiments

The air stream in the PPC sequence varied between 2.0 and 8.0 m^3 h^{-1}, having the VOC concentration maintained at 40 ± 5 ppm, providing residence times of 136.6 to 34.1 s in the PCD reactor (of which residence times of 44.1 to 11.0 s in the plasma zone) and 38.3 to 9.6 s in the PCO reactor, respectively. The VOC degradation performance was assessed from the ratio of its output (C_{out}) and input (C_{in}) concentrations with the error margin not exceeding 5 %. Air sampling started in 15 min after the reactors were switched on to ensure a steady state of experimental parameters.

2.4. Analyses

Air samples were collected using 20-mL vials and analyzed using gas chromatography-mass spectrometry GC-MS (QP2010 Plus, Shimadzu,

Japan). The GC used a capillary column Phenomenex ZB-WAXplus (Zebron), 30 m length, inner diameter 0.32 mm, and coating thickness 0.25 μm. The injection port temperature was maintained at 50 °C, and the column was kept at 30 °C. The MS used electron impact ionization and a single quadrupole mass analyzer.

m-Xylene oxidation by-products were analyzed in water samples by three-step liquid-liquid extraction with dichloromethane. Extracts were dried using anhydrous Na_2SO_4 and concentrated (1/10, v/v) by means of evaporation. Subsequently, the extracted by-products were analyzed with the GC-MS. The injection port temperature was maintained at 260 °C; GC temperature program started with holdup at 80 °C for 1 min with the following increase to 250 °C at 10 °C min^{-1}, and the final holdup for 5 min. Mass-spectra were obtained using electron impact ionization with the following scanning of ions in mass-analyzer over *m/z* range of 40–340 with the scan speed of 1.666 amu s^{-1}.

Gaseous ozone concentration below 340 ppm was measured using an ozone analyzer (Anseros Klaus Nonnenmacher GmbH, Germany). Concentrations above 400 ppm were measured with BMT 965 BT ozone analyzer (BMT Messtechnik GmbH, Germany). N_2O was measured with FT-IR spectrometry analysis (Interspec 200-X, Interspectrum OÜ, Estonia) at a bandwidth between 2256 and 2223 cm^{-1}, which had the least interference from other substances while a distinctive peak on the spectrum was still visible. Humidity and temperature were monitored with TPI597 digital hygrometer (Test Products International, Inc. USA). Spectrometry parameters of UV-A radiation within 315–400 nm were measured using a USB 2000+ UV–VIS spectrometer (Ocean Optics, USA).

3. Results and discussion

3.1. PCD oxidation of airborne m-xylene

The *m*-xylene PCD-oxidation rate was tested at varied air residence times and humidity with the results given in Fig. 2. Expectedly, the performance of the reactor improved at the residence time increased from 34.1 to 136.6 s, when the air flow rate decreased from 8.0 to 2.0 m^3 h^{-1}: noticeable changes are seen at lower pulse repetition rates, i.e., pulsed power input, whereas almost full oxidation was observed at higher frequency.

The effect of RH on oxidation is pronouncedly negative, demonstrating substantially lower *m*-xylene conversion degrees at 35 % compared to 2.5 % at 27 ± 3 °C. What is more surprising, oxidation efficiency was also lower in water-sprinkled reactor with RH 65 %. It was previously observed, however, that water sprinkling in the PCD reactor substantially accelerates oxidation of *m*-xylene serving a precursor for surface-borne hydroxyl radicals [19,32]. These observations seem to contradict each other: accelerated *m*-xylene PCD-oxidation observed with water sprinkling at its vapors concentration of 20 ppm [19] disappeared when the VOC's concentration was doubled. The authors explain the contradiction by the surface phenomena possibly taking place with the increased concentration of *m*-xylene.

Phenolic compounds formation as water-soluble intermediates in *m*-xylene oxidation is described below in this research. Doubling the *m*-xylene influx presumably increases the content of phenolic compounds and other intermediates in sprinkled water. These, being rapidly oxidized in PCD treatment [33], compete for oxidants at the gas-liquid interface, affecting the role of the water surface as a concentrator of short-living oxidants: more rapid utilization of OH-radicals at the interface in reactions with phenolic compounds and other rapidly reacting waterborne intermediates may reduce the concentration of oxidants at the plasma side of the interface thus interfering with oxidation of *m*-xylene vapors. This assumption requires proof, the simplest of which may consist of extended observations in variety of *m*-xylene and other BTEX-compounds concentrations. The experiments with toluene and benzene are on their way confirming the accelerated oxidation in sprinkled reactor.

On the other hand, oxidation of *m*-xylene proceeded faster in dry air compared to RH 35 % (Fig. 2A) [34,35]. The negative impact of increased humidity on the VOC oxidation in air may be explained by altered peak voltage and current in the pulse, decreasing the total amount of oxidants. Formation of ozone, e.g., is known to depend on air humidity confirmed in this study.

Table 1 summarizes energy yield data on xylene oxidation from selected studies for plug flow plasma reactors and also presents the results of the current study. The studies give incentives on important operational parameters including VOC concentrations, air flow rates, and relative humidity. The highest energy efficiency in this study was observed at the air flow rate of 6 m^3 h^{-1}. The energy yield is higher compared to previous study [19] due to increased input VOC concentration.

3.2. Ozone generation in PCD

Unwanted by-products of plasma application for VOCs abatement include ozone and nitrogen oxides. In clean dry air ozone is formed in a three-body collision as shown in Eq. (4), where M stands for the third collision partner, O, O_2, O_3 or N_2 [9].

$$O + O_2 + M \rightarrow O_3^{*} + M \rightarrow O_3 + M \quad (4)$$

Ozone output concentration was monitored showing ozone production at variations of air flowrate, relative humidity and pulse repetition frequency (Fig. 3). Concentration of ozone followed the tendency similar to *m*-xylene oxidation – ozone production increased at higher pulse repetition frequency and longer residence time. The dependence of ozone output on air humidity showed negative trend: ozone outlet concentration decreased with increased humidity, having nearly twice as much ozone generated in dry air (RH 2.5 %) compared to the humid one in sprinkled reactor (RH 65 %). Negative impact of water vapors on ozone formation in PCD may be explained by water molecule cleavage resultant in radical reaction routes, when hydrogen and hydroxyl radicals react with ozone initiating chain reactions of decomposition [13].

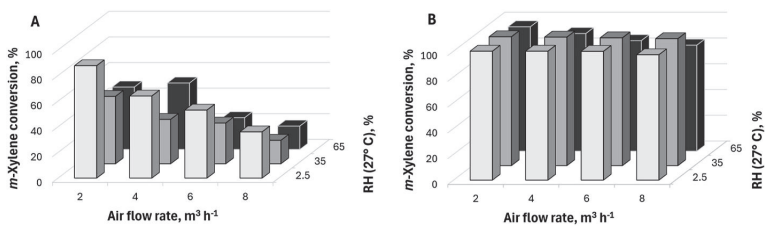

Fig. 2. *m*-Xylene PCD-oxidation degree at relative humidity variations vs air flow rate at pulse repetition frequencies 100 (A) and 800 (B) pps: *m*-xylene input concentration 40 ± 5 ppm, water circulation rate 9 L min^{-1} at RH 65 %, circulation water pH 6.0–6.5, error margin in *m*-xylene quantification ±5 %.

Table 1
Comparison of results in airborne xylene oxidation in plasma reactors.

Plasma reactor type	Initial xylene concentration, ppm	Gas flow rate, $m^3\ h^{-1}$	Removal, %	Energy yield, g $kW^{-1}h^{-1}$	Source
PCD (RH 2.5 %)	45.0 ± 5.0	2.0–8.0	36.0–100.0	3.9–49.4	Current study
PCD (RH 35 %)	45.0 ± 5.0	2.0–8.0	18.0–100.0	3.9–29.6	
PCD (RH 65 %)	45.0 ± 5.0	2.0–8.0	18.0–100.0	3.9–32.2	
PCD	20.0 ± 5.0	6.0	18.0–100.0	5.6–21.1	[19]
Dielectric Barrier Discharge	23.0–2303.0	0.1–1.0	95.0	20.0	[36]
	0.0–500.0	0.03–0.09	80.0	7.1	[37]

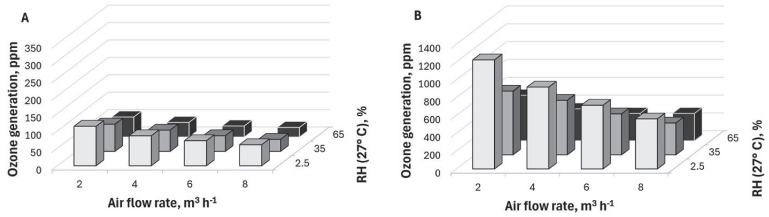

Fig. 3. Ozone outlet concentration from the PCD reactor at relative humidity variations vs air flow rate at pulse repetition frequencies 100 (A) and 800 (B) pps: *m*-xylene input concentration 40 ± 5 ppm, water circulation rate 9 L min^{-1} at RH 65 %, circulation water pH 6.0–6.5, error margin in ozone quantification ±5 %.

3.3. Nitrous oxide generation in PCD

Nitrous oxide N_2O is one of the relatively stable gaseous nitrogen oxides formed in plasma via various paths involving several reactions with excited nitrogen, nitrogen oxides, oxygen and ozone [13]. Nitrous oxide generation was quantified in the previous study of *m*-xylene oxidation, showing its behavior similar to the ozone generation, where high humidity and the water sprinkling reduced the yield of nitrogen-containing compounds: at the air flow rate of 6.0 $m^3\ h^{-1}$, *m*-xylene concentration of 20 ± 5 ppm, and pulse repetition frequency of 800 pps, the N_2O concentration comprised 7.1 and 3.7 ppm at RH 35 % and 65 % (sprinkled reactor), respectively [19]. In dry air at RH 2.5 %, the N_2O concentration reached 8.6 ppm at the doubled *m*-xylene content. The decreased N_2O formation in air at higher humidity is explained analogously to ozone formation by the interference from water vapors promoting side reactions.

A number of studies have been dedicated to the degradation of N_2O in PCO [38–40]. It has been shown that N_2O can be removed in photocatalytic batch reactors over several hours. This circumstance deprived the authors from studying N_2O oxidation in PCO reactor for substantially shorter retention times applied in the PPC device.

3.4. PCO oxidation of airborne m-xylene

The PCO reactor was studied as a standalone unit to follow the effects of relative humidity and residence time on *m*-xylene oxidation (Fig. 4). Two primary trends became evident: i) the amount of oxidized VOC increased with the residence time as observed previously [11], and ii) the increased air humidity enhances the PCO performance consistently with other studies [41]. Even though the underlying mechanisms are not always well understood, and various studies have reported differing results regarding humidity effect in PCO reactors [42], hydroxyl radicals formed on the photocatalyst (Eq. (3)) explain the observation. Another potential explanation is water vapor disrupting bonds of photocatalyst with oxidation by-products adsorbed on the surface, thereby improving the availability of active sites for adsorption and generation of reactive species. The overall effectiveness of the PCO reactor at given conditions is moderate having only a few ppm of *m*-xylene degraded. Nevertheless, the experiments proved that the VOC is oxidized in the PCO reactor at elevated air humidity: in dry air, *m*-xylene was barely oxidized (Fig. 4).

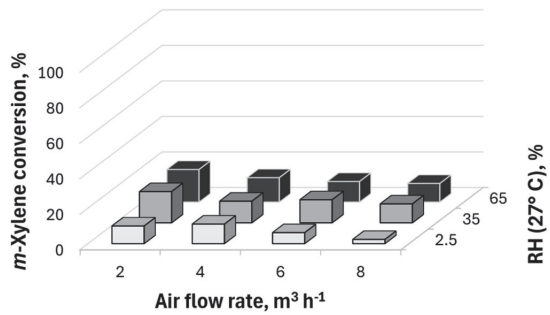

Fig. 4. *m*-Xylene PCO-conversion degree at relative humidity variations vs air flow rate: *m*-xylene input concentration 40 ± 5 ppm, irradiance at 315–400 nm 119 W m^{-2}, error margin in *m*-xylene quantification ±5 %.

3.5. Ozone degradation in PCO

Ozone degradation in the PCO reactor in absence of the VOC is shown in Fig. 5, certain ozone conversion is observed. At low humidity,

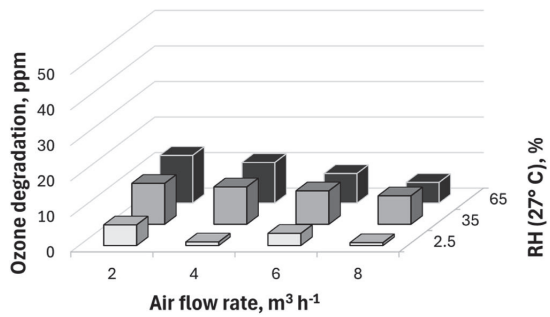

Fig. 5. Ozone PCO-degradation at relative humidity variations vs air flow rate: ozone inlet concentrations were generated in the PCD reactor and varied with relative humidity and the air flow rate at 100 pps; irradiance at 315–400 nm 119 W m^{-2}, error margin in m-xylene quantification ±5 %.

however, ozone appears to be stable showing only minor degradation even at the longest residence time. Photocatalytic oxidation was earlier reported following a pseudo-zero-order reaction kinetics having only a few ppm of ozone degraded regardless of the amount of ozone entering the reactor [11]. At elevated humidity, degradation of ozone becomes faster due to radical reactions shown in Eqs. (5) and (6) [16]:

$$O_3 + e^- \rightarrow O_3^{\cdot-} \rightarrow O^{\cdot-} + O_2 \quad (5)$$

$$O^{\cdot-}\left(O_3^{\cdot-}\right) + H_2O \rightarrow \cdot OH + OH^-(+O_2) \quad (6)$$

3.6. Oxidation of airborne m-xylene in post-plasma catalysis

The rationale behind using ozone in gas mixtures treated for PCO of VOCs is, among others, its ability to capture free electrons from the photocatalyst surface upon exposure to light. Such electron scavenging prevents the recombination of electron-hole pairs, increasing the availability of holes oxidizing target pollutants or producing •OH (Eq. (3)). Also, ozone admixtures extend the lifetime of the photocatalyst, making the combination of PPC with ozone beneficial for VOCs oxidation [43]. The results in *m*-xylene oxidation in the PPC combination are present in Fig. 6. At the maximum input pulsed power at 800 pps the conversion of *m*-xylene in the tandem is nearly identical to the one observed in PCD treatment for almost full oxidation of the VOC leaving little for subsequent PCO. At lower power, 100 pps, there is a noticeably improved PPC oxidation contributed by PCO in wet air, bringing the results closer to the dry air ones (Figs. 2A and 6A). This points out the impact of water vapors together with the residual ozone accelerating PCO of the VOC.

Ozone degradation in PCO following PCD is shown in Fig. 7. One can see that at 800 pps ozone degradation at high humidity was doubled as compared to ozone decomposition in absence of *m*-xylene (Fig. 5). This serves as clear evidence of ozone-assisted PCO of the VOC, in which ozone was utilized in oxidation of residual *m*-xylene under condition of high relative humidity. It could be argued that high humidity and the presence of water do play a very important role in the PPC reactor combination and observing only the target pollutant conversion is not sufficient to evaluate the reactor's performance.

3.7. Waterborne oxidation products of m-xylene

Accumulated waterborne products of *m*-xylene PCD-oxidation identified by means of GC-MS are given in Fig. 8 and refer to certain reaction pathways: hydroxylation of methyl group and aromatic ring with presumably subsequent ring opening, and nitration.

Hydroxylation proceeds via the sequence of hydrogen abstractions from the methyl groups induced by hydroxyl radicals with subsequent hydroxylation of resultant organic radicals or their reaction with oxygen and/or with water, producing identified compounds A and B, respectively. Series of oxidative transformations on the methyl group ends up with demethylation, hypothetical stage C, followed by hydroxylation of adjacent carbon atoms of aromatic ring with the ring opening producing dialdehyde compound E.

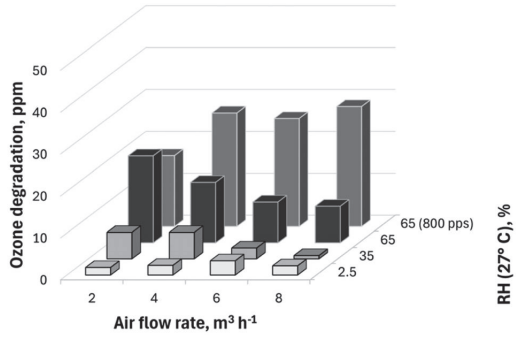

Fig. 7. Ozone degradation in the PPC reactor combination at different relative humidities, air flow rates and pulse repetition frequences. *m*-xylene input concentration 40 ± 5 ppm, water circulation rate 9 L min^{-1} (only at 65 % RH), water pH 6.0–6.5.

Stepwise hydroxylation of aromatic ring leads to the formation of 2,6-dimethylhydroquinone (compound G). The latter is then deprotonated and oxidized to quinone structure compound (compound H).

Phenolic intermediates also underwent nitration, giving two compounds K and L of equal molecular weight. The prerequisite for this reaction is plasma-induced formation of nitrogen oxides transformed further into nitric acid [19].

The products identified in water recycled in PCD reactor point out to the importance of sprinkling as means of absorption, preventing their possible emission with the outlet air stream.

3.8. PCO reactor scale-up

As seen from the experimental data, to be able to degrade ozone in the outlet stream of PCD, the PCO reactor should be scaled-up above the used photocatalytic surface. Data from Fig. 7 were used in calculation of the PCO efficiency in ozone degradation measured in ppm per cm^2 per second with irradiance in PCO 119 W m^{-2}. If the PCO reactor design remained unchanged and the volume would increase proportionally then the efficiency numbers comprised 0.0004, 0.0005 and 0.0018 ppm cm^{-2} s^{-1} for RH 2.5 %, 35 % and 65 % respectively. Fig. 9 represents the required area of the PCO reactor necessary to deplete ozone in the PCD outlet at 100 pps. The estimate shows that the necessary size of PCO reactor may require substantially larger PCO area, especially for ozone abatement in dry air: the PCO reactor would have to be nearly ten times smaller at RH 65 % or higher, which is because not only is the PCO more effective with higher humidity, but also the PCD produces less ozone when sprinkled.

4. Conclusions

The feasibility of electric discharge plasma combination with post-

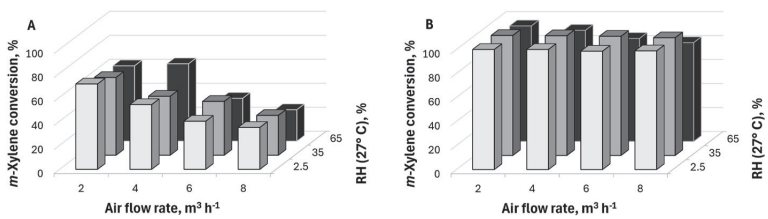

Fig. 6. *m*-Xylene oxidation in the post-plasma catalytic combination at relative humidity variations vs air flow rate: pulse repetition frequency 100 (A) and 800 (B) pps, m-xylene input concentration 40 ± 5 ppm, water circulation rate at RH 65 % - 9 L min^{-1}, sprinkling water pH 6.0–6.5, irradiance in PCO 119 W m^{-2}.

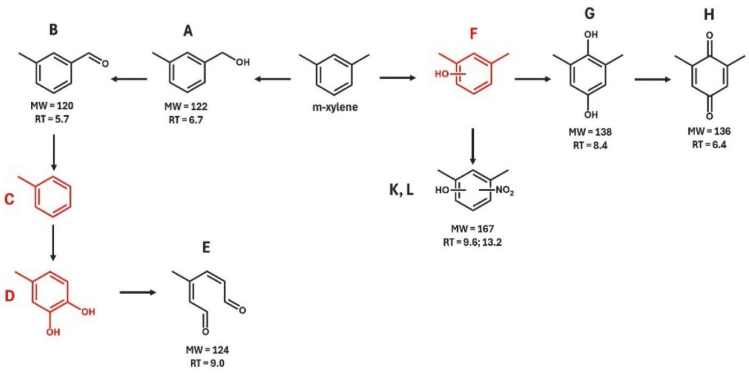

Fig. 8. Waterborne intermediate products of *m*-xylene PCD-oxidation: MW –molecular weight of compound, RT – retention time in a chromatogram; compounds indicated in red were not detected but considered as precursors of identified by-products; pulse repetition frequency 500 pps, m-xylene input concentration 40 ± 5 ppm, water circulation rate 9 L min^{-1}, sprinkling water pH 6.0–6.5, air flow rate 6 m^3 h^{-1}.

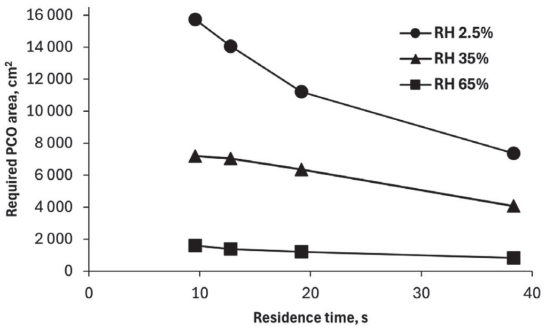

Fig. 9. Area of PCO reactor(s) for complete ozone depletion at RH variations vs residence time.

plasma photocatalysis was studied for *m*-xylene abatement in air. The results showed that water sprinkling in the PCD reactor, unlike with other BTEX-hydrocarbons, did not improve the *m*-xylene oxidation rate at given experimental conditions, i.e., at relatively higher VOC concentration (40 ppm). On the contrary, the PCD reactor performed better in dry air. High humidity in sprinkled PCD reactor, however, appeared crucial for subsequent PCO of *m*-xylene, proceeding noticeably faster than in dry air. Largely, in dry air, PCO had insignificant contribution to the overall *m*-xylene oxidation.

Ozone was produced in dry PCD reactor in significantly higher quantities than in sprinkled one. Besides, ozone degraded to a minor extent in PCO of dry air. Summarizing, treatment of dry air in PPC combination, although beneficial for *m*-xylene removal, resulted in substantial secondary pollution of treated air with ozone. At high relative humidity (RH 65 % at 25 °C) in sprinkled PCD reactor, lower production of ozone was supplemented with its prompt decomposition in PCO due to electron scavenging by ozone keeping the electron-hole pairs from recombining and formation of OH-radicals, thus making sprinkled PCD reactor application beneficial for the reduced ozone outlet from PPC.

N_2O followed a similar pattern to ozone formation in the PCD reactor where high humidity proved to prohibit nitrogen oxide formation. Yet PCO had no measurable effects on N_2O degradation due to limited residence time in the plug flow reactor.

The products of *m*-xylene oxidation detected in sprinkling water include intermediates of the methyl group dehydration with subsequent hydroxylation, mono- and di-hydroxylated aromatic ring, hydroquinone and quinone, and the opening of aromatic ring. The question of the lifetime of sprinkling aqueous solution and its further treatment needs an answer dependent on quantification of the products.

CRediT authorship contribution statement

Kristen Altof: Writing – original draft, Visualization, Formal analysis, Data curation, Conceptualization. **Marina Krichevskaya:** Writing – review & editing, Supervision. **Sergei Preis:** Writing – review & editing, Supervision. **Juri Bolobajev:** Writing – review & editing, Supervision, Formal analysis, Conceptualization.

Declaration of competing interest

The authors declare that they have no known competing financial interests or personal relationships that could have appeared to influence the work reported in this paper.

Acknowledgements

This work was funded by the Ministry of Education and Research through Centre of Excellence in Circular Economy for Strategic Mineral and Carbon Resources (01.01.2024–31.12.2030, TK228).

Data availability

Data will be made available on request.

References

[1] J.K. Pearson, European solvent VOC emission inventories based on industry-wide information, Atmos. Environ. 204 (2019) 118–124, https://doi.org/10.1016/j.atmosenv.2019.02.014.
[2] H. Rajabi, M.H. Mosleh, P. Mandal, A. Lea-Langton, M. Sedighi, Emissions of volatile organic compounds from crude oil processing – global emission inventory and environmental release, Sci. Total Environ. 727 (2020), https://doi.org/10.1016/j.scitotenv.2020.138654.
[3] X. Zhou, X. Zhou, C. Wang, H. Zhou, Environmental and human health impacts of volatile organic compounds: a perspective review, Chemosphere 313 (2023), https://doi.org/10.1016/j.chemosphere.2022.137489.
[4] European Parliament and of the Council of the European Union, Directive (EU) 2016/2284 of the European Parliament and of the Council of 14 December 2016 on the Reduction of National Emissions of Certain Atmospheric Pollutants, Amending Directive 2003/35/EC and Repealing Directive 2001/81/EC, 2016.
[5] K. Hirota, H. Sakai, M. Washio, T. Kojima, Application of electron beams for the treatment of VOC streams, Ind. Eng. Chem. Res. 43 (2004) 1185–1191, https://doi.org/10.1021/ie0340746.
[6] C. Du, X. Gong, Y. Lin, Decomposition of volatile organic compounds using Corona discharge plasma technology, J. Air Waste Manag. Assoc. 69 (2019) 879–899, https://doi.org/10.1080/10962247.2019.1582441.

[7] Joint research centre directorate B – growth and innovation circular economy and industrial leadership unit European IPPC bureau, Best Available Techniques (BAT) Reference Document for Common Waste Gas Management and Treatment Systems in the Chemical Sector, 2019. Brussels.

[8] P. Tikker, I. Kornev, S. Preis, Oxidation energy efficiency in water treatment with gas-phase pulsed Corona discharge as a function of spray density, J. Electrost. 106 (2020), https://doi.org/10.1016/j.elstat.2020.103466.

[9] Paul K. Chu, XinPei Lu, Low Temperature Plasma Technology, CRC Press, 2013, https://doi.org/10.1201/b15153.

[10] T. Batakliev, V. Georgiev, M. Anachkov, S. Rakovsky, G.E. Zaikov, Ozone decomposition, Interdiscip. Toxicol. 7 (2014) 47–59, https://doi.org/10.2478/intox-2014-0008.

[11] K. Altof, M. Krichevskaya, S. Preis, T. Tähemaa, J. Bolobajev, Ozone-assisted degradation of 2-methoxyethanol in a prototype plug flow photocatalytic reactor, Chem. Eng. J. 481 (2024), https://doi.org/10.1016/j.cej.2023.148488.

[12] A. Ogata, D. Ito, K. Mizuno, S. Kushiyama, A. Gal, T. Yamamoto, Effect of coexisting components on aromatic decomposition in a packed-bed plasma reactor, Appl. Catal. Gen. (2002), https://doi.org/10.1016/S0926-860X(02)00280-6.

[13] K.H. Becker, U. Kogelschatz, K.H. Schoenbach, R.J. Barker, Non-Equilibrium Air Plasmas at Atmospheric Pressure, CRC Press, 2004, https://doi.org/10.1201/9781482269123.

[14] M. Lee, M.B. Chang, Abatement of gas-phase *p*-Xylene via dielectric barrier discharges, Plasma Chem. Plasma Process. 23 (2003) 541–558, https://doi.org/10.1023/A:1023239122885.

[15] Kefeng Shang, Rino Morent, Nathalie De Geyter, Yongxin Wang, Zitong Yang, Plasma catalytic degradation of sulfamethoxazole in water with Fe/Mn-LDO catalyst: performance and mechanism, Separ. Purif. Technol. 360 (2025) 1383–5866, https://doi.org/10.1016/j.seppur.2024.131145. ISSN.

[16] H. Huang, W. Li, Destruction of toluene by ozone-enhanced photocatalysis: performance and mechanism, Appl. Catal., B 102 (2011) 449–453, https://doi.org/10.1016/j.apcatb.2010.12.025.

[17] S. Li, Y. Lin, G. Liu, C. Shi, Research status of volatile organic compound (VOC) removal technology and prospect of new strategies: a review, Environ. Sci. J. Integr. Environ. Res.: Process. Impacts (Issue 4) (2023), https://doi.org/10.1039/D2EM00436D.

[18] I. Kornev, S. Preis, Aqueous benzene oxidation in low-temperature plasma of pulsed Corona discharge, J. Adv. Oxid. Technol. 19 (2016), https://doi.org/10.1515/jaots-2016-0212.

[19] K. Altof, M. Krichevskaya, S. Preis, J. Bolobajev, Oxidation of airborne m-Xylene in pulsed Corona discharge: impact of water sprinkling, Chem. Eng. J. 8 (2024) 99, https://doi.org/10.3390/chemengineering8050099.

[20] I. Kornev, F. Saprykin, S. Preis, Stability and energy efficiency of pulsed corona discharge in treatment of dispersed high-conductivity aqueous solutions, J. Electrost. 89 (2017) (2017) 42–50, https://doi.org/10.1016/j.elstat.2017.07.001.

[21] M. Kask, J. Bolobajev, M. Krichevskaya, Gas-phase photocatalytic degradation of acetone and toluene, and their mixture in the presence of ozone in continuous multi-section reactor as possible air post-treatment for exhaust from pulsed corona discharge, Chem. Eng. J. 399 (2020), https://doi.org/10.1016/j.cej.2020.125815.

[22] Y. Zhang, Y. Zhu, S. Tao, Z. Zhang, M. Chen, Z. Jiang, W. Shangguan, Plasma-coupled catalysis in VOCs removal and CO2 conversion: efficiency enhancement and synergistic mechanism, Catal. Commun. 172 (2022), https://doi.org/10.1016/j.catcom.2022.106535.

[23] European Chemicals Agency, Substance infocard (Xylene). https://Echa.Europa.Eu/et/Substance-Information/-/Substanceinfo/100.014, 2024, 124.

[24] A.L. Bolden, C.F. Kwiatkowski, T. Colborn, New look at BTEX: are ambient levels a problem, Environ. Sci. Technol. 49 (2015) 5261–5276, https://doi.org/10.1021/es505316f.

[25] M. Zoveidavianpoor, A. Samsuri, S.R. Shadizadeh, Health, safety, and environmental challenges of xylene in upstream petroleum industry, Energy Environ. (2012), https://doi.org/10.1260/0958-305X.23.8.1339.

[26] Agency for Toxic Substances and Disease Registry, USA, Public health statement xylene. www.atsdr.cdc.gov/, 2007.

[27] K. Niaz, H. Bahadar, F. Maqbool, M. Abdollahi, A review of environmental and occupational exposure to xylene and its health concerns, EXCLI J. 14 (2015) 1167–1186, https://doi.org/10.17179/excli2015-623.

[28] L. Khezami, P. Nguyen-Tri, W.A. Saoud, A. Bouzaza, A. El Jery, D. Duc Nguyen, V. K. Gupta, A.A. Assadi, Recent progress in air treatment with combined photocatalytic/plasma processes: a review, J. Environ. Manag. 299 (2021), https://doi.org/10.1016/j.jenvman.2021.113588.

[29] P.J. Bruggeman, M.J. Kushner, B.R. Locke, J.G.E. Gardeniers, W.G. Graham, D. B. Graves, R.C.H.M. Hofman-Caris, D. Maric, J.P. Reid, E. Ceriani, D. Fernandez Rivas, J.E. Foster, S.C. Garrick, Y. Gorbanev, S. Hamaguchi, F. Iza, H. Jablonowski, E. Klimova, J. Kolb, F. Krcma, P. Lukes, Z. MacHala, I. Marinov, D. Mariotti, S. Mededovic Thagard, D. Minakata, E.C. Neyts, J. Pawlat, Z.L. Petrovic, R. Pflieger, S. Reuter, D.C. Schram, S. Schröter, M. Shiraiwa, B. Tarabová, P.A. Tsai, J.R.R. Verlet, T. Von Woedtke, K.R. Wilson, K. Yasui, G. Zvereva, Plasma-liquid interactions: a review and roadmap, Plasma Sources Sci. Technol. 25 (2016), https://doi.org/10.1088/0963-0252/25/5/053002.

[30] M. Sato, T. Ohgiyama, J.S. Clements, Formation of chemical species and their effects on microorganisms using a pulsed high-voltage discharge in water, IEEE Trans. Ind. Appl. 32 (1) (Jan.-Feb. 1996) 106–112, https://doi.org/10.1109/28.485820.

[31] M. Schiorlin, E. Marotta, M. Rea, C. Paradisi, Comparison of toluene removal in air at atmospheric conditions by different corona discharges, Environment. Sci. Technol. 43 (2009) 9386–9392, https://doi.org/10.1021/es9021816.

[32] A. Khadem, M.R. Khani, R. Hosseini rad, B. Shokri, S. Rashnoo, B. Ghobadian, Experimental analysis of volatile organic compounds conversion by a dielectric barrier discharge reactor to study the main products: Hydrogen, CO, CO_2, NO_x and hydrocarbons, Chem. Eng. Process. Process Intensif. 145 (2019), https://doi.org/10.1016/j.cep.2019.107660.

[33] J. Kornev, N. Yavorovsky, S. Preis, M. Khaskelberg, U. Isaev, B.-N. Chen, Generation of active oxidant species by pulsed dielectric barrier discharge in water-air mixtures, Ozone: Sci. Eng. 28 (2006) 207–215, https://doi.org/10.1080/01919510600704957.

[34] P. Ajo, I. Kornev, S. Preis, Pulsed Corona discharge induced hydroxyl radical transfer through the gas-liquid interface, Sci. Rep. 7 (2017), https://doi.org/10.1038/s41598-017-16333-1.

[35] S. Preis, I.C. Panorel, I. Kornev, H. Hatakka, J. Kallas, Pulsed corona discharge: the role of ozone and hydroxyl radical in aqueous pollutants oxidation, Water Sci. Technol. 68 (2013) 1536–1542, https://doi.org/10.2166/wst.2013.399.

[36] S.P. Bugaev, V.A. Kuvshinov, N.S. Sochugov, et al., Energy characteristics of the process of air scrubbing from hydrocarbon contaminants in a barrier-discharge reactor, Plasma Chem. Plasma Process. 16 (1996) 669–677, https://doi.org/10.1007/BF01447014.

[37] H.M. Lee, M.B. Chang, Abatement of gas-phase *p*-Xylene via dielectric barrier discharges, Plasma Chem. Plasma Process. 23 (2003) 541–558, https://doi.org/10.1023/A:1023239122885.

[38] J. Tan, H. Cheng, J. Liu, J. Sun, Y. Li, H. Wang, J. Liu, Z. Zhao, Room-temperature photocatalytic decomposition of N_2O over nanobelt-like Bi_2MoO_6, ChemistrySelect 4 (2019) 5338–5344, https://doi.org/10.1002/slct.201900323.

[39] L. Obalová, M. Reli, J. Lang, V. Matějka, J. Kukutschová, Z. Lacný, K. Kočí, Photocatalytic decomposition of nitrous oxide using TiO_2 and Ag-TiO_2 nanocomposite thin films, Catal. Today 209 (2013) 170–175, https://doi.org/10.1016/j.cattod.2012.11.012.

[40] K. Kočí, M. Reli, I. Troppová, M. Šihor, J. Kupková, P. Kustrowski, P. Praus, Photocatalytic decomposition of N_2O over TiO_2/g-C_3N_4 photocatalysts heterojunction, Appl. Surf. Sci. 396 (2017) 1685–1695, https://doi.org/10.1016/j.apsusc.2016.11.242.

[41] N. Bouazza, M.A. Lillo-Ródenas, A. Linares-Solano, Photocatalytic activity of TiO_2-based materials for the oxidation of propene and benzene at low concentration in presence of humidity, Appl. Catal., B 84 (2008) 691–698, https://doi.org/10.1016/j.apcatb.2008.06.002.

[42] A.H. Mamaghani, F. Haghighat, C.S. Lee, Photocatalytic oxidation technology for indoor environment air purification: the state-of-the-art, Appl. Catal., B 203 (2017) 247–269, https://doi.org/10.1016/j.apcatb.2016.10.037.

[43] M. Krichevskaya, S. Preis, A. Moiseev, N. Pronina, J. Deubener, Gas-phase photocatalytic oxidation of refractory VOCs mixtures: through the net of process limitations, Catal. Today 280 (2017) 93–98, https://doi.org/10.1016/j.cattod.2016.03.041.

Curriculum vitae

Personal data

Name: Kristen Altof
Date of birth: 16.02.1986
Place of birth: Tallinn, Estonia
Citizenship: Estonian

Contact data

E-mail: Kristen.altof@taltech.ee

Education

2021–2025 Tallinn University of Technology, Department of Materials and Environmental Technology, PhD
2017–2019 Tallinn University of Technology, MSc in Engineering
2008–2014 Berlin Technical University, BSc in Engineering

Language competence

Estonian Native speaker
English Fluent
German Fluent

Professional employment

2021–2025 Tallinn University of Technology, Department of Materials and Environmental Technology, early-stage researcher
2019 –… Energex Energy Experts OÜ, Chemical and Technology Engineer
Engineering calculations and technical analyses, energy and resource audits, digital diagnostics, grant applications, project management.
2016–2019 Buchen Industrial Services Baltikum OÜ, Project Manager
Management of maintenance projects in the chemical and energy industries in Estonia, Poland, and Germany.
2014–2015 Estover Piimatööstus OÜ, Head of Technical Department
Coordination of the department's operations, preparation of maintenance plans, resolution of emergency issues, implementation of development projects, and execution of automation projects.
2014 EstCube2 projekt, Intern
EstCube: Subsystem development and testing2014
2014 Vectronic Aerospace GmbH, Intern
Simulation software development

Defended dissertations

Kristen Altof, Master's Degree, 2019, (sup) Marina Kritševskaja, Comparison of Biogas Upgrading Methods Based on the Operating Parameters of Refining Technologies, Tallinn University of Technology School of Engineering, Department of Materials and Environmental Technology.

Field of research

Biosciences and Environment; Research into Substances Hazardous to the Environment.

Elulookirjeldus

Isikuandmed

Nimi: Kristen Altof
Sünniaeg: 16.02.1986
Sünnikoht: Tallinn, Eesti
Kodakondsus: Eesti

Kontaktandmed

E-post: Kristen.altof@taltech.ee

Hariduskäik

2021–2025 Tallinna Tehnikaülikool, Materjali- ja keskkonnatehnoloogia instituut, PhD
2017–2019 Tallinna Tehnikaülikool, tehnikateaduste magister
2008–2014 Berliini Tehnikaülikool, tehnikateaduste bakalaureus

Keelteoskus

Eesti keel Emakeel
Inglise keel Kõrgtase
Saksa keel Kõrgtase

Teenistuskäik

2021–2025 Tallinna Tehnikaülikool, Inseneriteaduskond, Materjali- ja keskkonnatehnoloogia instituut, nooremteadur
2019 –… Energex Energy Experts OÜ, Keemia- ja tehnoloogiainsener
Inseneriarvutused ja tehnilised analüüsid, energia- ja ressursiauditid, digidiagnostikad, toetuse taotlused, projektide juhtimine.
2016–2019 Buchen Industrial Services Baltikum OÜ, projektijuht
Hooldusprojektide juhtimine keemia- ja energiatööstustes Eestis, Poolas, Saksamaal.
2014–2015 Estover Piimatööstus OÜ, Tehnikaosakonna juhataja
Tehnikaosakonna töö koordineerimine, hooldusplaanide koostamine, avariiprobleemide lahendamine, arendusprojektide läbiviimine, automatiseerimisprojektide läbiviimine.
2014 EstCube2 projekt, praktikant
EstCube: Subsüsteemi arendus ja testimine
2014 Vectronic Aerospace GmbH, praktikant
Simulatsioonitarkvara arendus

Kaitstud lõputööd

Kristen Altof, magistrikraad, 2019, (juh) Marina Kritševskaja, Biogaasi väärindamistehnoloogiate võrdlus protsessis kasutatavate tehnoloogiliste seadmete tööparameetrite alusel, Tallinna Tehnikaülikool, Inseneriteaduskond, Materjali- ja keskkonnatehnoloogia instituut.

Uurimustöö põhisuunad

Bio- ja keskkonnateadused; Keskkonnaohtlikke aineid käsitlevad uuringud.

ISSN 2585-6901 (PDF)
ISBN 978-9916-80-503-9 (PDF)